

The Pennsylvania State University

The Graduate School

Department of Chemistry

**MEASUREMENTS AND CONTROL OF SINGLE MOLECULES AND THEIR
NANOSCALE ASSEMBLIES TO DEVELOP MOLECULAR MACHINERY**

A Dissertation in

Chemistry

by

Ajeet Kumar

© 2010 Ajeet Kumar

Submitted in Partial Fulfillment
of the Requirements
for the Degree of

Doctor of Philosophy

August 2010

The dissertation of Ajeet Kumar was reviewed and approved* by the following:

Paul S. Weiss
Distinguished Professor of Chemistry and Physics
Dissertation Advisor
Chair of Committee

A. W. Castleman, Jr.
Evan Pugh Professor of Chemistry and Physics
Eberly Distinguished Chair in Science

John V. Badding
Professor of Chemistry

Seong H. Kim
Professor of Chemical Engineering

Barbara J. Garrison
Shapiro Professor of Chemistry
Head of the Department of Chemistry

*Signatures are on file in the Graduate School

ABSTRACT

We explore functional molecules and assemblies on substrates. We induce motion, structural changes, and electronic changes in molecules and assemblies, which we measured using novel instrumentation.

We have controlled photo-induced isomerization of single azobenzene-functionalized molecules isolated in tailored *n*-alkanethiolate self-assembled monolayer matrices. We engineered the molecular design to suppress excited-state quenching from metal substrates and to form rigid assemblies of single tethered azobenzene molecules in the domains of the monolayer to limit steric constraints, and tip-induced and stochastic switching effects.

We prepared one-dimensional chain assemblies of azobenzene-functionalized molecules in the domain boundaries of *n*-alkanethiol matrices. We switched the chains of molecules from *trans* to *cis* using UV light and observed that the molecules in the chains isomerize in concert. This concerted switching was attributed to electronic coupling between the molecules within the chains. We employed electron-induced isomerization of azobenzene in the chains and established that π -orbital overlap of the molecules in the one-dimensional chain structures enables the electrons to delocalize along the chain.

We created assemblies of redox-active bistable rotaxane molecules on microscale levers to produce forces that bend the levers reversibly and generate *microscale* motion. Assembled rotaxane molecules generate cooperative forces, much like artificial molecular muscles, and constitute a seminal step toward molecular-machine-based nanoelectromechanical systems. We also controlled the conformational changes in rotaxanes at the single-molecule level and observed that conformational changes correlate

with the known redox states of rotaxanes. We observed that mechanical motions of these molecules are strongly influenced by their interactions with the surface and with neighboring molecules.

Assemblies of double-decker molecules, having two parallel porphyrin or phthalocyanine rings connected by rare earth metal cations, were created to study both rotary motion dynamics of isolated double-deckers, and the collective interactions of ensembles whose rotors interact as intermeshed gears. We demonstrate the ability to control the placements in arrays by lateral manipulations using a scanning tunneling microscope probe tip.

These studies demonstrate our abilities to create and to place isolated functional molecules and their assemblies. We are able to induce and to understand motion and structural and electronic changes in these nanoscale machineries assembled *via* bottom-up techniques.

TABLE OF CONTENTS

LIST OF FIGURES.....	viii
LIST OF SCHEMES.....	xiv
LIST OF ABBREVIATIONS.....	xv
ACKNOWLEDGMENTS.....	xvii
CHAPTER 1 CONTROLLING AND IMAGING MOLECULAR ASSEMBLIES.....	1
1.1 Introduction.....	1
1.2 Self-Assembled Monolayers.....	3
1.2.1 Insertion into Self-Assembled Monolayers.....	6
1.2.2 Co-Adsorption into Self-Assembled Monolayers.....	8
1.3 Scanning Tunneling Microscopy.....	8
1.3.1 Scanning Tunneling Microscopy Operation.....	10
1.4 Electrochemical Scanning Tunneling Microscopy.....	11
1.5 Thesis Overview.....	13
CHAPTER 2 REVERSIBLE PHOTO-SWITCHING OF SINGLE AZOBENZENE MOLECULES IN CONTROLLED NANOSCALE ENVIRONMENTS.....	16
2.1 Introduction.....	16
2.2 Experimental Procedure.....	20
2.2.1 Sample Preparation.....	20
2.2.2 Scanning Tunneling Microscopy.....	20
2.2.3 Apparent Height Determination.....	22
2.3 Results and Discussion.....	23
2.4 Conclusions and Future Directions.....	30
CHAPTER 3 SELF-ASSEMBLED ONE-DIMENSIONAL MOLECULAR WIRES OF AZOBENZENE: CONCERTED SWITCHING AND ELECTRON TRANSPORT.....	32
3.1 Introduction.....	32
3.2 Experimental Procedure.....	34
3.2.1 Sample Preparation.....	34
3.2.2 Scanning Tunneling Microscopy.....	36
3.2.3 Estimation of Electric Field in the Tunneling Junction.....	36

3.3 Results and Discussion.....	38
3.3.1 Chain Structure.....	38
3.3.2 Light-Induced Switching of Chains.....	38
3.3.3 Electron-Induced Switching of the 1L Chains.....	41
3.3.4 Electric Field Effects on Switching.....	43
3.3.5 Possible Routes for Electrons in Chain during Manipulation.....	44
3.3.6 Switching of the 2L Chains and Reversibility of Switching.....	45
3.3.7 Manipulation Time Period and Control Experiments.....	47
3.4 Conclusions and Future Directions.....	48
CHAPTER 4 A MECHANICAL ACTUATOR DRIVEN ELECTROCHEMICALLY BY ARTIFICIAL MOLECULAR MUSCLES.....	50
4.1 Introduction.....	50
4.2 Experimental Procedure.....	57
4.2.1 Preparation of Microcantilever Samples.....	57
4.2.2 Synthesis of Molecular Muscles and Control Compounds and Preparation of Monolayer Films.....	57
4.2.3 Electrochemical Atomic Force Microscopy.....	57
4.3 Results and Discussion.....	58
4.4 Conclusions and Future Directions.....	75
CHAPTER 5 CHANGING STATIONS IN SINGLE BISTABLE ROTAXANE MOLECULES UNDER ELECTROCHEMICAL CONTROL.....	76
5.1 Introduction.....	76
5.2 Experimental Procedure.....	77
5.2.1 Sample Preparations.....	77
5.2.2 Electrochemical Scanning Tunneling Microscopy.....	79
5.2.3 Cyclic Voltammetry.....	79
5.3 Results and Discussion.....	80
5.4 Conclusions and Future Directions.....	89
CHAPTER 6 MANIPULATION OF DOUBLE-DECKER PHTHALOCYANINE MOLECULES ON HOPG.....	90
6.1 Introduction.....	90
6.2 Experimental Procedure.....	91
6.2.1 Sample Preparation.....	91
6.2.2 Scanning tunneling microscope.....	93
6.3 Results and Discussion.....	94
6.3.1 Structure of the Thin Films.....	94

6.3.2 STM Probe Tip Manipulation of Molecules.....	98
6.3.2.1 Detaching Molecules from an Island using Probe Tip Manipulation.....	101
6.3.2.2 Splitting and Combining a Pair of Molecules Using Probe Tip Manipulation.....	101
6.4 Conclusions and Future Directions.....	104
CHAPTER 7 CONCLUSIONS AND FUTURE PROSPECTS.....	105
7.1 Switching of Single Molecule and Their One-Dimensional Assemblies.....	105
7.2 Rotaxane: An Artificial Muscle Molecule.....	109
7.3 Double-Decker Rotors.....	110
7.4 Concluding Remarks.....	110
REFERENCES.....	112

LIST OF FIGURES

- Figure 1.1 (A) Scanning tunneling microscopy image of a *n*-dodecanethiolate (C12) SAM assembled on a Au{111} substrate. Defects within the monolayer are inherent to the assembly and include substrate step edges (red arrows), substrate vacancy islands (teal arrows) and boundaries between of the alkanethiolate domains (green arrows). (B) Schematic of the packing of a C12 monolayer showing the tilt of the molecules. Carbon is represented by black circles, H by white, S by purple and Au by yellow. The alkanethiolate molecules are bound to the surface through a S-Au bond. (C) The SAMs pack on the surface in a $(\sqrt{3} \times \sqrt{3})R30^\circ$ lattice (red) relative to the underlying Au lattice (black). STM images are recorded with sample bias (V_s) = -1 V and tunneling current (I_t) = 2 pA.....4
- Figure 1.2 (A) Schematic of the SAM solution assembly. Gold substrates are placed into ethanolic solutions containing alkanethiol molecules resulting in an alkanethiolate SAM deposited on the substrates. (B) Schematic of insertion, which is performed by placing the Au{111} substrate with the preformed SAM into a solution containing the molecules to be inserted. (C) Schematic of co-adsorption, which is performed by placing the Au{111} substrate in mixture of total two thiols with a molar ratio of 1:4. The lower concentration molecules are placed within the domains of matrix. (D) Scanning tunneling microscopy image of an alkanethiolate SAM with molecules inserted at defect sites. (E) Scanning tunneling microscopy image of an alkanethiolate SAM with molecules co-adsorbed within domains. (V_s = -1 V; I_t = 2 pA).....7
- Figure 1.3 (A) An energy level diagram for a one-dimensional (1D) electron tunneling junction. The E_F of the tip and sample are offset by the applied bias voltage, V . The resultant current is exponentially proportional to the distance between the sample and the tip (z). LDOS = local density of states, Φ = work function of the metal. (B) Schematic of a STM tip rastering across a metal surface in constant current mode, where the tip is extended and retracted maintaining a constant tunneling current between tip and sample.....9
- Figure 1.4 Schematic of ECSTM. A bipotentiostat is used to control electrode potential in a four-electrode setup, including CE: counter electrode, RE: reference electrode.....12
- Figure 2.1 Scanning tunneling microscopy image of isolated azobenzene-functionalized single molecules (1, white protrusions) embedded in a C10 SAM films on Au{111}. For each molecule, extracted (black box) and background (red box) regions are automatically selected for each frame. The background corresponds to the SAM apparent height near the extracted molecule.

- Apparent height of 1 is measured to be $2.1 \pm 0.3 \text{ \AA}$21
- Figure 2.2 With time (1 hr), but no illumination, no change in apparent height was observed in scanning tunneling microscope images (Figure 2.2A & 2.2B) ($I_t = 2 \text{ pA}$; $V_s = 1.0 \text{ V}$). With sample bias polarity (V_s) change (but still no illumination), (2.2C) 1.0 V to (2.2D) -1.0 V, no significant change in apparent height was observed ($I_t = 2 \text{ pA}$) in the scanning tunneling microscope images.....24
- Figure 2.3 Azobenzene-functionalized molecules switch OFF and switch ON upon irradiation with UV ($\sim 365 \text{ nm}$) and visible ($\sim 450 \text{ nm}$) light, respectively. Images are recorded after irradiating (A) 0 min, (B) 10 min, (C) 35 min, (D) 60 min and (E) 160 min with ultraviolet light and visible light irradiation for (F) 30 min. Figures 2.3A-2.3E show switching OFF of single molecules with continued UV illumination. The squares in 2.3E and 2.3F show switching ON of molecules with visible illumination. The arrow in figure 2.3E shows switching ON of a molecule with UV illumination. Scanning tunneling microscope images are recorded at $V_s = 1 \text{ V}$ and $I_t = 2 \text{ pA}$. Contrast changes in the images are due to STM tip changes during imaging.....26
- Figure 2.4 Fraction of azobenzene-functionalized molecules in the ON state decreases as a function of time after UV irradiation ($\sim 12 \text{ mW/cm}^2$). The decay constant (τ) under these conditions is $54 \pm 15 \text{ min}$27
- Figure 2.5 Height profile of azobenzene functionalized molecules changes from I ($\sim 2.1 \pm 0.3 \text{ \AA}$) to II ($\sim 0.7 \pm 0.2 \text{ \AA}$) with UV light irradiation (switch OFF). With visible light exposure, the height profile changes from II ($\sim 0.7 \pm 0.2 \text{ \AA}$) to III ($\sim 1.5 \pm 0.3 \text{ \AA}$) (switch ON).....28
- Figure 3.1 (A) Formation of C10 SAMs with deposition in solution for 1 min leads to large numbers of defects. (B) Azobenzene-functionalized 1 molecules are inserted into the defect sites of loosely packed C10 SAM by immersing the preformed C10 SAM in solutions of molecule 1 for 4 min. (C) Vapor annealing of sample in C10 vapor adds matrix molecules to increase the sizes of domains of the matrix. During this packing, the C10 domains grow and push the molecules in the domain boundaries where they form 1D structures (white arrows). All STM images are recorded at $V_s = 1 \text{ V}$ and $I_t = 1 \text{ pA}$35
- Figure 3.2 (A) A representative STM image with chains of molecule 1 (yellow ovals) assembled at domain boundaries of a C10 SAM. (B) A STM image of a 2L chain at a domain boundary. The overlay of the black dots represent the phenyl ring arrangements in the herringbone structure. (C) A STM image of a 1L chain. Again black dots are shown to highlight the phenyl rings of the azobenzene moiety. (D) A schematic of the molecular arrangement in the 2L chain shows that it has two layers of molecules. Each pair of parallel molecules are separated by $8.9 \pm 0.4 \text{ \AA}$. All STM images are recorded at

- $V_s = 1 \text{ V}$ and $I_t = 1 \text{ pA}$37
- Figure 3.3 Photo-induced switching of chains is shown in the STM images. Both 1L and 2L chains switched OFF upon UV light exposure for $\sim 30 \text{ min}$ at $\sim 12 \text{ mW/cm}^2$. (A and B) All molecules in the 1L chain switched OFF completely. (C and D) Parts of the 2L chain did not switch OFF (red squares). Due to steric hinderance in the 2L chains, the molecules in the red box area do not have free space around them to switch to the *cis* form. All STM images were recorded at $V_s = 1 \text{ V}$ and $I_t = 1 \text{ pA}$39
- Figure 3.4 1L chain switched OFF by 2.0 eV electrons supplied by the STM tip. A and C show the position of the STM tip (black arrow) positioned above the 1L chain. All parts of the 1L chain switched OFF completely by applying a sample bias of 2.0 V for 2 min. However, a second 1L chain (yellow boxes) above the manipulated 1L chain (orange box) did *not* switch OFF due to the lack of sufficient coupling (black circle) between these two chains. All STM images are recorded at $V_s = 1 \text{ V}$ and $I_t = 1 \text{ pA}$42
- Figure 3.5 Series of STM images are shown of a 2L chain switching between the ON and the OFF states, for two cycles. A sample bias of 2.0 V applied by the STM probe tip (black arrows) switches the $\sim 130 \text{ \AA}$ long 2L chain (A and C). The switching is reversible. The OFF chain switched ON when left unperturbed for 30-100 min with thermal relaxation (B and D). Parts of the chain did not switch OFF (B, red squares) due to steric hinderance in 2L chains. All STM images are recorded at $V_s = 1 \text{ V}$ and $I_t = 1 \text{ pA}$46
- Figure 4.1 Schematic of the experimental setup used for in situ electrochemical activation of the palindromic bistable [3]rotaxanes molecules. The inset shows the reversible electrochemical oxidation and reduction of R^{8+} to produce the microcantilever deflection. (WE: working electrode, CE: counter electrode, RE: reference electrode).....56
- Figure 4.2 Deflection signature (colored lines) in response to a triangular sweep (purple lines) of the electrochemical potential for (a) a bare microcantilever (orange line, 5 mV s^{-1}) and (b) a microcantilever modified with a monolayer film of the palindromic bistable [3]rotaxane R^{8+} (green line) on one side of the microcantilever (20 mV s^{-1}). The directions of the arrows indicate the corresponding y-axis of the parameter plotted.....59
- Figure 4.3 Deflection vs. applied potential with respect to the working electrode for a bare microcantilever (orange line, 5 mV s^{-1}) as well as for microcantilevers coated with monolayer films of the bistable [3]rotaxane R^{8+} (green line, 20 mV s^{-1}), the dumbbell D (black line, 20 mV s^{-1}), and 1-dodecanethiol C12 (dark grey line, 20 mV s^{-1}).....63

- Figure 4.4 Time-dependent operation of microcantilevers coated with: (a) the palindromic bistable [3]rotaxane R^{8+} (green line), (b) the dumbbell D (black line), and (c) 1-dodecanthiol C12 (dark grey line), when subjected to a series of oxidation and reduction potential steps (purple lines).....66
- Figure 4.5 Comparison of the downward deflection as a result of the application of an oxidizing potential (squares) and the upward deflection caused by the application of reducing potential (circles) in a microcantilever modified with a bistable [3]rotaxane R^{8+} monolayer film followed through five actuation cycles. Solid lines represent the best fits.....69
- Figure 4.6 Actuation of a microcantilever coated with R^{8+} molecules when subjected to three types of electrochemical potential variations. In Stage I, seven steps of alternating oxidizing and reducing potentials were applied. In Stage II, no external potential was applied for 175 sec. This period enabled recovery of the cantilever, as noted from the fit (dotted line) of the deflection signature observed in Stage II. In Stage III, five steps of alternating oxidizing and reducing potentials were applied.....72
- Figure 5.1 Structure and motion of a bistable rotaxane molecule, R, adsorbed on Au{111} investigated using electrochemical scanning tunneling microscopy. (A) The tetracationic cyclobis(paraquat-p-phenylene) ring (CBPQT⁴⁺, blue) is known to move along the thread between two recognition sites (tetrathiafulvalene, TTF, green and 1,5-dioxynaphthalene, DNP, red stations) depending on the redox state of the TTF unit. (B) The protrusions are assigned as CBPQT⁴⁺ rings. (C) In its reduced state at +0.12 V, the CBPQT⁴⁺ ring prefers to encircle the TTF station. (D) Upon oxidation (+0.12 V to +0.53 V) of TTF into a radical cation, electrostatic repulsion propels the ring to the DNP station (blue arrow). (E) Upon reduction (+0.53 V to +0.12 V) of TTF to neutrality, the DNP station relaxes back to its thermodynamically favorable position, the TTF station (red arrow). Image conditions: $V_s = 0.3$ V; $I_t = 2$ pA. The Faradaic current was typically less than 10 pA.....78
- Figure 5.2 STM images of Au{111} under 0.1 M HClO₄ at electrode potential of +0.35 V vs. Ag/AgCl electrode ($V_s = 0.3$ V; $I_t = 2$ pA). (A) Control experiment, no molecules (vertical scale: 10 Å); (B) dumbbell component of R^{4+} on Au{111} (CH₂Cl₂: 5 sec, 5 μM adsorption) (vertical scale: 15 Å); (C) R^{4+} on Au{111}. The protrusions are due to the CBPQT⁴⁺ rings (vertical scale: 20 Å). Image conditions: $V_s = 0.3$ V; $I_t = 2$ pA. The Faradaic current was typically less than 10 pA.....81
- Figure 5.3 Cyclic voltammogram of R^{4+} adsorbed on Au under 0.1 M HClO₄.....82
- Figure 5.4 A STM image of R^{4+} adsorbed on Au{111} under 0.1 M HClO₄ solution. The three images with potentials +0.12 V, +0.53 V, and +0.12 V are superimposed and the protrusions on all three images have been marked. The trajectories of

- a large number of motions of CBPQT⁴⁺ rings after potential steps from +0.12 V to +0.53 V and back to +0.12 V are marked with blue and red lines, respectively, as in Figure 5.1C-E (320 Å × 320 Å).....84
- Figure 5.5 Histogram of measured displacements of protrusions over 10 min at different potentials. (A) The surface was equilibrated at +0.12 V; (B) the surface was equilibrated at +0.53 V; (C) the potential was stepped from +0.12 V to +0.53 V and displacements were measured by comparing images acquired before and after the potential step; (D) the potential was stepped back from +0.53 V to +0.12 V and again the displacements were measured.....86
- Figure 5.6 Polar graph of displacement vectors after the potential step from +0.53 V to +0.12 V. The angle is referenced against the trajectories after the potential was stepped from +0.12 V to +0.53 V. The angular distribution suggests that the protrusions have the tendency to move in opposite directions when molecules are reduced back to the original state.....88
- Figure 6.1 (A) STM images of thin films of a mixture of H₂Pc(OC₈H₁₇)₈ and (Nc)Sm[Pc(OC₈H₁₇)₈] on HOPG. (B) An area of the mixed monolayer occupied with DD molecules. Dark areas correspond to H₂Pc(OC₈H₁₇)₈, lattice constants: a = 2.5 ± 0.1 nm and b = 2.4 ± 0.1 nm. Lighter areas correspond to DD molecules: lattice constants: l = 3.0 ± 0.1 nm and k = 3.0 ± 0.1 nm. STM images are recorded at V_s = -0.5 V and I_t = 2 pA.....95
- Figure 6.2 With time (30 min), few changes in the mixed monolayer of DD and H₂Pc(OC₈H₁₇)₈ molecules were observed in STM images (I_t = 2 pA; V_s = -0.5 V). Circles show one desorbed molecule.....96
- Figure 6.3 A-I. Oscilloscope traces for the z-position of the STM tip (yellow) and tunneling current (blue) during the manipulation step of molecules. The corresponding sample bias voltage and current values are given as (V_s; I_t). J. Mixed monolayer of DD and H₂Pc(OC₈H₁₇)₈ molecules on HOPG. The green arrow is the direction of tip movement with (-0.3 V; 21 pA). The molecule being manipulated moved along the white arrow. K. Image of the area after manipulation. Another molecule was pushed upward (pink arrows). STM images are recorded at V_s = -0.5 V and I_t = 2 pA.....97
- Figure 6.4 A. Oscilloscope traces for the manipulation of an island of DD molecules. Manipulation condition was V_s = -0.3 V; I_t = 21 pA. B. Island of DD molecules is manipulated using STM. Tip moved along the green arrow, breaking the island. C. Circled molecule broke away from island. A few molecules desorbed after manipulation (black arrows). Molecule with pink arrow stayed intact with the island. STM images are recorded at V_s = -0.5 V and I_t = 2 pA.....102

Figure 6.5 A pair of DD molecules is split and combined using manipulation ($V_s = -0.1$ V and $I_t = 21$ pA). A-B. Probe tip is placed between the molecules and the manipulation step was applied to split the pair. The Probe tip was moved along the green arrow. However, the molecules 1 and 2 moved along the white arrows. C-D. Molecule 3 was manipulated to make a pair with 4. The probe tip was moved along the green line. However, 3 moved along the white lines and pushed 4, as shown in 6.5C. STM images were recorded at $V_s -0.5$ V and $I_t = 2$ pA.....103

LIST OF SCHEMES

- Scheme 2.1 Isolated azobenzene-functionalized single molecules (1) embedded in 1-decanethiolate (C10) SAM on Au{111}. Photo-induced changes in apparent height of the azobenzene-functionalized molecules in STM images are due to isomerization of the azobenzene moiety between *trans* and *cis*, and are defined as ON (apparent height = $2.1 \pm 0.3 \text{ \AA}$) and OFF (apparent height = $0.7 \pm 0.2 \text{ \AA}$) states, respectively.....19
- Scheme 4.1 Molecular structures of (a) a palindromic bistable [3]rotaxane R^{8+} , (b) a disulfide-tethered dumbbell D (control compound related to R^{8+}), and (c) 1-dodecanethiol C12 (control compound).....53
- Scheme 6.1 Molecular structures of double-decker molecule (Nc)Sm[Pc(OC₈H₁₇)₈] (upper) and Pc(OC₈H₁₇)₈ (lower). Nc = naphthalocyanine; Pc = phthalocyanine.....92

LIST OF ABBREVIATIONS

Molecules	
C10	Decanethiolate
C12	Dodecanethiolate
A1	Azobenzene-functionalized molecule
R ⁸⁺	Bistable [3]rotaxane
R ⁴⁺	[2]rotaxane
TTF	Tetrathiafulvalene
NP	Naphthalene
CBPQT	Cyclobis(paraquat- <i>para</i> -phenylene)
DNP	dioxynaphthalene
Pc	Pthalocyanine
Por	Porphyrins
Nc	Naphthalocyanine

Other Acronyms	
SAM	Self-assembled monolayer
LDOS	Local density of states
1D	One-dimensional
2D	Two-dimensional
DD	Double-decker
HOPG	Highly ordered pyrolytic graphite
1L	One-layer chain
2L	Two-layer chain
RT	Room temperature
LM	Lateral manipulation
RT	Room temperature
I _t	Tunneling current set point
V _s	Applied sample bias
z	Tip-sample distance
E _F	Fermi level
τ	Decay constant
rms	Root mean square

Characterization Tools

STM	Scanning tunneling microscopy
ECSTM	Electrochemical scanning tunneling microscopy
AFM	Atomic force microscopy
CV	Cyclic Voltammetry

ACKNOWLEDGMENTS

I would like to take this opportunity to thank each and every individual who have contributed to my personal and professional development during my stay at Penn State. Here is a partial list of these wonderful people.

First I would like to thank my graduate advisor Prof. Paul Weiss. Thank you for welcoming me into your group and providing me with the opportunity and the resources to be as creative as I like, inspiring me to do my best, and making sure I am progressing along a forward path. Your effort in making us learn, both scientifically and otherwise, has driven most of my achievements and has helped me gain the most confidence in my scientific abilities.

I thank my committee members Prof. A Welford Castleman, Prof. John Badding, and Prof. Seong Kim. I appreciate the time and effort you have put into being on my committee. I gratefully acknowledge financial support from the National Science Foundation, the Materials Research Science and Engineering Center (MRSEC) at Penn State, and the Department of Energy (DE-FG02-07ER15877). I would also like to thank our collaborators: Prof. Vincent Crespi and Prof. Tony Huang at Penn State, Prof. James Tour at Rice University, and Prof. Fraser Stoddart at Northwestern University.

I would like to thank all of the former and present Weiss group members that I have had the pleasure of meeting. Their willingness to go out of their way to assist colleagues has helped to build a friendly atmosphere in our lab. Dr. Tao Ye, thank you for your support and guidance in starting on all of my projects and always being there for me. I have looked to you as a source of inspiration, strength, and fellowship. Thanks to

everyone who was here when I arrived and welcomed me into the group: Rachel Smith, Arrelaine Dameron, Beth Anderson, Julia Heetderks, Sanjini Nanyakkara, Hector Saavedra, Amanda Moore, Thomas Mullen, Adam Kurland, Meaghan Blake, Nate Hohman, Moonhee Kim, Rong Zhang, Mitchel Shuster, Amit Vaish, and thanks to the postdocs who have been here and have given me scientific advice: Luis Fernandez, Susan Gillmor, Patrick Han, Dongbo Li, Peng-Peng Zhang, Shelley Claridge, Wei Xu, and Wei-Ssu Liao. I wish the best of luck to those who came after me in their continuing research and all future endeavors: Bala Pathem, Andrea Giordano, John Thomas, Sarawut Cheunkar, Jeff Lawrence, Huan Cao, Jeffrey Schwartz, and Daniel Dewey.

My special thanks to my parents. Through their works and deeds, they always tell me how important it is to see good sides in the trying times and stay true to aspirations. I cannot imagine how I could come this far without their unconditional love and support. Thank you for always encouraging me and allowing me to follow my dreams. Thanks to my siblings, Divya, Indu, and Kundan: for their love. Thanks to my good friends at State College, who made my stay at Penn State more enjoyable.

Finally, to my wife, Priti, without your love, support, and encouragement this work would not have been completed. You are my best chosen friend, companion, and guide.

Chapter 1

CONTROLLING AND IMAGING MOLECULAR ASSEMBLIES

1.1 Introduction

Inspired by the inherent promise and opportunities in nanotechnology, the scientific community has been attempting to decrease the characteristic length scales that define mechanical, electronic, and other devices [1,2]. This has driven tremendous progress in new techniques for the assembly and construction of devices and machines with functional components based on nanoscale building blocks. Remarkable advances have been achieved in chemical synthesis, nanoscale assembly, and molecular control and measurements that have enabled the development of molecular-scale machines [3-12]. Ultimately, success at miniaturization will make machines at the molecular level operate with the macroscopic concepts of motion.

A molecular machine or electronic device consists of a discrete number of molecules or other nanoscale components, each capable of performing mechanical movements or undergoing electronic property changes in response to external stimuli [13,14]. Nanoscale devices can be as simple as a single molecule undergoing mechanical/electronic changes; they also may work hierarchically or together in concert to perform complex functions, as in biological systems. These molecular devices, like macroscopic systems, need to be powered by electrical [3,6,15], chemical [4,16], electrochemical [17], or optical [18-21] means.

Functional molecules that can either change conductivity or move with external stimuli are ideal for molecular motors or molecular electronics. Significant effort has been made to design and to synthesize such molecules [4,22-25]. These functional molecules, if to be used in actual devices, need to be put at interfaces or in other nanoscale environments where we can restrict their degree of freedom and direct their motion to generate useful work. Arranging functional molecules and their assemblies on substrates provides technologically relevant test conditions [26,27]. Substrates can be designed to restrict motion and give direction to the motion of molecules. A major challenge for this kind of research includes not only synthesizing molecules and fabricating precise assemblies in controlled environments, but also accessing their properties and functions at the molecular and nanometer scales. Scanning probe microscopy techniques have proven to be very significant in control and measurements of molecular electronics and molecular motors.

This dissertation explores the design of molecules and their assemblies on substrates. Novel instrumentation has been developed and employed to understand motion and structural changes in single molecules and their directed assemblies. We will discuss how we have designed molecules and created nanoscale environments to control photo-isomerization of single-isolated molecules on a Au{111} surface. The photo- and electron-induced isomerization of one-dimensional molecular assemblies was also studied. Further, we used molecular motion of artificial molecular-muscles to generate large forces on the macroscopic scale. Single-molecule insights of the motion of artificial muscle molecules help us design more efficient molecules. The remainder of this chapter

will introduce self-assembly techniques and discuss various scanning tunneling microscopy (STM) instrumentation, including electrochemical STM (ECSTM).

1.2 Self-Assembled Monolayers

In the 1940's, Zisman *et al.* discovered that an alkanolic acid could self-organize into a monolayer on a clean platinum surface driven by chemisorption from the solution phase [28]. Monolayers prepared by this method are called self-assembled monolayers (SAMs). These monolayers provide a simple route to engineer the surface properties of metals, semiconductors, and other materials. These are spontaneously formed organic assemblies directed by the chemical and physical properties of the molecules [29]. Chemically functionalized headgroups of molecules or ligands that form SAMs have a specific affinity for a substrate that typically enables them to displace adsorbed adventitious materials.

A number of headgroup/surface combinations have been studied, such as ROH/Si, RCOOH/Ni, and $R(\text{PO}_4)^{2-}/\text{TiO}_2$ [29]. However, the most widely characterized systems are alkanethiolates adsorbed on Au{111} substrates [30-32]. Alkanethiolate SAMs on Au{111} are well ordered and highly stable due to the strong gold-sulphur bond (~44 kcal/mol) and the stabilizing van der Waals forces (~1 kcal/mol per methylene unit) between adjacent alkyl chains. Alkanethiolate SAMs are easy to prepare and are of high structural order [29]. These monolayers can serve as templates for area-selective deposition of metals and a variety of guest molecules. Since one can tailor the interaction

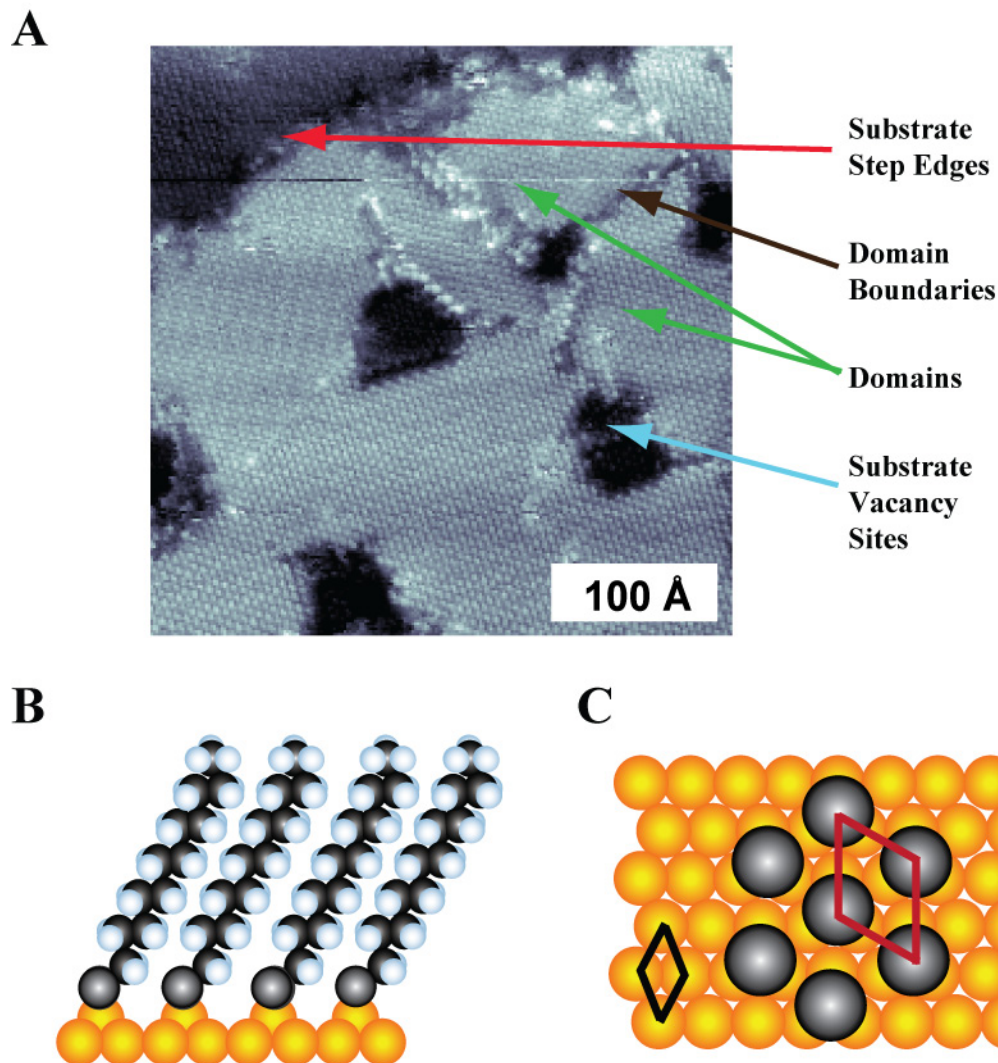


Figure 1.1: (A) Scanning tunneling microscopy image of a *n*-dodecanethiolate (C12) SAM assembled on a Au{111} substrate. Defects within the monolayer are inherent to the assembly and include substrate step edges (red arrows), substrate vacancy islands (teal arrows) and boundaries between of the alkanethiolate domains (green arrows). (B) Schematic of the packing of a C12 monolayer showing the tilt of the molecules. Carbon is represented by black circles, H by white, S by purple and Au by yellow. The alkanethiolate molecules are bound to the surface through a S-Au bond. (C) The SAMs pack on the surface in a $(\sqrt{3} \times \sqrt{3})R30^\circ$ lattice (red) relative to the underlying Au lattice (black). Image is recorded with sample bias (V_s) = -1 V and tunneling current (I_t) = 2 pA.

between SAMs and other molecules or particles by modifying the terminal groups, they have been used for many types of molecular assemblies, including molecular electronics and mechanical devices discussed here.

A representative STM image of an *n*-dodecanethiolate (**C12**) SAM deposited on Au{111} is shown in Figure 1.1A, where arrows highlight the characteristic features of **C12** SAMs. This imaged SAM includes several key features, such as substrate defects, including substrate step edges (red arrows), substrate vacancy islands, domains, and domain boundaries. Step edges are boundaries between terraces of the gold substrate that differ in height by one or more Au atom. Substrate vacancy islands (teal arrows) are one Au atom deep substrate defects formed through Au{111} substrate reconstruction. During solution deposition, *n*-alkanethiol molecules reorganize the surface energy, and Au atoms get ejected from the surface to reconstruct into a different lattice [33]. Domains of **C12** and domain boundaries between two converging structured areas are shown (brown and green, respectively) [34-37]. The alkyl chains arrange with a molecular tilt angle of $\sim 30^\circ$ with respect to the Au surface normal to maximize the van der Waals interactions [31,38,39]. Self-assembled monolayers with short chain *n*-alkanethiols generally form a close-packed ($\sqrt{3} \times \sqrt{3}$) $R30^\circ$ lattice with respect to the underlying Au{111} lattice (Figure 1.1B,C). However, in longer chains (>10 Carbon) due to the changing intermolecular and the sulfur-gold interactions, another close-packed superlattice $c(4 \times 2)$ exists [31,40-42]. The lattice spacing for the alkanethiolate SAMs is 4.99 Å [31].

1.2.1 Insertion into Self-Assembled Monolayers

To create isolated single molecules within host SAM matrices, we use a strategy to insert molecules that primarily adsorb in the defect sites of SAMs. For example, this strategy allows us to measure the conductivity of molecules inserted into SAM matrices [43]. We study single molecules individually and compare them to the ensemble measurements. Thus, we gain an understanding into the interplay of single molecules working collectively to the properties of bundles of molecules, or to the creation of assemblies. The schematic in Figure 1.2B shows the insertion strategy used in parts of this dissertation. Specific molecules that were used for insertion, as well as their concentrations, will be given within the relevant chapters. First, *n*-alkanethiolate matrices are created with varying degrees of ordering in the matrix, which depends on the time allowed for assembly (Figure 1.2A). Longer assembly times lead to higher degrees of order, while shorter assembly times result in more defect sites. Insertion is usually achieved through solution deposition, and large numbers of defects in SAM matrices enable higher insertion [44-48]. Next, the preformed SAMs are placed in a solution containing the molecules to be inserted (Figure 1.2B). When the inserted molecules are imaged with STM, they may appear as protrusions from the host SAM, as shown in Figure 1.2D.

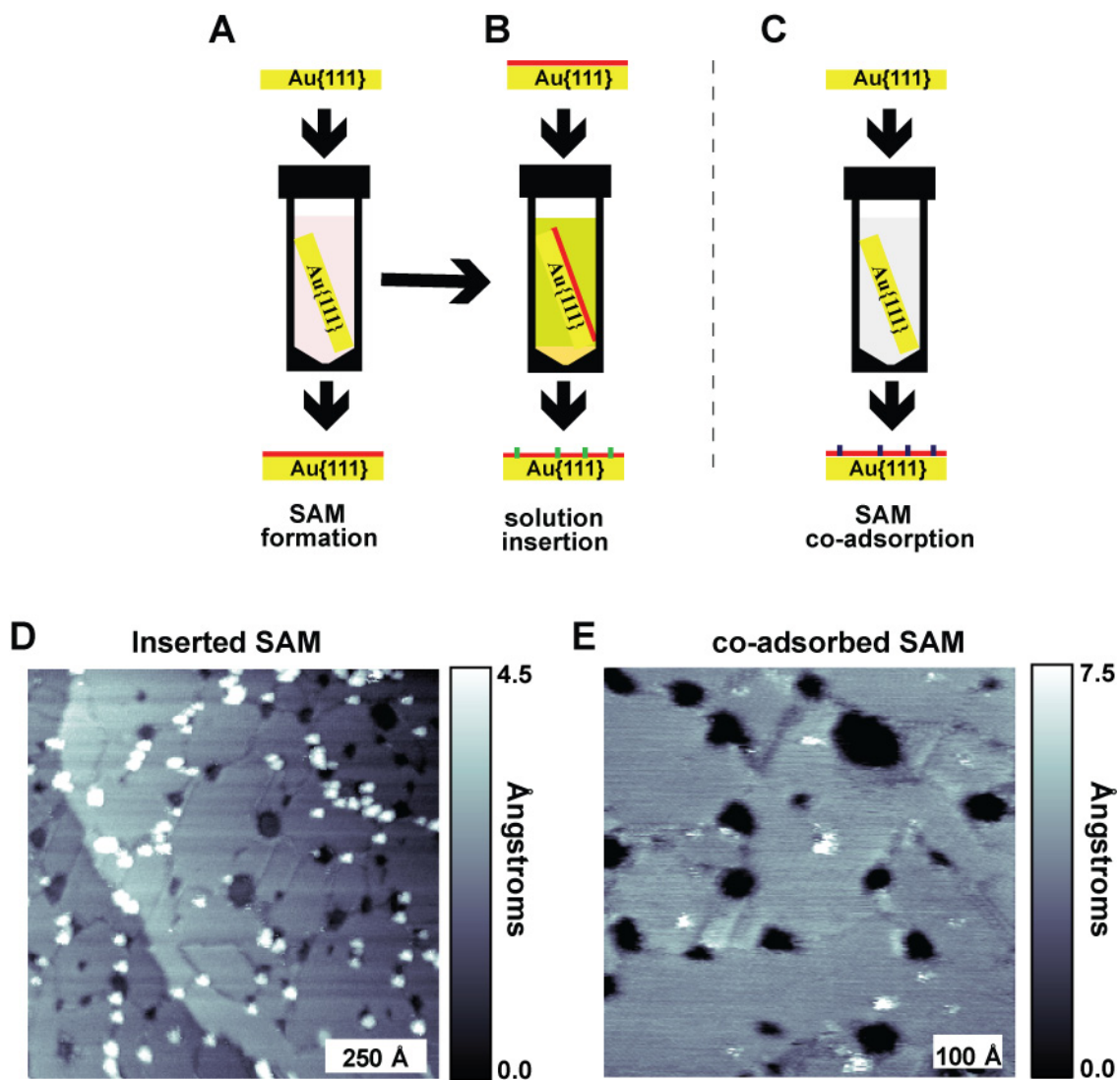


Figure 1.2: (A) Schematic of the SAM solution assembly. Gold substrates are placed into ethanolic solutions containing alkanethiol molecules resulting in an alkanethiolate SAM deposited on the substrates. (B) Schematic of insertion, which is performed by placing the Au{111} substrate with the preformed SAM into a solution containing the molecules to be inserted. (C) Schematic of co-adsorption, which is performed by placing the Au{111} substrate in mixture of total two thiols with a molar ratio of 1:4. The lower concentration molecules are placed within the domains of matrix. (D) Scanning tunneling microscopy image of an alkanethiolate SAM with molecules inserted at defect sites. (E) Scanning tunneling microscopy image of an alkanethiolate SAM with molecules co-adsorbed within domains. ($V_s = -1$ V; $I_t = 2$ pA)

1.2.2 Co-Adsorption into Self-Assembled Monolayers

A mixture of molecules in solution can form multi-component SAMs [40,49]. The ordering of the resulting matrix after solution deposition of mixed species can form a variety of monolayer depending on the nature and concentration of the molecules being assembled. For example, mixed monolayers prepared from two types of *n*-alkanethiolate molecules with similar lengths but different pendant functionality form phase-segregated SAMs separated as domains of common pendant functionality [50,51]. Isolated single molecules can also be formed by co-adsorption (Figure 1.2C). The molecule in need of isolation should have a similar headgroup structure, so that it is compatible with the matrix. Using this strategy, the molecules are adsorbed within the domains of the matrix, unlike the insertion process (Figure 1.2E). The details of the molecule combinations are discussed in relevant chapters.

1.3 Scanning Tunneling Microscopy

Since the invention of STM in 1981 [52-54], it has developed into an invaluable tool for probing and understanding interactions and electronic structures on surfaces. STM is used to determine atomic arrangements of a flat conducting or semiconducting surface by rastering with an atomically sharp tip and thus rendering real-space images. It is one of a family of several scanning probe microscopy techniques involving a local probe in proximity to the surface. Many books [55,56] and reviews [53,54,57] have been written to describe its development, theory, and use in detail. In this chapter, we will introduce the theory of imaging in air and liquid environments.

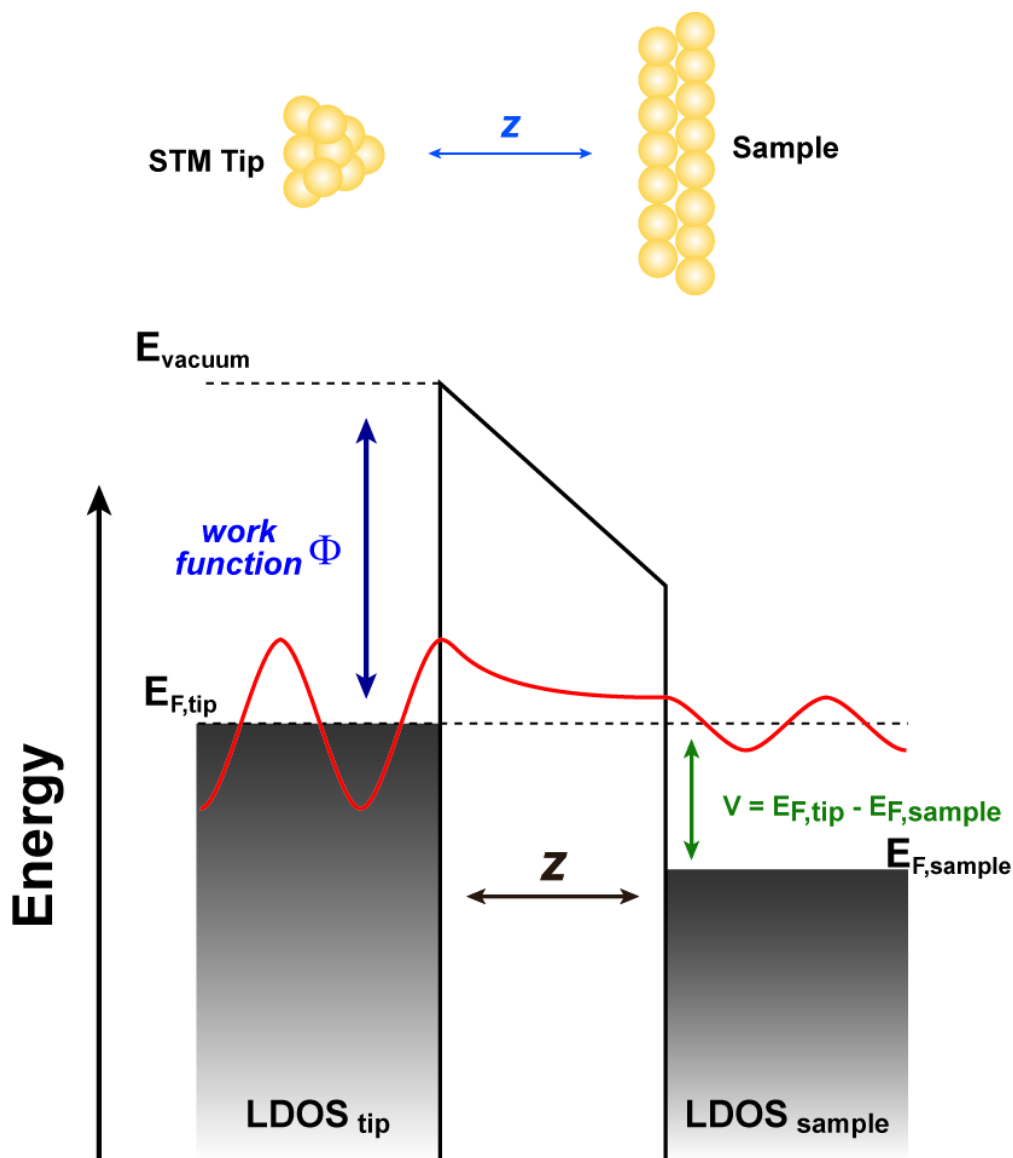


Figure 1.3: (A) An energy level diagram for a one-dimensional (1D) electron tunneling junction. The E_F of the tip and sample are offset by the applied bias voltage, V . The resultant current is exponentially proportional to the distance between the sample and the tip (z). LDOS = local density of states, Φ = work function of the metal. (B) Schematic of a STM tip rastering across a metal surface in constant current mode, where the tip is extended and retracted maintaining a constant tunneling current between tip and sample.

1.3.1 Scanning Tunneling Microscopy Operation

In STM an atomically sharp probe tip, usually made of W or Pt-Ir alloy, is brought in close proximity (3-10 Å) to a substrate using a piezoelectric transducer. At these distances, the electron wavefunction of the tip overlap with the electronic wavefunction of the surface. By applying a voltage across this junction, the electrons quantum mechanically tunnel through this classically forbidden potential energy barrier. A one-dimensional (1D) energy level diagram of this process is depicted in Figure 1.3. The polarity of the bias voltage will determine the path of the tunneling electron. For example, if a positive voltage is applied across the tip and the sample, electrons will tunnel from the occupied Fermi level of tip ($E_{F,tip}$) to the unoccupied levels of the sample ($E_{F,sample}$) (Figure 1.3). By changing the bias polarity, electron flow occurs in the opposite direction (from sample to tip).

In classical mechanics, an electron with energy E moving in a potential barrier $U(z)$ is forbidden to cross the barrier when $E < U(z)$. However, in quantum mechanics, electrons have a non-zero probability to cross through the barrier when $E < U(z)$. The wavefunction (ψ) of an electron in a one-dimensional tunneling junction with a rectangular potential barrier is defined by:

$$\psi(z) = \psi(0)e^{-\kappa z}, \quad 1.1$$

where

$$\kappa = \frac{\sqrt{2m(V-E)}}{\hbar}, \quad 1.2$$

z is the tip-sample separation, m is the mass of an electron, V is the barrier potential, E is the energy of the tunneling electron, and \hbar is Planck's constant. The probability

distribution of the electron is proportional to the square of the wavefunction giving a tunneling current I :

$$I(z) \propto |\psi(z)|^2 \propto e^{-2\kappa z}. \quad \mathbf{1.3}$$

For small biases, the exponential current decay is about an order of magnitude per Å change in z because the quantity $(V-E)$ can be approximated as the work function (Φ) of the metal. Because of this, the STM is very sensitive (tenths to thousandths of Ångstroms) to both lateral and vertical changes in topography [58,59].

The STM can image the surface by rastering the probe tip in one of two modes: constant-current or constant-height. In constant-current mode, a feedback loop is employed to maintain a constant tunneling current. The tip height, mounted on the piezoelectric tube, responds to changes in topography. Thus, the recorded topographic image is a convolution of the geometric structure and the local density of states (LDOS) of the tip or sample. In constant-height mode, the probe tip stays at a constant height while rastering across the surface and records the resulting current, I_t . The experiments discussed throughout this dissertation were performed in constant-current mode.

1.4 Electrochemical Scanning Tunneling Microscopy

Although originally developed for studies under vacuum and ambient environments, STM quickly found applications in *in-situ* probing of electrochemical interfaces [60]. For ECSTM, the tip generates a faradaic current that is dependent on the

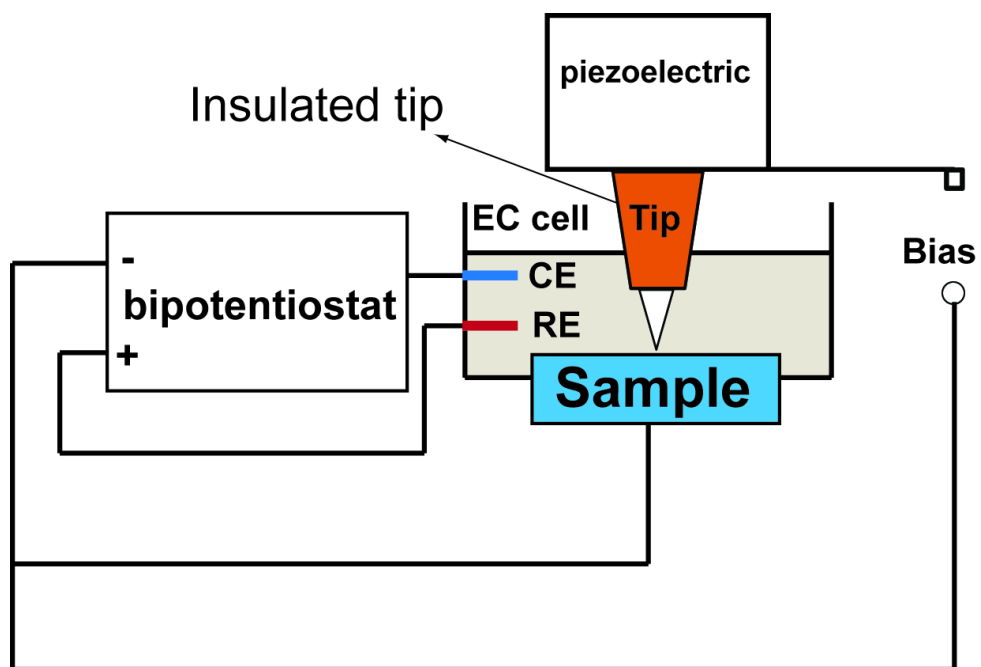


Figure 1.4: Schematic of ECSTM. A bipotentiostat is used to control electrode potential in a four-electrode setup, including CE: counter electrode, RE: reference electrode.

tip potential. The faradaic current from a bare metallic tip overwhelms the tunneling current. Therefore, it is necessary to coat the tip, except the apex, with an insulating material (Figure 1.4) [60]. Another important feature of ECSTM is that a bipotentiostat is required to control the potential of the tip and the potential of the surface independently (Figure 1.4). Therefore, the tip bias is the difference between the potentials of the tip and the surface. It turns out that if cleanliness of samples and electrolytes is maintained, ECSTM is often capable of resolution significantly better than that under ambient environments and even comparable to that achieved under ultra-high vacuum.

1.5 Dissertation Overview

The research that is described in this dissertation is primarily related to the design of molecules and their assemblies on substrates for their application in molecular electronics and molecular motors. Novel instrumentation has been employed to understand motion and structural changes in single molecules and their directed assemblies.

We have studied photo-induced isomerization of single azobenzene-functionalized molecules isolated in tailored *n*-alkanethiolate SAM matrices on Au{111} (Chapter 2). Using molecular engineering, we are able to suppress excited-state quenching from the metal substrate and form rigid assemblies of single tethered azobenzene molecules in the domains of the monolayer to limit steric constraints, as well as tip-induced and stochastic switching effects.

In Chapter 3, we prepared one-dimensional (1D) chain structures of these molecules in the domain boundaries of *n*-alkanethiol matrix. We switched the chain

structure from *trans* to *cis* using ultraviolet (UV) light and observed that the molecules in the chain isomerize in concert. Molecules in the chain couple electronically. To demonstrate the extent of the electronic coupling, we employed electron-induced isomerization of azobenzenes to demonstrate that electrons can propagate between the two ends of the chains.

To develop molecular machines, molecules that can undergo restricted motion upon external stimuli to generate useful work are necessary. For example, rotaxane molecules are a model system of artificial muscle that responds to electrochemical potential changes. In Chapter 4, redox-controllable, bistable rotaxane molecules (artificial molecular muscles) are coated on microcantilevers and subjected to alternating oxidizing and reducing electrochemical potentials to deflect the microcantilevers reversibly.

Using ECSTM, we observed electrochemically controlled station changes of individual bistable rotaxane molecules *in situ* (Chapter 5). Motions of the movable rings were correlated with redox states of one of the resting stations and displayed partial reversibility. Such insights are important for nanoelectromechanical and nanoelectronic devices based on mechanically interlocked compounds. We understand that bistable rotaxane molecules with *rigid* dumbbells should enable consistent and fully reversible motions, as well as direct visualization of the rings *and* the shafts of the molecules.

Control of lateral arrangements of molecules in two-dimensional (2D) arrays and their exposed chemical functionalities is necessary for the development of molecular-scale devices. Preciseness in the distances between double-decker (DD) molecules is a key element in building functional arrays of DD-based molecular rotors. In Chapter 6,

we demonstrate the ability to control the molecular placements in DD arrays using phthalocyanine as bottom ligands on highly ordered pyrolytic graphite (HOPG) substrates. We used the probe tip of a liquid-cell STM to manipulate single DD molecules.

The results of these projects are summarized and future prospects are discussed in Chapter 7.

Chapter 2

REVERSIBLE PHOTO-SWITCHING OF SINGLE AZOBENZENE MOLECULES IN CONTROLLED NANOSCALE ENVIRONMENTS

2.1 Introduction

In this chapter, we look at photo-induced isomerization of single azobenzene-functionalized molecules isolated in tailored alkanethiolate monolayer matrices on Au{111}. Using molecular engineering, we are able to suppress excited-state quenching from the metal substrate and to form rigid assemblies of single tethered azobenzene molecules in the domains of the monolayer to limit steric constraints, as well as tip-induced and stochastic switching effects.

A major challenge of molecular electronics is to design and to incorporate single molecules as transistors, diodes, or switches into circuits [6,61-64]. Molecular switches are typically regulated by an electric field [15,65,66], a scanning tunneling microscope (STM) tip [44,67-69], or by a chemical/electrochemical reaction [4]. These activation methods are relatively slow and may interfere with the function of nanosized circuits, which can impose limitations on device applications. However, far-field illumination or other stimuli are more feasible driving factors to power nanoscale switches [3,19,21] because of the ease of addressability, picosecond response time, and compatibility with a broad range of ambient environments, such as solvents, electrolytes, or gases. Therefore, photochromic molecules that can reversibly photo-switch between two different conductance states could serve as more practical molecular switches.

Azobenzenes, which can reversibly isomerize between *cis* and *trans* forms under photoillumination, have been studied to control their switching on metal electrodes [70-72]. Other molecules that have been studied for their photochromic switching are diarylethenes [1,73,74] and stilbenes [75]. However, evidence of photo-induced switching of single molecules on metal electrodes is often complicated by surface quenching [71,74], steric hindrance, and non-photo-induced switching [44,46,68-72,74,76,77]. In most single-molecule switching studies, active molecules have been attached at domain boundaries and vacancy islands of host alkanethiolate matrices. Since molecules attached at domain boundaries and vacancy islands are loosely packed and less stable, they are influenced by fluctuations [44,46,69] and therefore switch randomly due to non-photo-induced effects.

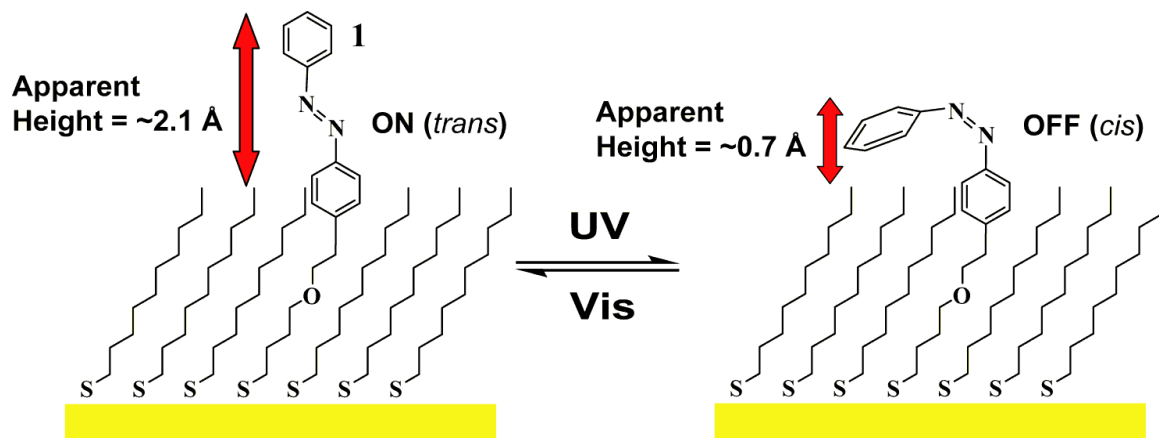
The development of a practical molecular-scale optoelectronic device will also require control over switching in ambient conditions (atmospheric pressure and room temperature). However, such control over reversible switching has neither been achieved in ambient [70,72,74] nor under ultrahigh vacuum or cryogenic temperatures [71,78]. Here, we report reversible photo-switching of azobenzene-functionalized single molecules (**1**) when assembled on Au{111}. Control was achieved in ambient conditions by appropriately designing the tether and tuning the rigid assembly of the molecule to limit surface quenching and non-photo-induced switching effects.

Surface quenching is dependent upon photo-induced electron transfer from an excited state of a photochromic molecule to the gold substrate [79]. If electronic coupling between the molecule and the substrate is strong, the excited state is quenched and isomerization does not occur. To overcome this problem, Comstock *et al.* attached

tert-butyl legs to an azobenzene moiety to reduce coupling [71]. These molecules were irradiated for long periods (~3 hr) at cryogenic and ultrahigh vacuum conditions and yet only partial isomerization and one reversible switching event were observed. Furthermore, the events were convoluted by stochastic or tip-induced switching.

Steric constraints of tightly packed matrices can restrict conformational changes, thus hindering isomerization in azobenzenes. Pace *et al.* used a self-assembled azobenzene monolayer and irradiated the surface with UV light to observe photoisomerization [72]. Based on changes in contrast in the images, they concluded that there must have been photoisomerization of the monolayer. They did *not* observe any changes in packing density, suggesting high steric hindrance that would restrict the conformational changes expected in the molecule upon isomerization. We note that such contrast changes in STM images are also commonly produced by tip-induced effects [80,81].

We designed an azobenzene-functionalized molecule, 4-[2-(4-phenylazo-phenyl)-ethoxy]-butane-1-thiol (**1**, shown as the thiolate), to chemisorb *within* domains of 1-decanethiolate (**C10**) self-assembled monolayers (Scheme **2.1**) [82]. Rigid assembly of **1** surrounded by **C10** molecules minimizes conformational changes at and near the gold-sulfur bond (as opposed to the case of molecules adsorbed at defects such as domain boundaries). The molecular design renders stability due to favorable intermolecular interactions with the monolayer and reduces steric constraints and electronic coupling between the excited state orbitals of the molecule and the Au substrate. The molecular tethering scheme allows the azobenzene moiety to protrude from the **C10** matrix



Scheme 2.1: Isolated azobenzene-functionalized single molecules (**1**) embedded in 1-decanethiolate (C10) SAM on Au{111}. Photo-induced changes in apparent height of the azobenzene-functionalized molecules in STM images are due to isomerization of the azobenzene moiety between *trans* and *cis*, and are defined as ON (apparent height = 2.1 ± 0.3 Å) and OFF (apparent height = 0.7 ± 0.2 Å) states, respectively, under typical scanning condition of $V_s = -1$ V and $I_t = 2$ pA.

(Scheme 2.1), minimizing electronic coupling and steric hindrance. Previously, it was shown that electronic coupling can be reduced by increasing the length, replacing a methylene in the backbone with an ether linkage [83], and reducing the π -conjugation of the tether [43,82]. Hence, by minimizing steric hindrance, surface quenching, and non-photoinduced switching effects, isolated molecules of **1** attached to Au{111} could be controlled and reversibly switched between ON and OFF states by irradiation under ambient conditions (*vide infra*). We correlated these states with *trans* and *cis* isomers of the azobenzene, respectively.

2.2 Experimental Procedure

2.2.1 Sample Preparation

Single molecules were prepared on Au{111} by including them in the domains of the **C10** monolayer through co-assembly (Figure 2.1). An ethanolic mixture of **1** and **C10** were co-adsorbed with a total thiol concentration of 1 mM and a molar ratio of 1:4, respectively, for 24 hr under a nitrogen atmosphere. The sample was then annealed in **C10** vapor (for 2 hr at 80 °C) to add matrix molecules to increase the packing of the matrix [84].

2.2.2 Scanning Tunneling Microscopy

Please refer to Chapter 1 for a description of STM operation. Here, the azobenzene-functionalized molecule (**1**), were analyzed using a custom-built scanning

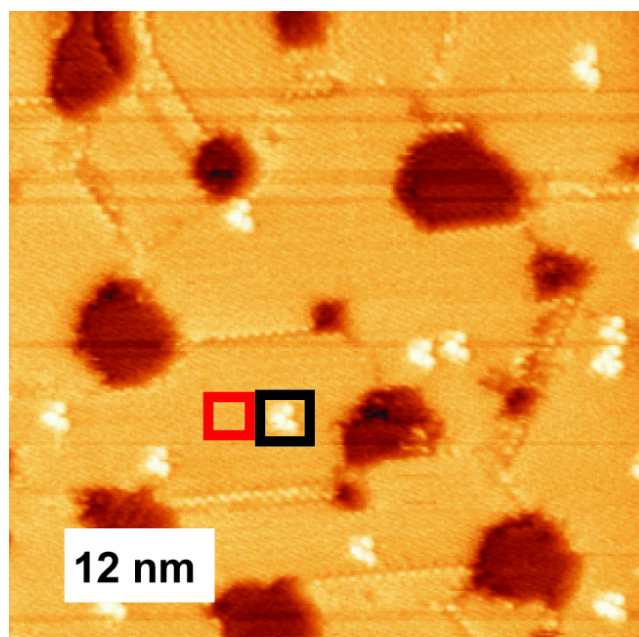


Figure 2.1: Scanning tunneling microscopy image of isolated azobenzene-functionalized single molecules (**1**, white protrusions) embedded in a **C10** SAM films on Au{111}. For each molecule, extracted (black box) and background (red box) regions are automatically selected for each frame. The background corresponds to the SAM apparent height near the extracted molecule. Apparent height of **1** is measured to be $2.1 \pm 0.3 \text{ \AA}$ imaged under scanning condition of $V_s = -1 \text{ V}$ and $I_t = 2 \text{ pA}$.

tunneling microscope, mounted with an optical fiber, operating under ambient conditions [82]. Successive STM images were acquired over the same area for several (up to 4) hours to determine the behavior of the molecules co-adsorbed with host matrices. Many high-resolution time-lapse series of images have been recorded. An optical fiber (5 mm diameter) is attached in the STM set-up to illuminate the sample *in situ*. UV and visible light emitting diodes with peak emission wavelengths of 365 nm and 440 nm, respectively, were used as the light source. Light intensities at the outlet of the optical fiber for sample illumination were $\sim 12 \text{ mW/cm}^2$ and $\sim 6 \text{ mW/cm}^2$ for UV and visible light, respectively.

2.2.3 Apparent Height Determination

Drift from thermal fluctuations and creep, due to the piezoelectric translators, can change the area imaged, so a tracking algorithm was used to correct for drift during acquisition and for post-acquisition analyses [45]. Several azobenzene-functionalized molecules were present in the STM image within domains of the matrix. Figure 2.1 shows a $50 \times 50 \text{ nm}^2$ each area with a single molecule highlighted (black box) to illustrate our data extraction procedure. A second box (adjacent, red box) was extracted, proximate to the molecule of interest, to maintain a consistent background. The median of the top five pixel values for each extracted frame of the inserted molecule determined the raw imaged height of the inserted molecule. The smaller extracted SAM background area was selected to contain neither substrate vacancies nor step edge sites. The mean value of this extracted area was used as the background. The difference between the raw extracted height of the molecule and the background yielded the apparent height, thereby

reducing background variations in the apparent height due to the local environment of the inserted molecule. Theoretical physical height of the molecule was calculated using Spartan (Spartan, Wavefunction Inc, CA) for windows.

2.3 Results and Discussion

The density of single molecules within the domains was consistent throughout the sample and these were imaged as 2.1 ± 0.3 Å apparent *protrusions* from the **C10** matrix, defined as the ON state (for tunneling conditions of 1 V sample bias, and 2 pA tunneling current). When imaged continuously for an hour without illumination, no switching events were observed (Figure 2.2). We then scanned the same sample with a range of bias polarities (1.0 V to -1.0 V) (Figure 2.2), and again, no switching events were observed. Thus, the designed tether and the new assembly limit the molecules' ability to switch stochastically or by tip-induced effects, in contrast to what we previously observed for oligo(phenylene-ethynylene) molecules when allowed conformational freedom at domain boundaries and other defects [44,46,68,69,76,77].

Isolated molecules within domains were exposed to UV light (~365 nm) and imaged with STM at increasing UV illumination times. The molecules switched to the OFF state, characterized by an apparent height reduction of ~1.4 Å (Figure 2.3). We observed that an increasing number of molecules switched off with longer UV illumination times. The OFF state of **1** appeared to protrude 0.7 ± 0.2 Å above the **C10** matrix in STM images at these tunneling conditions (1 V sample bias, 2 pA tunneling current). Figures 2.3B-2.3E show the molecules switching from the ON

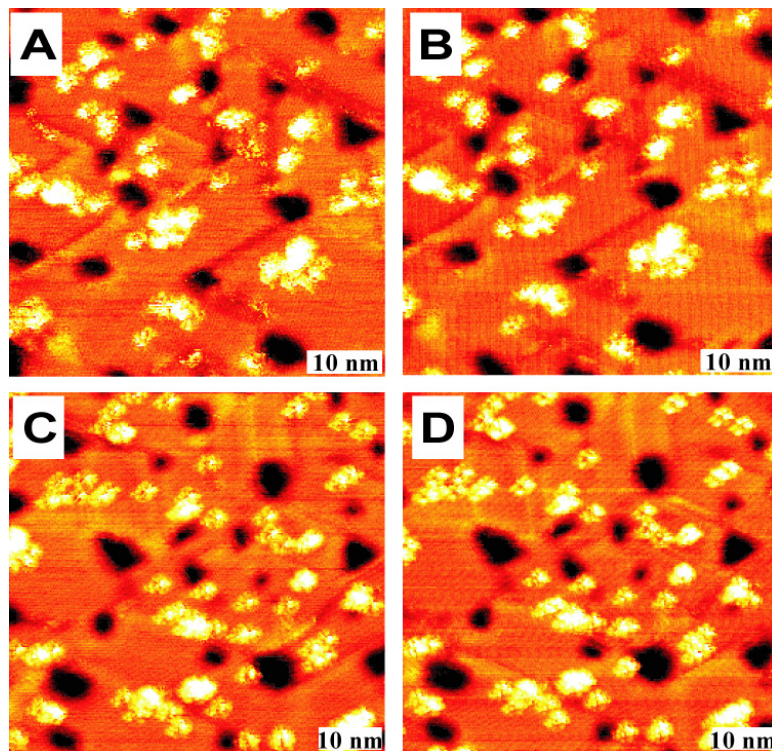


Figure 2.2: With time (1 hr), but no illumination, no change in apparent height was observed in scanning tunneling microscope images (Figure 2.2A & 2.2B) ($I_t = 2$ pA; $V_s = 1.0$ V). With sample bias polarity (V_s) change (but still no illumination), (2.2C) 1.0 V to (2.2D) -1.0 V, no significant change in apparent height was observed ($I_t = 2$ pA) in the scanning tunneling microscope images.

state to the OFF state after 10, 35, 60 and 160 min, respectively, of UV exposure. The number of molecules that switched as a function of exposure time shows an exponential time dependence with a decay constant of 54 ± 15 min (Figure 2.4) under these conditions (~ 12 mW/cm²). The error bars are determined by the standard deviations of the observed numbers of molecules in three sets of observations. The slower decay constant as compared to that in solution is likely due to the electronic coupling of the azobenzene moiety with the Au substrate, which is reduced by the inclusion of the tether, but still appears to be significant in deactivating isomerization.

Previously, in an ensemble measurement, Weisner *et al.* [85] demonstrated an exponential dependence of azobenzene photoisomerization on illumination time. The exponential time dependence and elimination of other potential switching effects indicate that photoexcitation causes switching due to photoisomerization. All the protrusions in the images (Figure 2.3A-2.3F) represent molecules of **1**, and are found only when **1** is co-assembled with the matrix. The similarities of the shapes and sizes of the protrusions in each image suggest that each protrusion corresponds to a single molecule; the shape and size of each is a map of the STM tip and some of the contrast changes in different images are due to STM tip changes during imaging [63].

Theoretical calculations predict the *trans* isomer of azobenzene to be $\sim 100\times$ more conductive than the *cis* isomer [86]. When **1** isomerized from *trans* to *cis* on Au{111} (as shown in Scheme 2.1), the actual height, in contrast to apparent height, decreases by ~ 4 Å due to conformational changes about the N-N double bond. Hence, both

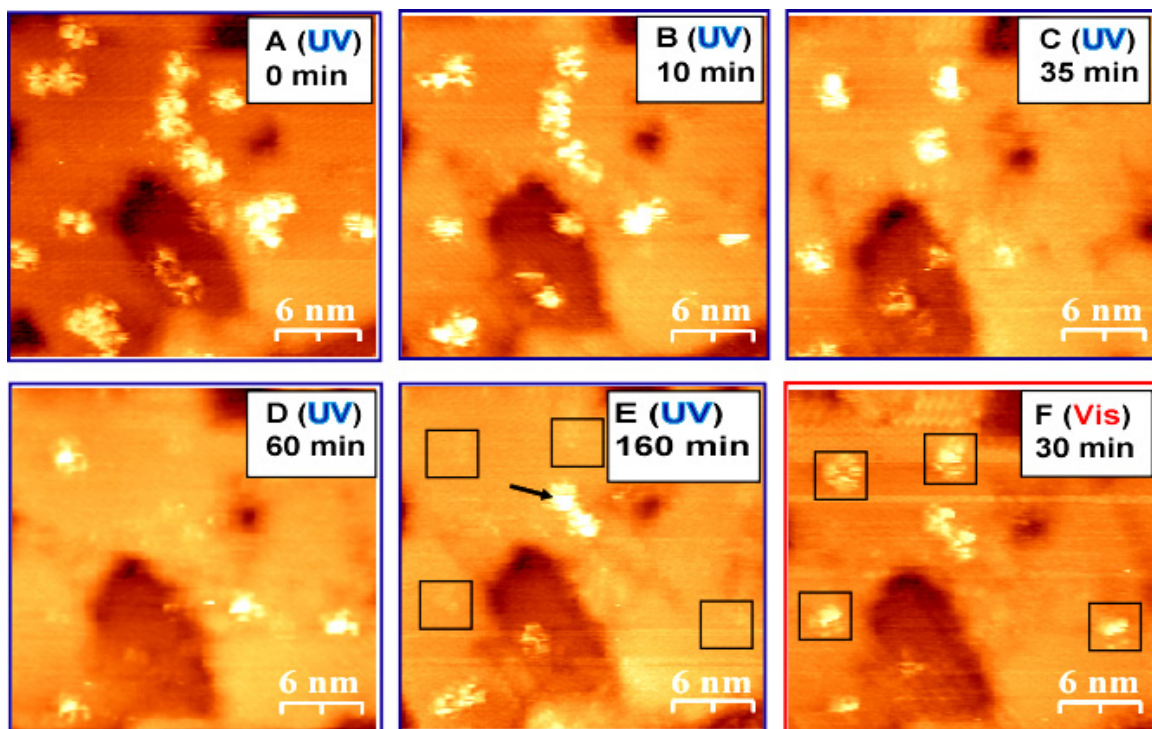


Figure 2.3: Azobenzene-functionalized molecules switch OFF and switch ON upon irradiation with UV (~ 365 nm) and visible (~ 450 nm) light, respectively. Images are recorded after irradiating (A) 0 min, (B) 10 min, (C) 35 min, (D) 60 min and (E) 160 min with ultraviolet light and visible light irradiation for (F) 30 min. Figures 2.3A-2.3E show switching OFF of single molecules with continued UV illumination. The squares in 2.3E and 2.3F show switching ON of molecules with visible illumination. The arrow in Figure 2.3E shows switching ON of a molecule with UV illumination. Scanning tunneling microscope images are recorded at $V_s = 1$ V and $I_t = 2$ pA. Contrast changes in the images are due to STM tip changes during imaging.

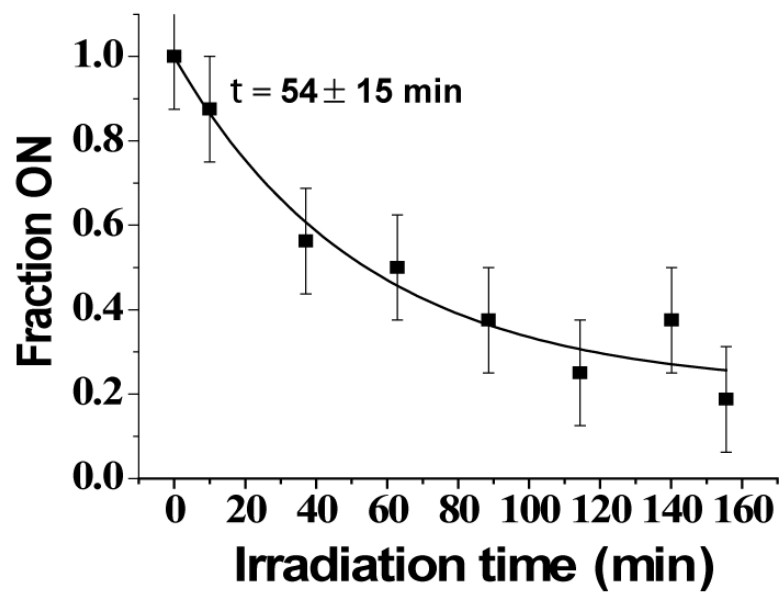


Figure 2.4: Fraction of azobenzene-functionalized molecules in the ON state decreases as a function of time after UV irradiation ($\sim 12 \text{ mW/cm}^2$). The decay constant (τ) under these conditions is $54 \pm 15 \text{ min}$.

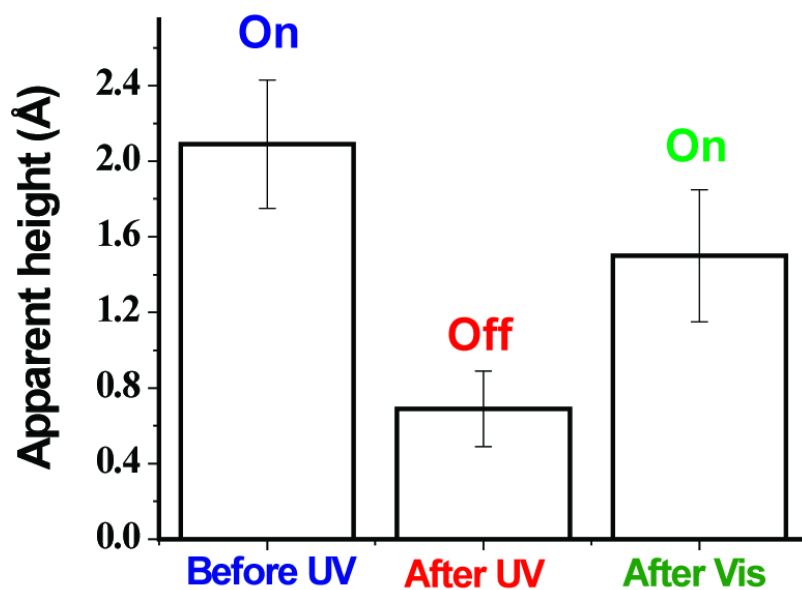


Figure 2.5: Height profile of azobenzene functionalized molecules changes from I ($\sim 2.1 \pm 0.3 \text{ \AA}$) to II ($\sim 0.7 \pm 0.2 \text{ \AA}$) with UV light irradiation (switch OFF). With visible light exposure, the height profile changes from II ($\sim 0.7 \pm 0.2 \text{ \AA}$) to III ($\sim 1.6 \pm 0.3 \text{ \AA}$) (switch ON).

conductivity and height contribute to the observed reduction in apparent height (ON to OFF, *trans* to *cis*), since STM images are a convolution of physical height and electronic structure.

After 160 min of UV illumination, more than 90% of the azobenzene-functionalized molecules isomerized from *trans* to *cis*. Subsequent illumination with visible light (~ 450 nm, ~ 6 mW/cm²) for 30 min switched nearly 50% of **1** back to the ON state (Figure 2.3F). The squares in Figure 1E and 1F highlight a few switching ON events.

In the gas and solution phases [87,88], visible light is known to photoisomerize azobenzene from *cis* to *trans*; hence, we conclude that the azobenzene-functionalized molecules have been reversibly photo-switched at the single-molecule level. The reversibility of photo-switching was further established by comparing the apparent height profiles of molecules [44] on the sample before and after exposure with UV and visible light. Nearly ~ 150 molecules were sampled before and after UV irradiation (to switch to the OFF state), and after visible illumination (to switch to the ON state) and the apparent heights were plotted (Figure 2.5). Drift arising from thermal fluctuations induced by light and creep in the STM piezoelectric imaging mechanism makes it difficult to observe a single feature for very long times (greater than 5 hr). Several STM image frames of a scan area 80×80 nm² with ~ 30 -40 azobenzene-functionalized molecules in each were used to collect apparent height changes. The apparent heights before UV, after UV, and after visible illumination are 2.1 ± 0.3 Å, 0.7 ± 0.2 Å, and 1.6 ± 0.3 Å, respectively. After visible illumination, the sample includes *both* ON and OFF molecules, thus giving a lower apparent height distribution compared to the initial ON state.

Figure **2.3E** (arrow) shows a molecule in the ON state, which was OFF in Figure **2.3D** even after UV illumination. The absorption band of *cis* molecules overlaps with UV light and thus, irradiation with UV for sufficiently long times (1-2 hr) occasionally triggers isomerization from *cis* to *trans* [87]. Figure **2.3F** (squares) shows reversible switching to ON ~50% of the total OFF molecules after visible illumination for 30 min. Thermal *cis-trans* isomerization of azobenzene has been reported to take place on timescales of 10-30 hr [89] but we observed some switching in 30 min (Figures **2.3E** & **2.3F**). The visible light, with an intensity ($\sim 6 \text{ mW/cm}^2$) lower than that of typical ambient light, is too weak to induce significant heating that could thermally isomerize the azobenzene moiety. Thus, based on our observations of fast response of switching compared to thermal isomerization and kinetic studies by Liu *et al.* [89], isomerization of *cis* to *trans* here is photo-induced rather than from thermal relaxation.

2.4 Conclusions and Future Directions

We showed that the molecular tether and assembly isolated the azobenzene moiety from the metal substrate and the rigid assembly of **1** within the domains of the host matrix rendered stability, due to which control over reversible photo-switching was achieved. The rigid assembly can potentially be utilized in stabilizing single molecules for other switching studies in which the matrix plays a key or interfering role. With stability in ambient conditions and an improved understanding of photo-switches, assembly of practical molecular devices may become possible. In order to test these ideas, we are now studying assemblies of these photoswitches.

The conductivity of the tether played a crucial role in electronically decoupling the azobenzene moiety from the Au substrate. However, the degree of electronic coupling needs to be understood in detail. To this end, we are working on different tethers with varying conductivities and studying the efficiency of photo-isomerization of the azobenzene moiety.

Chapter 3

SELF-ASSEMBLED ONE-DIMENSIONAL MOLECULAR CHAINS OF AZOBENZENE: CONCERTED SWITCHING AND ELECTRON TRANSPORT

3.1 Introduction

In Chapter 2, we demonstrated that azobenzene-functionalized molecules can be attached to a Au{111} substrate as isolated single units. We also demonstrated that the molecules can switch between *trans* and *cis* isomers using UV and visible light, respectively. In this chapter, we prepare 1D chain structures of these molecules in the domain boundaries of decanethiolate SAM matrices. We switch the chain structures from *trans* to *cis* using UV light and observe that the molecules in the chain isomerize in concert. This concerted switching is attributed to the electronic coupling between the molecules within the chains. To demonstrate the extent of the electronic coupling we employed a STM probe tip for electron-induced isomerization of azobenzenes. We observe that electrons can travel between the two ends of the chains.

Control over creation and electronic properties of molecular 1D structures on surfaces is one of the most challenging quests in the development of molecular and organic devices [1,6,61,90,91]. Self-assembly—the autonomous process utilizing non-covalent interactions, such as hydrogen bonds, van der waals interactions, and π - π interactions to organize molecules—is a promising technology for the production of such 1D, 2D, and 3D structures [92-95]. Resulting from proximity of molecules in 1D assemblies and depending on the coupling, the energy levels of molecules might be expected to delocalize, leading to an increased mobility of electrons inside the 1D

structures. So far, only theoretical studies have been able to demonstrate such delocalization of electrons and have predicted that lateral conductance through 1D systems can be substantial [96-101]. Experimental efforts have been hindered by the difficulty in establishing electrodes at the ends of the 1D chains. Electronic band dispersion due to electron delocalization in organic monolayers have nevertheless been studied using STM [99,102,103]. If electron delocalization is appreciable in a 1D chain of molecules, the effect of any electronic perturbation, such as driven conductivity changes in a molecule, should also be observed throughout the chain. To date, no such system has been studied. Understanding the propagation of effects can be instrumental for greater insights into electron-transport mechanisms; much needed to advance the fields of molecular and organic electronics.

We created 1D molecular chains of azobenzene-functionalized molecules (**1**) using self-assembly on Au{111}. The azobenzene-functionalized molecule **1** has previously been shown to switch from *trans* to *cis* conformation upon stimulation with UV light [20]; here, we switched 1D chains composed of molecule **1** with UV light and observed that the molecules in each chain isomerized in concert. Since electrons can also isomerize azobenzenes [66,104,105], we explored the concerted isomerization of the molecules in 1D chains by employing electron-induced isomerization of the chains. We utilized an ambient STM probe tip for electrons to induce the isomerization at one end of the chains and observed the isomerization of the entire >100 Å long chains. Since STM tunneling is a localized event, it is not directly responsible for the switching of the whole chain. However, the tunneling electrons, entering the chain at one end, apparently travel along the 1D structure and induce isomerization of all the molecules in the chain. We

hypothesize that π -orbital overlap of the molecules in the 1D structures results in delocalization along the chain, as in a conductor.

3.2 Experimental Procedure

3.2.1 Sample Preparation

One-dimensional chain structures were prepared on Au{111} by assembling azobenzene-functionalized molecules between the domains of a **C10** monolayer. We used insertion techniques (described in Chapter 1) along with heat treatment to prepare the chains. The process involved three key steps. In step A, **C10** molecules were adsorbed on the Au{111} substrate by immersing a flame-annealed Au{111}/mica surface in an ethanolic solution of **C10** (1 mM) for 1 min. This led to the formation of a SAM with a large number of defects and disordered areas (Figure 3.1A). In step B, the sample was immersed in an ethanolic solution containing molecule **1** (0.2 mM) for ~4 min. During this process, molecule **1** inserts into the vacant and disordered areas of the loosely packed **C10** matrix (Figure 3.1B). Subsequently, in step C, the sample was annealed in **C10** vapor (for 2 hr at 80 °C) to increase the degree of order in the matrix domains by the addition of **C10** molecules [84]. During this packing, the **C10** domains grow and push the azobenzene-functionalized molecules to domain boundaries where they form 1D structures (Figure 3.1C). After this procedure, no or few (0-10 per $500 \times 500 \text{ \AA}^2$) single molecules were present in the area of the sample probed. During the vapor-annealing process, the intermolecular interactions between the inserted molecules is critical for the molecules to remain attached to the surface.

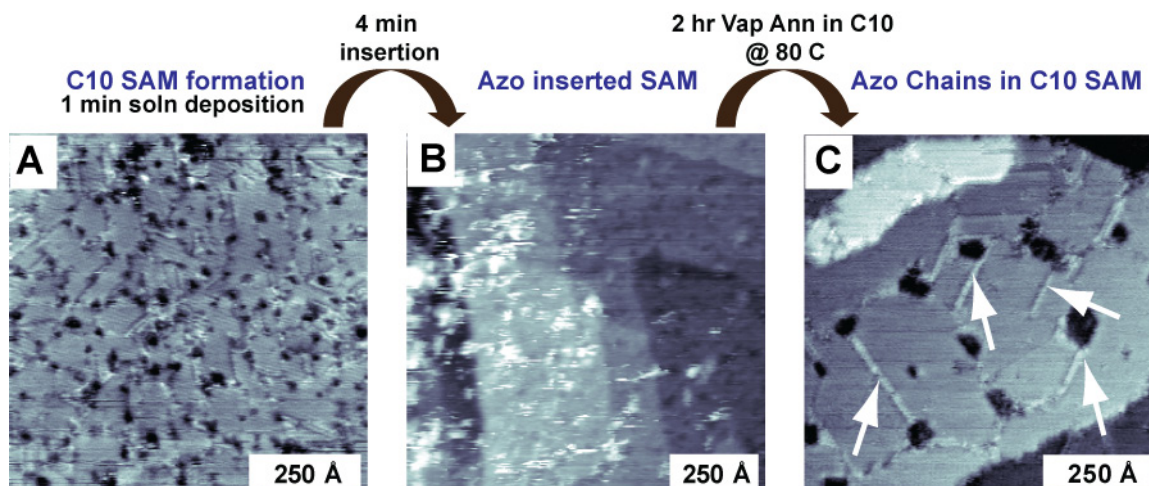


Figure 3.1: (A) Formation of C10 SAMs with deposition in solution for 1 min leads to large numbers of defects. (B) Azobenzene-functionalized **1** molecules are inserted into the defect sites of loosely packed C10 SAM by immersing the preformed C10 SAM in solutions of molecule **1** for 4 min. (C) Vapor annealing of sample in C10 vapor adds matrix molecules to increase the sizes of domains of the matrix. During this packing, the C10 domains grow and push the molecules in the domain boundaries where they form 1D structures (white arrows). All STM images are recorded at $V_s = 1$ V and $I_t = 1$ pA.

3.2.2 Scanning Tunneling Microscopy

Refer to Chapter 1 and 2 for a detailed description of STM operation. Here, the chain structures of molecule 1 were analyzed and manipulated using a custom-built STM, with an attached optical fiber, operating under ambient conditions [82]. Chain structures were switched from *trans* to *cis* conformations using 2.0 eV electrons tunneling from the STM probe tip to the sample [66,104]. A 2.0 V sample bias was maintained across the tunnel junction for 0-5 min with a current of 1 pA. After switching from the *trans* to *cis* conformation, the sample was left unperturbed for 30-120 min in order for the molecules to relax thermally back to the *trans* state.

3.2.2 Estimation of Electric Field in the Tunneling Junction

During imaging, the STM tip rasters over the SAM. Molecule 1, when attached to the Au substrate, protrudes ~ 21 Å from the substrate (molecular heights were calculated using Spartan for Windows, Wavefunction Inc, CA). Hence, during imaging of molecule 1 on Au{111}, the STM tip is at least 21 Å from the substrate. Considering a simple case of a parallel plate capacitor with homogeneous electric field separated by 21 Å with a potential difference of 2.0 V, the electric field (potential/distance) between the plates is estimated to be 0.09 V/Å. Under manipulation conditions, the sample bias was increased to 2.0 V, which moves the STM tip away from the substrate to maintain 1 pA tunneling current. Hence, the electric field during manipulation can be estimated to be less than 0.09 V/Å.

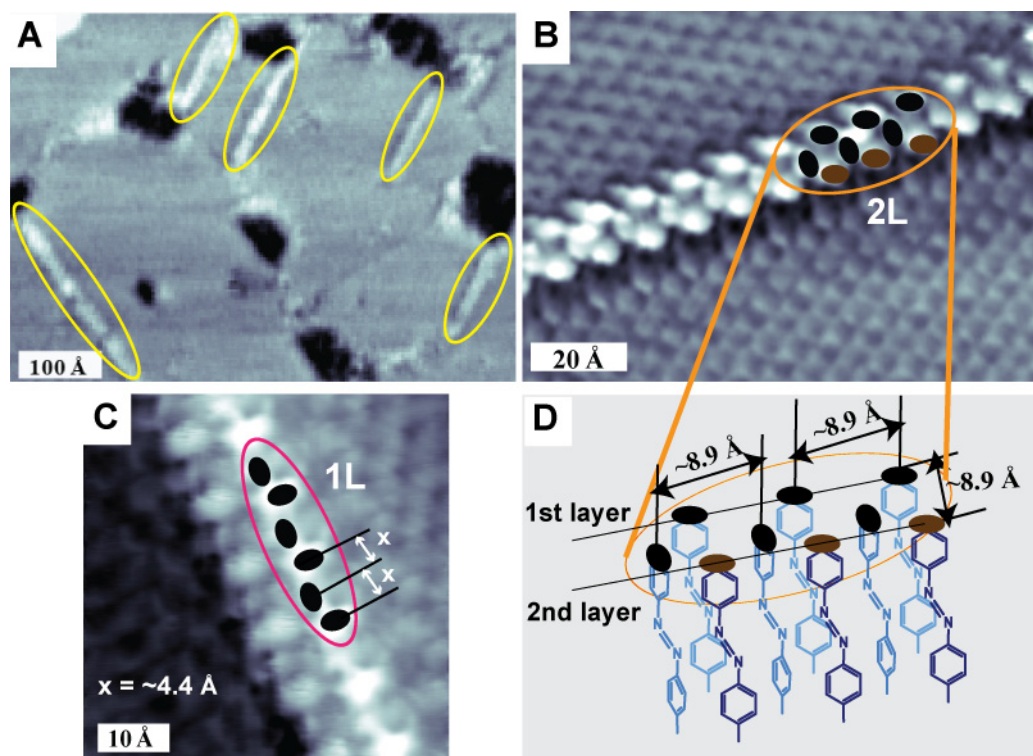


Figure 3.2: (A) A representative STM image with chains of molecule **1** (yellow ovals) assembled at domain boundaries of a **C10** SAM. (B) A STM image of a **2L** chain at a domain boundary. The overlay of the black ovals represent the phenyl ring arrangements in the herringbone structure. (C) A STM image of a **1L** chain. Again black ovals are shown to highlight the phenyl rings of the azobenzene moiety. (D) A schematic of the molecular arrangement in the **2L** chain shows that it has two layers of molecules. Each pair of parallel molecules are separated by $8.9 \pm 0.4 \text{ \AA}$. All STM images are recorded at $V_s = 1 \text{ V}$ and $I_t = 1 \text{ pA}$.

3.3 Results and Discussion

3.3.1 Chain Structure

Molecules assemble into herringbone arrangements to form the chain structures. Chains were typically formed with two types of structures, namely: one-layer (**1L**) and two-layer (**2L**) chains (Figure 3.2). STM images in Figure 3.2 show the molecular arrangements in the chains. Similar herringbone structures have been observed previously in various azobenzene-based SAMs on Au{111} [106,107]. The **1L** chain has an arrangement where adjacent molecules with phenyl rings have lateral separations of ~ 4.4 Å oriented at $\sim 90^\circ$ to each other (Figure 3.2C and 3.2D, black ovals). Alternate molecules are oriented parallel to each other with a spacing of 8.9 ± 0.4 Å. The **2L** chain has an additional layer of molecules, second layer, as compared to **1L** chains (Figure 3.2B and 3.2D, brown ovals). Each pair of parallel molecules are separated by 8.9 ± 0.4 Å (Figure 3.2D). Both types of chains are equally abundant on the sample ($5-8$ per 1000×1000 Å²) and the length of the chains, typically, varied between 30-200 Å. The apparent heights of the chains above the matrix under these conditions are ~ 2 Å, consistent with our previous experiments on single azobenzene-functionalized molecules, discussed in Chapter 2 [20].

3.3.2 Light-Induced Switching of Chains

Azobenzenes can be switched between two stable isomers (*trans* and *cis*) with light [70-72,78], electrons [66,104], or electric field [65], when attached to a Au{111} substrate. In Chapter 2, we assembled single isolated molecules of **1** on Au{111} and

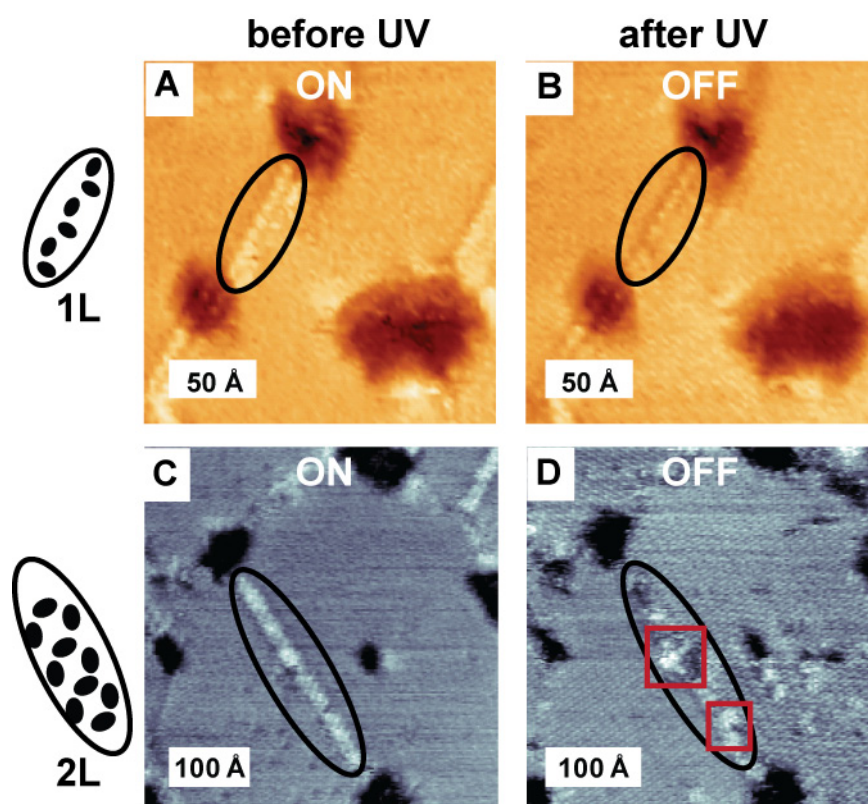


Figure 3.3: Photo-induced switching of chains is shown in the STM images. Both **1L** and **2L** chains switched OFF upon UV light exposure for ~ 30 min at ~ 12 mW/cm². (**A** and **B**) All molecules in the **1L** chain switched OFF completely. (**C** and **D**) Parts of the **2L** chain did not switch OFF (red squares). Due to steric hinderance in the **2L** chains, the molecules in the red box area do not have free space around them to switch to the *cis* form. All STM images were recorded at $V_s = 1$ V and $I_t = 1$ pA.

demonstrated their photo-induced isomerization. Here, we prepared 1D assemblies of molecule **1** in domain boundaries of **C10** matrix. Figure **3.3** shows STM images of **1L** and **2L** chains switching OFF upon exposing to UV light for 30 min at ~ 12 mW/cm².

We compared the switched OFF states of the **1L** and **2L** chains, shown in Figure **3.3C** and **3.3D**, respectively. We observed that the **1L** chain switched OFF completely (i.e., all molecules switched OFF), however, some parts of the **2L** chain did not switch OFF (Figure **3.3D**, red squares). We attribute this difference to one extra layer of molecules in the **2L** chains compared to the **1L** chains. Due to this extra layer, the molecules in the **2L** chains are apparently sterically hindered and do not have sufficient free space around them to switch to the *cis* form. Steric hindrance is affecting only a few parts of the chain, possibly, because of the growth mechanism of these chains. Molecules self-assemble to form the most energetically stable structures. During this process, some part of the chain may orient differently than others.

The photo-induced switching of the molecules in the chains is markedly different from the switching of single molecules discussed in Chapter 2. The individual molecules (Figure **2.3** and discussion in Chapter 2) switched OFF independently with UV illumination. However, the molecules in the chains either switched OFF completely (in **1L**) or switched in bundles (in **2L**). Concerted switching indicates that the molecules arranged in the chains are coupled. To explore the nature of this coupling we employed electron-induced switching of azobenzene molecules (*vide infra*).

3.3.3 Electron-Induced Switching of the 1L Chains

To understand the intermolecular electronic coupling in the 1D chains of molecule **1** on Au{111}, we induced isomerization, selectively, at one end of the assembly and looked for the effects of this isomerization on other parts of the chain. During isomerization from *trans* to *cis* (or vice versa), azobenzenes require energy from an external source and cross through an excited electronic or transient ionic state to switch between the two isomers [14]. Here, we employed STM tunneling electrons (2.0 eV) to isomerize the azobenzene moieties in molecule **1**, arranged in 1D on Au{111}. We positioned the STM probe tip at one point above a **1L** chain (black arrow in Figure 3.4A) and applied a sample bias of 2.0 V. The STM was operating in constant-current mode with tunneling current of 1.0 pA and all images were recorded at $V_s = 1.0$ V and $I_t = 1$ pA. With the STM probe tip placed above the **1L** chain, we increased the sample bias from 1.0 V (imaging condition) to 2.0 V (manipulation condition) and maintained the bias for 2 min. The STM topographs recorded before and after excitation are shown in Figure 3.4. We observed that all parts of the **1L** chains switched OFF (i.e., isomerized from *trans* to *cis*) (Figure 3.4B and 3.4D).

Tunneling electrons were supplied only at one end of each chain; however, we observed switching of the entire (in this example ~ 90 Å long) **1L** chain. Since, tunneling is a localized phenomenon [108], we expect that tunneling at one end of the chain would not *directly* affect isomerization of the other end. During isomerization, the electrons, supplied to the molecules at one end, delocalized along the chain to induce isomerization in all molecules of the **1L** chain. This indicates that the molecules within the chain are

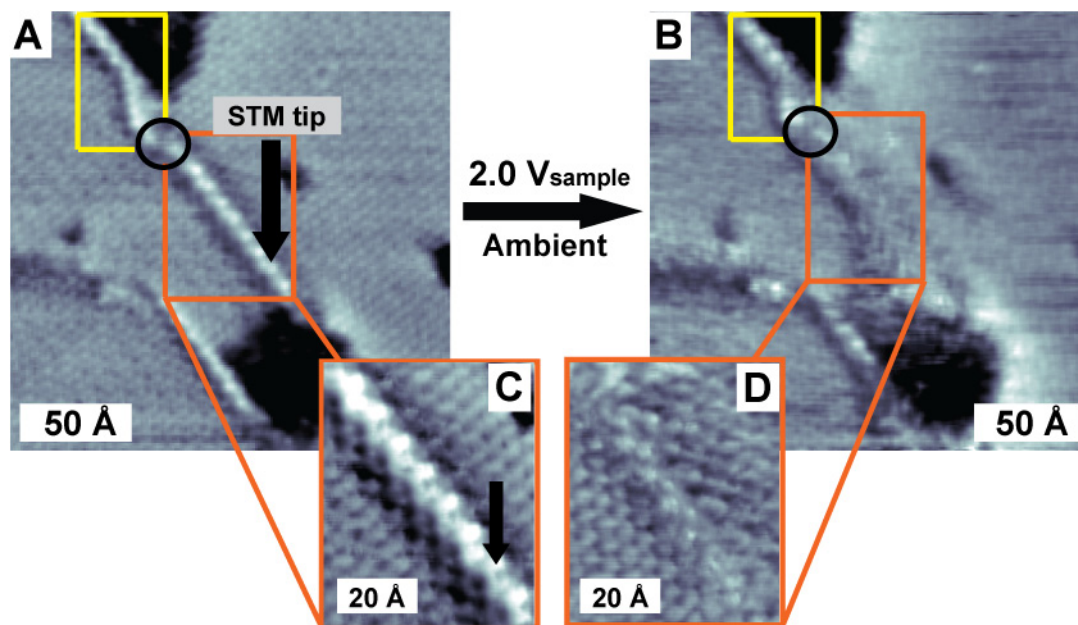


Figure 3.4: 1L chain switched OFF by 2.0 eV electrons supplied by the STM tip. A and C show the position of the STM tip (black arrow) positioned above the 1L chain. All parts of the 1L chain switched OFF completely by applying a sample bias of 2.0 V for 2 min. However, a second 1L chain (yellow boxes) above the manipulated 1L chain (orange box) did *not* switch OFF due to the lack of sufficient coupling (black circle) between these two chains. All STM images are recorded at $V_s = 1$ V and $I_t = 1$ pA.

sufficiently coupled through their π -orbital overlap for excitation across the chain. To understand this phenomenon in greater detail, theoretical calculations are being performed by our collaborator, Prof. Vincent Crespi at Penn State.

Further experimental evidence for delocalization of electrons in the **1L** chain can be observed in Figure **3.4A** and **3.4B**. The **1L** chain excited under manipulation completely isomerized, however, a proximate **1L** chain (yellow box) located above the manipulated chain did not switch OFF. This second **1L** chain is not physically connected to the first (Figure **3.5**, black circle) and electrons did not couple sufficiently to the second chain.

The possibility of conformational changes in one molecule inducing isomerization in the neighbouring molecule in the chain, like a domino or cascade effect [109], can be excluded because isomerization of azobenzene is an energy activated (1.8-3.5 eV) process [87,110]. An endothermic change in conformation of one molecule (~ 0.7 eV) [110] cannot provide sufficient energy to activate the isomerization of a neighbouring molecule.

3.3.4 Electric Field Effects on Switching

Azobenzene-functionalized molecules are also known to switch between *trans* and *cis* isomers with electric fields [65]. Alemani *et al.* reported switching of azobenzenes with conditions from $V_s = 1.5$ V and tip-sample distances (z) of 4 Å to $V_s = 6.5$ V and $z = 36$ Å. At this extreme condition of $V_s = 6.5$ V and $z = 36$ Å, where no tunneling current is flowing, switching of azobenzenes was still observed. Thus, electric fields, equal or higher to 0.18 V/Å, applied across the STM tunneling junction are needed

to switch azobenzene-functionalized molecules. They also observed that the applied field induced switching in areas of $500 \times 500 \text{ \AA}^2$ under the tip. In our experiments, the electric fields in the STM junction during the manipulation period were less than 0.09 V/\AA and the tunneling electrons were not affecting the disconnected chain located 90 \AA away from the manipulating STM tip location. Salfrank and coworkers have reported that an electric field greater than 1.5 V/\AA is needed to switch azobenzene molecules [110]. Hence, the possibility of the electric fields in the tunneling junction inducing the switching of the chains can be ruled out here.

3.3.5 Possible Routes for Electrons in Chain during Manipulation

Electrons with 2 eV energy were continuously tunneling through the molecules during manipulation. Once electrons are supplied to an azobenzene molecule, they can either tunnel to the substrate or delocalize to the other electronically coupled molecules within the chain. As electrons are delocalized along the chain, they can tunnel to the substrate from any of the positions on the chain. The electrons may also lose energy by inducing isomerization of the azobenzenes from the *trans* to the *cis* form. At any given time, all three phenomena: tunneling to the substrate, delocalization within the chain, and isomerization of azobenzenes, may occur during manipulation. The process occurring at the shortest time-scale should dominate. Since the entire chain was typically switched OFF, we believe that the delocalization of electrons occurs at the fastest time scale and hence, the electrons were able to populate the orbitals of azobenzene moieties in the chain before they tunneled to the substrate or isomerized the azobenzenes. To understand our observations, theoretical calculations are being performed to estimate the time scales

at which these three phenomena of tunneling, delocalization, and isomerization take place during the switching of the molecules in the chain.

3.3.6 Switching of the 2L Chains and Reversibility of Switching

Similar to **1L** chains, 2.0 eV electrons supplied at one end of the **2L** chains switched OFF all or most parts of the **2L** chains. Figure **3.5A** and **3.5B** shows that a **2L** chain switched OFF with a sample bias of 2.0 V applied for 5 min. Again, the electrons supplied at one end of the chain propagate along the chain to the other end and continuously populate the orbitals of all the molecules, resulting in their isomerization. The **2L** chain shown in Figure **3.5A** is ~ 130 Å long and was switched OFF, unlike the second **1L** chain (yellow box in Figure **3.4A**), located ~ 90 Å away from the STM probe tip, which remained unswitched during manipulation. In the **2L** chain, shown in Figure **3.5**, the molecules, separated as far away as ~ 110 Å from the molecules under the probe tip, are electronically coupled and isomerized *via* manipulation. Hence, we conclude that the switching is induced by electrons and not by electric field.

We observed a difference in the switching behavior of the **1L** and **2L** chains, similar to the observation made in photo-induced switching in section **3.3.2**. The molecules in the red boxes in Figure **3.5B** did not switch OFF with rest of the **2L** chain. Because the **2L** chains have an extra layer of molecules as compared to the **1L** chains, **2L** chains are sterically hindered and some molecules apparently do not have enough free space around them to switch to the *cis* form.

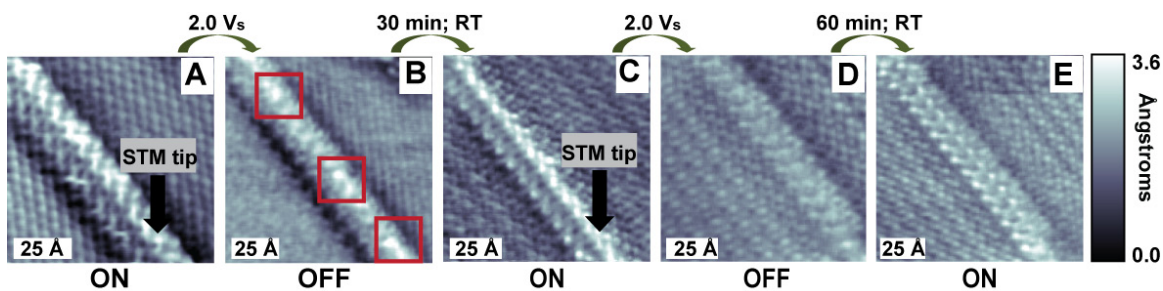


Figure 3.5: Series of STM images are shown of a **2L** chain switching between the ON and the OFF states, for two cycles. A sample bias of 2.0 V applied by the STM probe tip (black arrows) switches the ~ 130 Å long **2L** chain (**A** and **C**). The switching is reversible. The OFF chain switched ON when left unperturbed for 30-100 min with thermal relaxation at room temperature (RT) (**B** and **D**). Parts of the chain did not switch OFF (**B**, red squares) due to steric hinderance in 2L chains. All STM images are recorded at $V_s = 1$ V and $I_t = 1$ pA.

Switching of chains were observed to be a reversible process (i.e., chains can switch between the ON and the OFF states, multiple times). After the **2L** chain was switched OFF by applying a sample bias of 2.0 V for 5 min (Figure **3.5**), the sample was imaged at scanning parameters of $V_s = 1.0$ V and $I_t = 1$ pA. We observed that the molecules began to switch back to the ON state (*trans*) from the OFF state (*cis*) after 30 min (Figure **3.5C**), without further manipulation. The azobenzenes are known to switch back to the thermodynamically more stable *trans* form *via* thermal relaxation. The reversibility of switching was demonstrated multiple times. Figure **3.5** shows the **2L** chains switching between ON and OFF states for two complete cycles.

3.3.7 Manipulation Time Period and Control Experiments

The manipulation time period required to switch the chains varied from 0-5 min in different experiments. The variable time period is associated with the placement of the tip above the molecules and the lifetime of switching of the azobenzene moiety in the chains. The STM, operating in ambient conditions, had a drift of < 0.5 Å/min in the x and y directions. During the manipulation time period of 0-5 min, the STM probe tip moves due to drift and induces isomerization only when in position above a molecule. Additionally, when the tip is positioned above the molecule it isomerizes the molecule, with a finite probability. The electrons would either excite the azobenzene moieties or tunnel elastically to the substrate. Further, each excitation may yield into isomerization or it may get quenched due to proximity to the Au substrate, thus, it may require multiple excitations to induce isomerization in the entire chain.

In STM topographic images, domain boundaries of pure **C10** SAM sometimes appear as chains of molecules [82], similar to the chains of molecule **1** in **C10** SAM domain boundaries. However, the apparent heights of these **C10** boundaries are less than 1 Å as compared to ~2 Å of molecule **1** under these conditions. The **C10** domain boundaries, appearing as chains, were observed to be unstable under imaging conditions (i.e., they move into nearby vacancy sites). At many locations when they are stable under imaging conditions, domain boundaries did not move and remained unresponsive to manipulation, unlike the switching of the chains.

3.4 Conclusions and Future Directions

We prepared 1D chain structures of azobenzene-functionalized molecules at the domain boundaries of decanethiolate SAM matrix. We switched the chain structures from *trans* to *cis* using UV light and observed that the molecules in the chain isomerize in concert. The concerted isomerization indicates that the molecules in the chains are electronically coupled. To demonstrate the extent of the electronic coupling, we employed electron-induced isomerization of azobenzenes. We believe that electrons are propagating between the two ends of the chains due to favorable molecular orbital overlap. Theoretical investigations are underway to quantify the extent of coupling.

The switching of both types of chains due to excitation propagating along the chains suggests that these chains are well coupled. These molecular structures can be grown easily; however, further work is required to develop control over their placement on substrates, as well as their lengths scales. Fundamental understanding of electronic coupling and transport mechanisms will also need to be developed to design and to

fabricate more robust and efficient conducting molecular chains. Efforts are currently underway to expand the library of molecules that can be assembled as molecular chains in a variety of host matrices.

Chapter 4

A MECHANICAL ACTUATOR DRIVEN ELECTROCHEMICALLY BY ARTIFICIAL MOLECULAR MUSCLES

4.1 Introduction

To develop molecular machines, molecules that can undergo restricted motion upon external stimuli to generate useful work are necessary. For example, rotaxane molecules are a model system for artificial muscle that responds to electrochemical potential changes. In this chapter, redox-controllable, bistable [3]rotaxane molecules (artificial molecular muscles), are coated on a microcantilever and subjected to alternating oxidizing and reducing electrochemical potentials to deflect the microcantilevers reversibly.

Inspired by the inherent promise of and opportunities in nanotechnology, the scientific community has been attempting to decrease the characteristic length scales that define mechanical, electronic, and other devices [111,112]. A wide range of applications, including robotic, optical and microfluidic systems, call for microscale and nanoscale actuators [113]. However, most conventional electrostatic and piezoelectric materials require high driving voltages and must be fabricated using photolithography and other top-down manufacturing techniques that cannot easily achieve [114] feature sizes below 100 nm. In contrast, bottom-up approaches [115] that employ atoms and molecules as their fundamental building blocks and working units can potentially deliver mechanical operations on much reduced size scales [2,9,116,117]. Recently, research has been directed towards developing an integrated approach that combines the functionality of

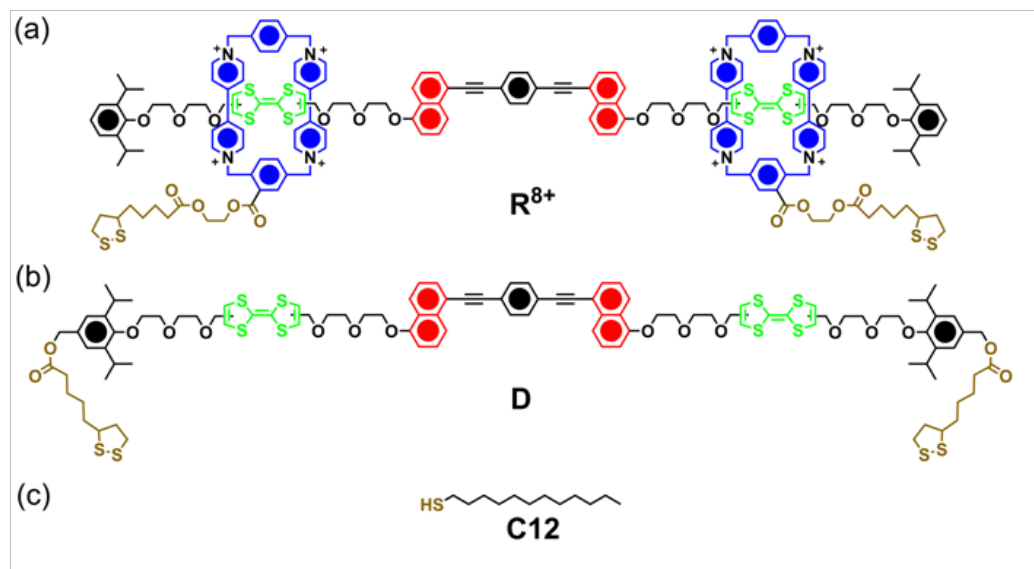
bottom-up assembly with top-down techniques for the manufacture of hybrid nanoelectromechanical systems (NEMS) [118].

A number of nanomechanical actuators [115,119-131] have been fabricated by hybrid top-down/bottom-up approaches. Electromechanical expansion in sheets of single-walled carbon nanotubes, proposed by Baughman *et al.* [119], have resulted in micro-scale actuation with strains higher than those obtained using conventional ferroelectrics. The phenomenon of hydrogel swelling by radiative forces was used by Juodkazis *et al.* [120] to build light-sensitive actuators. Redox-activated electrostatic repulsion in polymer molecules, such as polyaniline [126] and polypyrrole [130], have also been employed to power reversible actuation in microcantilevers. Raguse *et al.* [127] have utilized the intercalation of ions in nanoparticle films to achieve electrochemical actuation. These systems rely upon the bulk response of materials, and recently, researchers have started to harness work from molecular-scale mechanical motions. For example, Shu *et al.* [129] demonstrated the controlled, reversible actuation of a microcantilever, using pH-controlled configurational changes (duplex to i-motif) in self-assembled monolayer (SAM) matrices of DNA. While a monolayer of a photosensitive protein complex (bacteriorhodopsin) has been employed by Thomas *et al.* [123] and Ren *et al.* [128] to actuate microcantilevers photochemically, other experimentalists [125] have exercised photochemical control upon the conformational (*cis/trans*) isomerization of azobenzene molecules to actuate microcantilevers.

Artificial molecular machinery [2,3,9,12,13,22,64,115,116,132-141] has emerged as one of the most attractive alternatives for performing controllable mechanical work that begins at the nanoscale. These molecular machines have proven to be integral to the

operation and performance of many nanoscale and microscale systems, including molecular electronics [46,64,117,132,141-149], nanovalves for drug delivery [150-155], tunable electrochromic devices [17,148,156-158], as well as light-powered devices for transporting liquid over millimeters [159] and rotating microscale objects [73]. The class of artificial molecular switches, based on bistable rotaxanes, are especially promising [160,161]. These particular nanomachines are mechanically interlocked compounds [162] composed of a dumbbell-shaped component that is encircled by one or more ring components [146,163]. Bistable, donor-acceptor rotaxanes have many advantages as actuation materials. They can generate tunable strains, *e.g.*, up to 42%, while the strain generated [114] by traditional piezoelectric actuators is typically less than 1% [164,165]. They can also undergo controlled mechanical motion following the input of a variety of external stimuli (chemical, electrochemical and optical), while traditional actuators [113,166] and biomotors [167] usually rely on a single stimulus. Bistable [2]rotaxanes also offer the synthetically tunable property of hysteretic switching by taking advantage of a metastable state [86,142,156,168]. In this manner, the molecules can persist in their actuated state long after the stimulus is removed. Most importantly, bistable rotaxanes can deliver controllable mechanical motions at molecular level — a characteristic that most existing micro/nano actuators [111,118-123,125-131] do not possess — and thus can be ideal for applications where ultras-small nanoactuators are needed.

We recently extended research beyond simple bistable [2]rotaxanes, by designing and synthesizing a disulfide-tethered, palindromic, bistable [3]rotaxane \mathbf{R}^{8+} (Scheme 1)



Scheme 4.1: Molecular structures of (a) a palindromic bistable [3]rotaxane R^{8+} , (b) a disulfide-tethered dumbbell molecule **D** (control compound related to R^{8+} having no ring), and (c) 1-dodecanethiol **C12** (control compound).

that mimics [164,165] biological skeletal muscle's contraction and extension. Skeletal muscles convert chemical energy to mechanical energy by the cumulative actions of myosin biomotors [169]. Coherent and cooperative configurational changes in this biosystem are harnessed in order to obtain macroscopic muscle contraction and expansion [170,171]. By imitation of the changes in shape that occur in skeletal muscles, the palindromic, bistable [3]rotaxane \mathbf{R}^{8+} undergoes controllable mechanical motions in the presence of external stimuli. It has a pair of redox-active tetrathiafulvalene (TTF) units, a pair of naphthalene (NP) stations separated by a di(ethylene glycol) spacer, and two movable tetracationic, cyclobis(paraquat-*para*-phenylene) (CBPQT⁴⁺) rings (Scheme 1). In the ground state co-conformation, both the CBPQT⁴⁺ rings encircle the TTF units, courtesy of electron donor-acceptor interactions [165]. Oxidation of the TTF units causes the CBPQT⁴⁺ rings to move towards the NP stations because of the electrostatic repulsion between the rings and the positively charged TTF²⁺ units. Reducing the TTF²⁺ dications back to their neutral state causes the rings to shuttle back onto the TTF units. The incorporation of a disulfide tether onto each CBPQT⁴⁺ ring component provides a point of attachment to gold surfaces. More critically, this connection provides the means to transfer the energy of contraction within the artificial muscle molecules to an underlying substrate.

The collective motions induced by oxidation and reduction of ~8 billion muscle molecules can be harnessed to perform mechanical work on a microcantilever [164,165]. Reversible flexing of a micro-cantilever coated with \mathbf{R}^{8+} during the cyclic injection of oxidizing and reducing solutions was correlated to the collective contraction and extension-relaxation of the surface-bound muscle molecules. This work constituted a

starting point in molecular-muscle-based NEMS. However, the introduction of different chemicals into the system is a slow and inconvenient process that is associated with the gradual accumulation of waste products. Succinctly, chemically controlled actuation is not optimal for many engineering applications. Compared to chemical methods, electrochemically or photochemically induced oxidations and reductions have many advantages – (i) devices can be switched much faster, (ii) they can work without producing chemical waste, and (iii) either electricity or light can be used for both inducing (writing) and detecting (reading) mechanical molecular motions in devices.

Here, we demonstrate the feasibility of electrochemically controlled surface-bound molecular muscles and use the collective mechanical motions of the bistable molecules to perform mechanical work on a larger scale. The electrochemically-induced movements employing the rotaxane molecules bend the cantilevers in the opposite direction to those observed for the control systems, in which electrolyte adsorption appears to play a major role. We were not able to determine the exact nature of the oxidation states of the TTF units (+1 or +2) within the surface-bound rotaxanes. However, the observed thermal relaxation of the proposed metastable state ($k = 1.2 \times 10^{-2} \text{ s}^{-1}$) monitored in the device's deflection is consistent with internal movements resulting from the TTF units' oxidation in the molecules [86,142,156,168,172], as well as the primary role of the molecular muscles in bending the microcantilevers up and down.

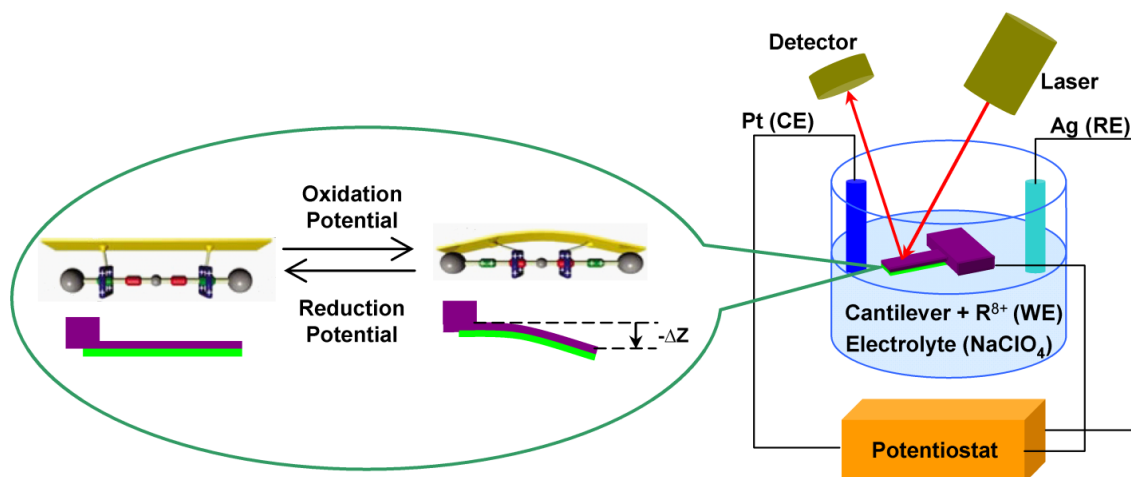


Figure 4.1: Schematic of the experimental setup used for in situ electrochemical activation of the palindromic bistable [3]rotaxanes molecules. The inset shows the reversible electrochemical oxidation and reduction of R^{8+} to produce the microcantilever deflection. (WE: working electrode, CE: counter electrode, RE: reference electrode).

4.2 Experimental Procedure

4.2.1 Preparation of Microcantilever Samples

Commercial rectangular silicon microcantilevers (NanoAndMore Inc, Lady's Island, SC) of length 500 μm , width 100 μm , and thickness 1 μm were used in all the experiments. One side of the microcantilevers was coated with a 20-nm-thick gold layer by the manufacturer. Before a monolayer film was deposited, each microcantilever was cleaned for 5 min with UV/ozone and then washed with deionized water.

4.2.2 Synthesis of Molecular Muscles and Control Compounds and Preparation of Monolayer Films

The palindromic bistable [3]rotaxane \mathbf{R}^{8+} and the control dumbbell compound \mathbf{D} , having no ring component, were synthesized using a method reported earlier [150,165]. 1-Dodecanethiol, $\mathbf{C12}$ (Sigma- Aldrich), was used without further purification. Microcantilevers were cleaned and then placed for 48 h in solutions containing the target molecule, in order to form monolayer films on the gold layers.

4.2.3 Electrochemical Atomic Force Microscopy

A scanning probe microscope combined with an electrochemical cell supply (Pico SPM 2500, Molecular Imaging) was used in all of the experiments. Before each experiment, the electrolyte (0.1 M NaClO_4) employed in the electrochemistry setup was purged with nitrogen gas. Both counter and reference electrodes were cleaned by ultrasonication in water and acetone before each experiment. At the end of each experiment, the potential of the reference electrode (Ag) was adjusted with respect to that of a AgCl solution. The sensitivity of each microcantilever was calibrated by fitting the

slopes of force curves, in order to measure the cantilever deflection (nm) by means of the photodiode signal (V) (Figure 4.1). The deflection data and applied voltage signals were obtained with 2 ms time resolution, and were later averaged from 100 data points. The signals were analyzed and plotted using MATLAB 7.0 (The Mathworks, Natick, MA) and Origin Pro (Origin Lab Co., Northampton, MA).

4.3 Results and Discussions

In order to detect the mechanical work exerted by the surface-bound, palindromic, bistable [3]rotaxane \mathbf{R}^{8+} on microcantilevers during electrochemical activation, we combined (Figure 4.1) an optical deflection technique based on atomic force microscopy (AFM) with an *in situ* electrochemical method. A microcantilever coated on one side with gold was used as a working electrode, a silver wire as a quasi-reference electrode, and a platinum wire as a counter electrode. These three electrodes were placed in a Teflon cell filled with aqueous electrolyte (0.1 M NaClO₄). The silver wire pseudoreference electrode was subsequently calibrated against a Ag/AgCl 3 M KCl reference. The data illustrated in Figures 4.2–4.4 represent the calibrated redox potentials. The gold surface of the microcantilever was coated with a monolayer film of \mathbf{R}^{8+} molecules and the redox state was changed by applying a desired potential using a potentiostat (CHIInstrument, Inc.). A laser beam reflected by the silicon side of the microcantilever was collected by a split photodiode. The deflections in the

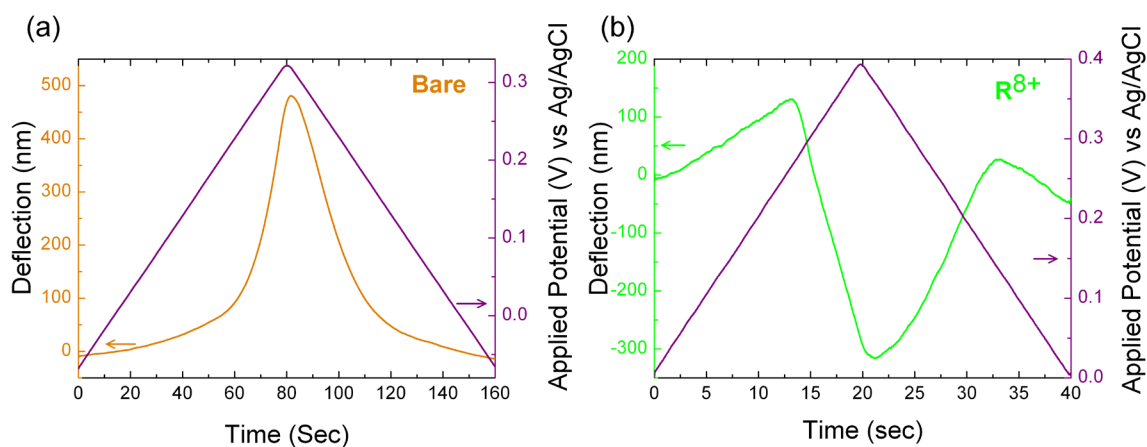


Figure 4.2: Deflection signature (colored lines) in response to a triangular sweep (purple lines) of the electrochemical potential for (a) a bare microcantilever (orange line, 5 mV s^{-1}) and (b) a microcantilever modified with a monolayer film of the palindromic bistable [3]rotaxane R^{8+} (green line) on one side of the microcantilever (20 mV s^{-1}). The directions of the arrows indicate the corresponding y-axis of the parameter plotted.

microcantilever during electrochemical activation of the muscle molecules were measured from the variations in the reflected laser beam position on the photodiode.

Previously, redox-activated mechanical switching of \mathbf{R}^{8+} molecules in solution was characterized extensively using cyclic voltammetry and UV-visible spectroelectrochemistry [165]. When \mathbf{R}^{8+} molecules are attached to surfaces, our expectation is that, upon the application of a sufficiently oxidizing potential, the TTF units in \mathbf{R}^{8+} will become positively charged, causing the surface-bound rings to move towards the NP units. Consequently, this action will increase the bending moment of the supporting microcantilever. A reducing potential will regenerate the neutral TTF units, causing the rings to move back to these TTF units. The deflection in the microcantilever would then decrease. Therefore, by applying an electrochemical potential, it will be possible to harness the collective mechanical motions from surface-bound molecular muscles and to control the deflection of the microcantilever.

To describe the direction of the microcantilever deflection, we use the terms “down” for deflection of the microcantilever towards the gold side (negative deflection), and “up” for deflection away from the gold side (positive deflection). To determine the mechanical work exerted by molecular muscles on the microcantilevers, all competing forces acting against the mechanical work performed by molecular muscles should be low in magnitude or, ideally, non-existent. Such competing forces, however, do exist in microcantilevers during electrochemical activation. They include electrostatic repulsion forces at solid-liquid interfaces and surface stress induced by specific adsorption and desorption of ionic species in the electrolyte [173]. To assess the influence of these competing forces, we subjected a nominally bare gold-precoated microcantilever without

a molecular muscle monolayer film to a sweep of triangular potential. Figure 4.2a shows the performance of a bare microcantilever subjected to anodic and cathodic sweeps of electrochemical potential at a slow scan rate of 2 mV/sec. The bare microcantilever was deflected upwards during the anodic sweep and deflected back down again to the neutral position during the cathodic one. Based on the magnitudes of surface stress reported in earlier work [173-176], we attribute this deflection signature to the specific adsorption of perchlorate (ClO_4^-) counterions onto the gold-coated side of the microcantilever.

We expected that, upon the oxidation of the TTF units and the consequent contraction of the distance between the rings, the collective moments of deflection caused by the many muscle molecules would flex the microcantilever (Figure 4.1) in the negative direction, that is, *opposing* the competing effect (Figure 4.2a) of specific adsorption by perchlorate counterions. *Both* effects were observed (Figure 4.2b) in triangular sweep experiments performed on a microcantilever coated with a monolayer film of \mathbf{R}^{8+} molecules. During the anodic sweep, the initial deflection went upward. However, after reaching a potential of +0.24 V, the microcantilever started to deflect downwards for various scan rates of applied potential.

In comparison to larger scan rates (50 mV/sec), smaller scan rates (20 and 25 mV/sec) produced larger deflections. This could be due to partial redox activation of \mathbf{R}^{8+} molecules at larger scan rates. Qualitatively, the deflection signatures of different \mathbf{R}^{8+} -coated cantilevers were reproducible. The right ordinate of the graph shows the surface stress, $\Delta\sigma$, which can be determined by the following equation:

$$\Delta\sigma = -\frac{Et^2}{3L^2(1-\nu)} \Delta z \quad 4.1$$

where $E/(1-\nu)$ is the bi-axial Young's modulus of cantilever (230 Gpa); L is the length of the cantilever, (460 μm , considering the effect of laser spot diameter); t is thickness of the cantilever (1 μm); and Δz is deflection. Variations in the magnitudes were observed for different cantilevers and could be attributed to factors such as the differences in the mechanical properties of individual cantilevers, and position of laser beam.

The observed downward deflection was attributed to the collective motions of surface-bound muscle molecules that generate tensile stress on the microcantilevers. Subsequent application of a cathodic sweep caused the microcantilever to return to its original position. This restoration was believed to occur because the reduction of the TTF^{2+/+} units should lead to shuttling of the rings back to their original positions. When the potential went below +0.12 V, the microcantilever deflected downward, an observation that we attribute to the desorption of perchlorate counterions from the microcantilever occurring in the background. The initial deflection (when the driving potential is below +0.24 V) in the \mathbf{R}^{8+} -coated cantilevers, attributed to the specific ion adsorption, was higher than what was observed in bare cantilevers. This phenomenon may have occurred due to the presence of positive charges on \mathbf{R}^{8+} , which makes the cantilever surface highly charged and more prone to specific adsorption than bare cantilevers. Another cantilever coated with \mathbf{R}^{8+} molecules also showed similar deflection signatures for the same potential window and scan rate, indicating good reproducibility of our experiments. It should also be noted that the magnitude of deflection observed here

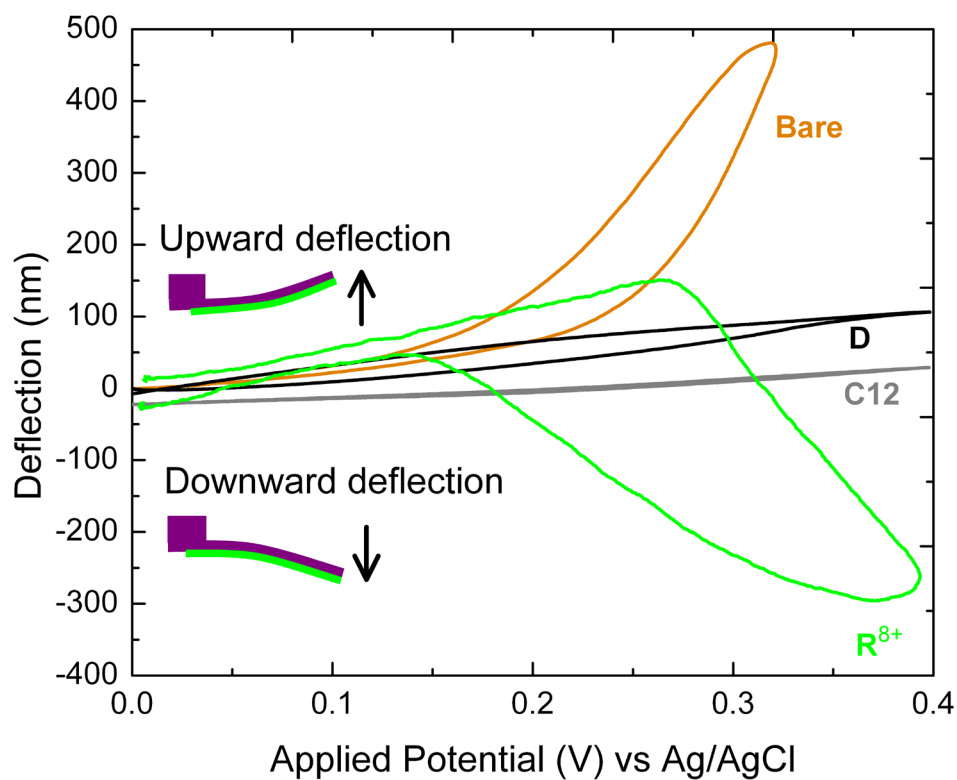


Figure 4.3: Deflection vs. applied potential with respect to the working electrode for a bare microcantilever (orange line, 5 mV s^{-1}) as well as for microcantilevers coated with monolayer films of the bistable [3]rotaxane \mathbf{R}^{8+} (green line, 20 mV s^{-1}), the control dumbbell molecule \mathbf{D} (black line, 20 mV s^{-1}), and 1-dodecanethiol $\mathbf{C12}$ (dark grey line, 20 mV s^{-1}).

is much larger than the ones observed in our previous studies [164,165], which utilized chemical stimuli and were likely limited by the diffusion and partial activation of the molecules.

To determine other effects that could contribute to the deflection of the cantilever, such as electron injection into the cantilever, we conducted control experiments with monolayer films composed of two different compounds. The first control compound (Scheme 4.1b) was a disulfide-tethered dumbbell compound **D**. This compound contains a pair of TTF and NP units with the same relative geometry as that present in \mathbf{R}^{8+} and retains the redox activity of the [3]rotaxane. However, **D** lacks mechanically mobile CBPQT⁴⁺ rings, while the disulfide tethers are attached at the two stoppers of the dumbbell. The second control compound (Scheme 4.1c) was **C12**, which lacks both moving elements and redox-active units, yet is known to form well-ordered SAMs that would thus block adsorption of other species [177-182]. Neither control compound was expected to perform mechanical work on the microcantilever, but it is expected that oxidation of **D** changes the electronic structure of the gold metal and creates tensile stresses on the cantilever.

To test these hypotheses, monolayer films of the control molecules, assembled on microcantilevers, were subjected to triangular sweeps (Figure 4.3) at slow scan rates of 20 mV s⁻¹. The deflection for both control compounds was opposite to that observed in the case of \mathbf{R}^{8+} . This opposite movement indicates that the mechanically active, disulfide-tethered CBPQT⁴⁺ rings in \mathbf{R}^{8+} are essential for the redox-controlled bending of the cantilever beams. The small upward deflections of the microcantilevers coated with control compounds were attributed to the adsorption of perchlorate counterions on the

gold side of the microcantilever. The potential-induced deflections, observed for microcantilevers coated with any of the monolayers (**R**⁸⁺, **D**, or **C12**), were smaller in magnitude than those observed for bare microcantilevers. In these cases, the monolayers served as protective blocking layers that decreased adsorption. The adsorption for the ordered SAMs of the **C12**-coated microcantilevers was somewhat less pronounced than that observed for microcantilevers coated with **D**, as well as for those coated with **R**⁸⁺ prior to the onset of downward deflection. We attribute this to the well-ordered, dense surface packing of the **C12** SAM providing the best protection (of the films studied) from ion adsorption. The upward deflection in the case of **D**-coated microcantilevers suggests that the effects from specific ion adsorption dominate over the tensile stresses induced by the injection of electrons into the cantilever.

We have also performed dynamic studies in which the potential steps were alternated on a microcantilever coated with molecular muscles (Figure 4.4a) in order to initiate oxidation and reduction and the deflections were measured as a function of time. On the basis of the observed deflection curves (Figure 4.3), the voltages of +0.4 V and +0.2 V were selected in order to effect the TTF unit's oxidation and reduction, respectively. It was observed that at +0.40 V, the microcantilever deflects downward, and at a lower potential, +0.20 V, where TTF is reduced to its neutral state, the microcantilever is deflected upwards. The alternate bending down and up of the microcantilever corresponds to the alternate oxidation and reduction of the surface-coated muscle molecules, respectively. We applied similar alternating potential steps to other

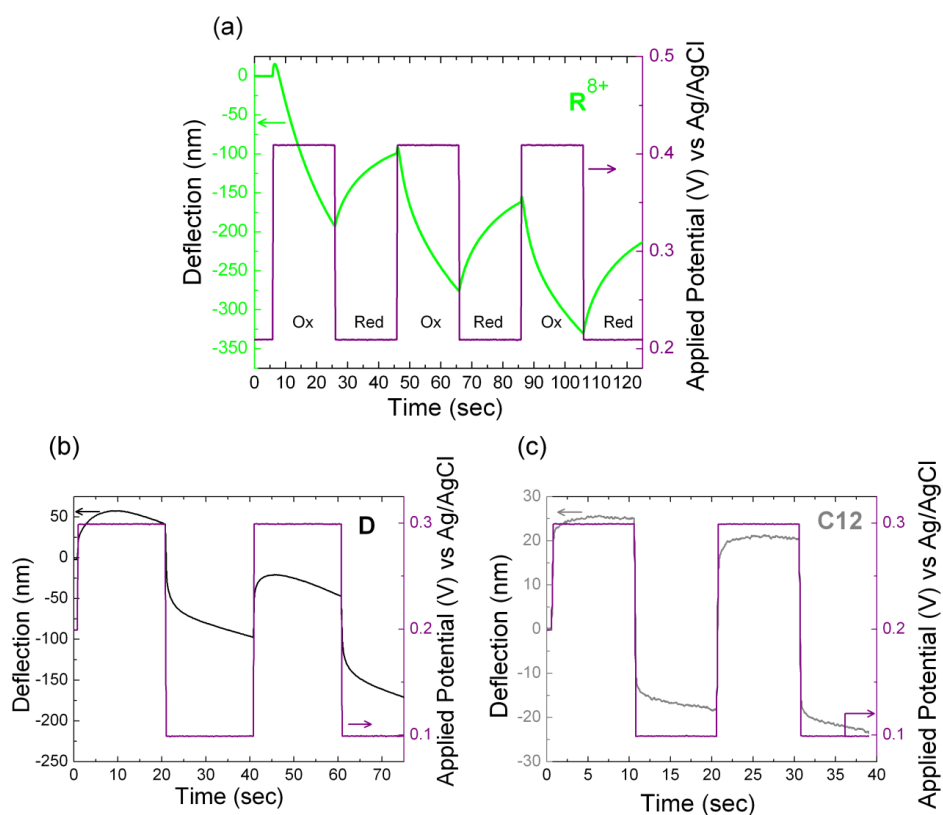


Figure 4.4: Time-dependent operation of microcantilevers coated with: (a) the palindromic bistable [3]rotaxane R^{8+} (green line), (b) the control dumbbell molecule **D** (black line), and (c) 1-dodecanthiol **C12** (dark grey line), when subjected to a series of oxidation and reduction potential steps (purple lines).

microcantilevers, coated either with the control compounds **D** or **C12**. The cantilevers bent upward during the application of a higher potential step and bent downward during the application of a lower potential step (Figures **4.4b** and **4.4c**). Both deflections were in the opposite directions to those observed (Figure **4.4a**) for the \mathbf{R}^{8+} -coated microcantilevers.

When we repeated the redox chemistry, we observed (Figure **4.4a**) a gradual downward deflection of the cantilever. This overlying strain effect, or creep [183], has been observed in other electrochemical actuator systems [184-188]. The creep in these systems is purportedly caused by the disentanglement of the adsorbed molecular components [186,188]. We believe that a similar creep mechanism may apply here, but in our case, arising from a reorganization of the muscle molecules within the monolayer film that plays an important role during the electrochemical perturbation. Similar behavior—the gradual deflection towards the coated side of the cantilever—was also observed in the microcantilevers coated with **D** (Figure **4.4b**) and **C12** (Figure **4.4c**). However, such behavior was not observed in experiments (data not shown) conducted on bare microcantilevers. These observations are consistent with our hypothesis on the creep mechanism. The creep of microcantilevers coated with **C12** was substantially less pronounced than that for **D**- or \mathbf{R}^{8+} -coated microcantilevers. One would expect molecules such as **C12**, which form more organized monolayer films, to experience far less reorganization. We further note that recent investigations have indicated the importance of the substrate atoms in thiolate motion on gold, so that we may also expect substrate atoms to move when substantial molecular forces are applied [48,189,190].

The deflections of cantilever caused by the two competing effects, anion adsorption and electron transfer into the cantilever, can be estimated from the response of the **D**-coated cantilevers. The dumbbell molecule **D** is similar to **R**⁸⁺, except for lacking the moving rings. Figure 4.3 indicates that the expected deflections from the two competing effects reach maximum deflections of ~250 nm in the upward direction. Therefore, experimentally, the total deflection produced by the muscle contraction alone can be estimated to be ~550 nm.

We attempted to quantify the magnitude of the deflection observed analytically in the microcantilever coated with **R**⁸⁺ using cantilever mechanics. The deflection, Δz , caused by the collective contractions and extensions of molecular muscles can be quantified using a special case of Euler-Bernoulli's beam equation, which includes a moment at the free end of beam, and is given by:

$$\Delta z = \frac{M_{beam} L^2}{2E'I}, \quad 4.2$$

where M_{beam} is the collective deflection moment on the beam; L is the total length of the beam (450 μm , considering the effect of laser spot diameter); E' is the biaxial Young's modulus of the microcantilever (additional stiffness due to Au and **R**⁸⁺ monolayer is neglected) and is given by $E/(1-\nu)$, where E is Young's Modulus (187.5 GPa), and ν is the Poisson's ratio (0.182) [191], and I is the area moment of inertia of the beam's cross-section. The spacer, di(ethylene-glycol), between the two DNP sites of the molecular muscle improves the rigidity of the molecule. In an idealized model for quantitative analysis, we assume that the molecular muscles are rigid and the interactions between

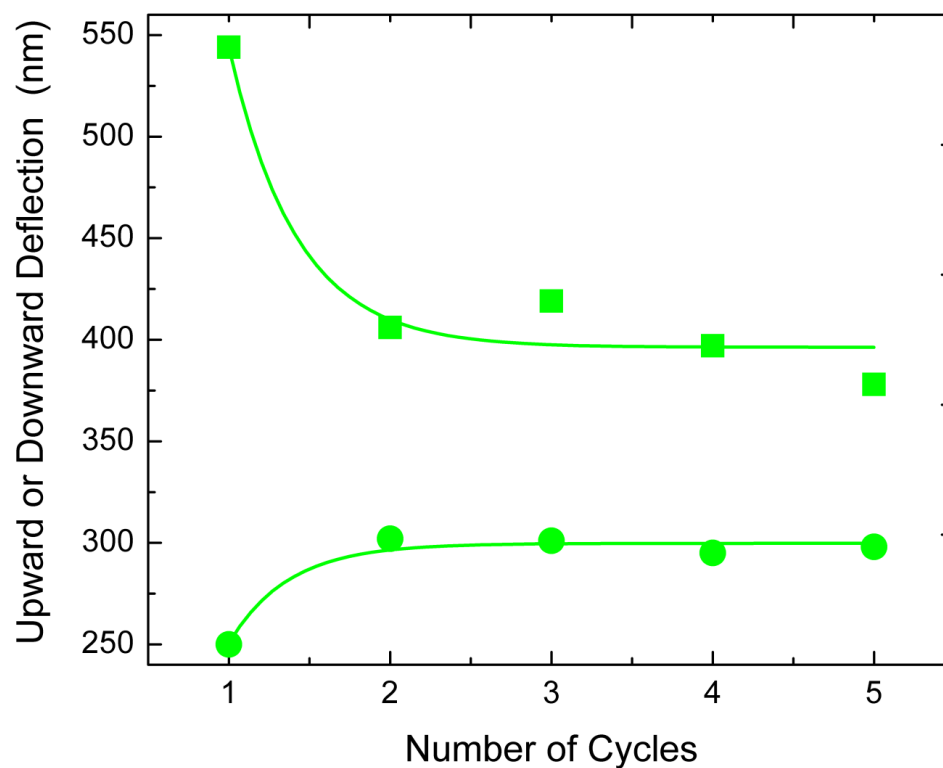


Figure 4.5: Comparison of the downward deflection as a result of the application of an oxidizing potential (squares) and the upward deflection caused by the application of reducing potential (circles) in a microcantilever modified with a bistable [3]rotaxane \mathbf{R}^{8+} monolayer film followed through five actuation cycles. Solid lines represent the exponential best fits.

neighboring molecules are negligible. With these assumptions, the collective deflection moment of the beam is given by:

$$M_{beam} = N \cdot 2 \cdot P \cdot (t/2) \cdot f_1 \cdot f_2 \cdot f_3, \quad 4.3$$

where N is the total number of molecules adsorbed along the width of the microcantilever; P is the Coulombic repulsion force causing the ring to move away from the TTF unit; t is the beam thickness (1 μm); f_1 is the surface coverage factor; and f_2 and f_3 are the constants corresponding to the idealized geometry and the molecule's orientation, respectively (assumed to be random). Since only the molecular segment

between the two rings generated a moment that contributed to the deflection, $f_2 = \frac{L_1}{L_2}$,

length of the molecule. For a molecule in its extended inter-ring co-conformation, L_1 was 4.2 nm and L_2 was 7.4 nm [165]. With the molecules and deposition protocol employed, we do not expect all the molecules to be fully extended; thus, L_1 and L_2 would vary and they could each be smaller than indicated above. Since the molecules were randomly aligned and only the force exerted along the longitudinal axis of the beam will contribute to deflection, $f_3 = 2/\pi$. The number of molecules along the width was approximated as

$\frac{w}{b}$, where b was the breadth of each rotaxane (1 nm) and w was the breadth of the cantilever (100 μm). The success of the model to quantify the deflection observed in the experiments lies in the ability to predict the repulsion force between CBPQT⁴⁺ ring and the TTF²⁺ station accurately. Assuming the TTF unit is oxidized to TTF²⁺ and neglecting the effects of 1) electrolyte, 2) presence of counter-anions, and 3) orientation of molecule, we can use the actuation energetics of a similar molecule reported by Brough *et al.* [192].

By augmenting the force spectroscopy data with molecule dynamics simulations and considering the effects of thermal fluctuations as a function of the probe's loading rate, they were able to predict the actuation energy, W , between TTF^{2+} and CBPQT^{4+} . A value of 65 kcal/mol was determined to be the actuation energy, a value that also matches *ab initio* calculations. To convert actuation energy, W , to average actuation force, P , we divide W with the distance between TTF^{2+} and DNP, $d = 1.4$ nm, giving a value of 320 pN. Using this magnitude for the force and assuming a surface coverage of 100%, the theoretical displacement was predicted to be 620 nm. This value is slightly larger than the magnitude of deflection (~ 550 nm) observed in the experiments, but well within the accuracy of the various assumptions made in the model.

The first cycle of oxidation and reduction caused a larger deflection than did subsequent cycles. The extent of the deflection stabilized (Figure 4.5) after the first cycle. We attribute the sudden changes in the downward and upward deflection at the end of the first cycle to the incomplete recovery of the ground state co-conformation from the metastable state co-conformation [86,142,156,168], which leaves only a portion of the muscle molecules active for subsequent cycles. This observation suggested that a microcantilever, if left in a reducing environment after a series of oxidation and reduction cycles, should have most of the surface-bound rotaxane molecules recover to their ground state co-conformation. With a new set of actuation cycles, the first cycle would once again exhibit large changes in downward and upward deflection.

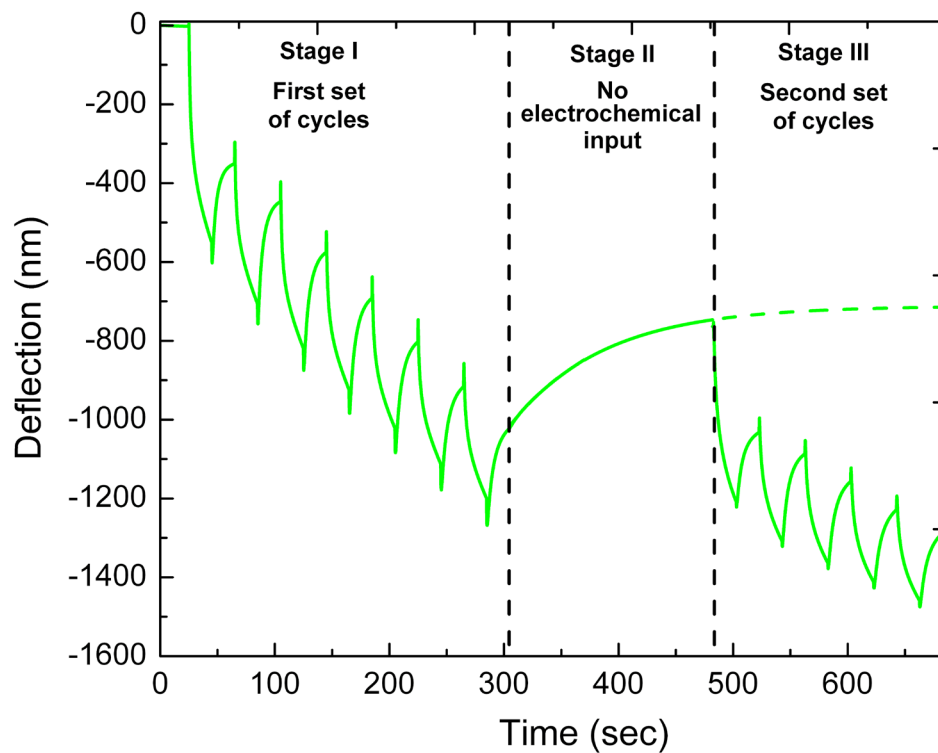


Figure 4.6: Actuation of a microcantilever coated with \mathbf{R}^{8+} molecules when subjected to three types of electrochemical potential variations. In Stage I, seven steps of alternating oxidizing and reducing potentials were applied. In Stage II, no external potential was applied for 175 sec. This period enabled recovery of the cantilever, as noted from the fit (dotted line) of the deflection signature observed in Stage II. In Stage III, five steps of alternating oxidizing and reducing potentials were applied.

To test this hypothesis, we applied three stages of potential variations (Figure 4.6) while the cantilever deflection was recorded. Stage I included seven steps of alternating oxidation and reduction potentials with 20 sec intervals at each potential for each step. During these steps, the microcantilever bent alternately downwards and upwards, as expected for these artificial molecular muscles. Large changes in the downward and upward deflections were observed in the first cycle of actuation, followed by constant upward and downward deflections in the following actuation cycles. Sudden changes or “spikes” in the deflection of the microcantilever were observed at the end of each oxidation and reduction stage, and are most likely a result of the desorption and adsorption of the perchlorate counterions. In Stage II, the microcantilever was left electrochemically unperturbed at an open circuit potential—*i.e.*, no potential applied—for ~175 sec. During this stage, the cantilever deflected upward with a first-order decay ($k = 0.012 \text{ s}^{-1}$). The recovery of the cantilever position appeared to be incomplete, possibly as a result of the irreversible creep observed in Stage I. A time interval of 175 s was chosen for Stage II in order to ensure saturation of the recovery process. In Stage III, we again applied alternating redox potentials with the same durations as those applied in Stage I. We observed deflection signatures similar to those in Stage I. Large changes in the downward and upward deflections were again observed in the first cycle of operation. These changes were followed by constant upward and downward deflections in later cycles within the error of our measurements.

The observation of an exponential decay for the relaxation of the \mathbf{R}^{8+} -coated microcantilever’s deflection curve is consistent with the behavior of bistable [2]rotaxanes in solution [168,172], embedded in polymer matrices [156], and self-assembled onto gold

surfaces [86]. In these previous cases, the relaxations of the molecules were observed directly using electrochemistry and it was found that the rates of motion slowed down [142,168] as the rotaxanes were transferred into more highly condensed phases. Their kinetic behavior was found to correlate with the thermal relaxation of the electrical signature from a device that has rotaxanes incorporated within them as Langmuir-Blodgett monolayers [142,168]. Therefore, we posit that the first-order decay in the deflection of the microcantilever arises from the thermally activated motion of the mobile rings from the NP stations back to the neutral TTF stations. The rate constant correlates with an activation barrier of $\Delta G^\ddagger = 20 \text{ kcal mol}^{-1}$. On the basis of solution-phase studies [165] on the molecular muscle prototype to \mathbf{R}^{8+} , the corresponding barrier was estimated to be less than 14 kcal mol^{-1} . Consequently, there is an increase of 6 kcal mol^{-1} on going from solution to surface-bound devices. This increase is greater than the $\sim 2 \text{ kcal mol}^{-1}$ expected on the basis of the bistable rotaxane studied, first in solution, and then self-assembled onto gold electrodes. Slower than usual thermal relaxation has been observed for the *cis-to-trans* isomerization [193] in single polymer strands incorporating multiple azobenzene units when these strands are placed under loads by utilizing microcantilevers in force spectroscopy experiments. We concur with the rationalization presented in this previous report that the load-induced motion is no longer able to proceed along the lowest pathway possible. The exponential decay arises either when configurationally active molecules (azobenzene), or when active rotaxanes with two mobile rings (\mathbf{R}^{8+}) relax in confluence with an applied restoring force. The data suggest that the active units are not interacting with each other. Nevertheless, the observation of a relaxation process is a

crucial molecular signature that confirms the dominant role that the surface-bound rotaxanes serve in bending the microcantilevers.

4.4 Conclusions and Future Directions

We have demonstrated that surface-bound artificial muscle molecules, when electrochemically activated, cause a microcantilever to bend. Conversely, microcantilever beams that are coated with redox-active but mechanically inert control compounds—the dumbbell of the [3]rotaxane or **C12**—do not display the same bending characteristics. Moreover, using beam theory and analysis, it has been shown that these observations are consistent with the hypothesis that the cumulative nanoscale movements of the surface-bound “molecular muscles” can be activated electrochemically and harnessed to perform much larger-scale mechanical work. The observed “creep” phenomenon in the dynamic studies most likely results from the reorganization of the molecules in the films. Compared with their chemically-driven counterparts [164,165], the electrochemically-driven molecular-muscle-based actuators can be operated much faster, more conveniently, and with larger responses.

Although challenges remain, the results constitute a key step towards functional NEMS based on artificial molecular muscles. We believe that: (i) by improving the assembly conditions, (ii) by increasing the rigidity of the muscle molecules, and (iii) by incorporating a blocking layer in a matrix around the active components, the artificial molecular muscle-based NEMS can be optimized even further. Understanding the interaction of rotaxane molecules with the substrate on a single-molecule level is also important to design efficient molecular muscles.

Chapter 5

CHANGING STATIONS IN SINGLE BISTABLE ROTAXANE MOLECULES UNDER ELECTROCHEMICAL CONTROL

5.1 Introduction

Mechanically interlocked molecules, such as bistable catenanes or rotaxanes [9,12,22,194-197] having addressable rings, have potential applications in areas ranging from molecular-scale electronics [117], to display technologies [198], to nanoelectromechanical devices [101,199]. Functional components of these molecular machines can be triggered by external stimuli, such as redox reactions [200], light [201], metal ion complexation [202], and pH [203]. Solution-phase measurements have been used to characterize the structures and functions [195] of these molecular switches. However, to realize the full potential of these functional molecules at the nanoscale, it is imperative to understand their operation at the single-molecule level under environments relevant to actual device operation [101,117,198]. Recently, progress has been made in measuring collections of molecules in condensed monolayers and polymer gel matrices [66,172]. Few examples illustrate STM tip manipulation of rotaxane molecules on substrates [204,205]. However, serial manipulation of switchable molecules is far less practical than parallel electrochemical, optical, and chemical control of molecules [199].

Thus far, most rotaxane molecules are inherently flexible and have poorly defined conformations and orientations when adsorbed on surfaces, rendering them difficult to resolve individually with scanning probe microscopes. Because of the limited knowledge of the molecular geometries and the conformations of such single molecules on

substrates, the effects of the nanoscale environments on the station changes remain unaddressed. In this chapter, we have developed molecular designs that reduce the mobilities of the molecules significantly. We were able to assemble bistable rotaxane molecules in orientations conducive to direct STM measurements of their station changes. An ECSTM has been employed to observe molecular motion *in situ* [45,140] and we observed that single-molecule station changes correlate with the redox states of bistable rotaxanes [195]. We found that the mechanical motions of these mechanically interlocked molecules are influenced by their interactions with the surface and with neighboring molecules, as well as by the conformations of the dumbbell components.

5.2 Experimental Procedure

5.2.1 Sample Preparation

The [2]rotaxane molecule (\mathbf{R}^{4+}), with disulfide groups attached to the stoppers on the dumbbell termini (Figure 5.1A), has been designed to bind at each end to Au{111}. After cleaning a Au{111} single crystal disc with piranha solution (3:1 mixture of H_2SO_4 and H_2O_2)[‡], the Au{111} disc was hydrogen flame annealed and cooled under argon before being immersed in the \mathbf{R}^{4+} 4PF_6 solution ($\sim 10 \mu\text{M}$). Only 10-20 seconds of immersion was necessary to achieve the desired coverage (5-6 molecules/ 1000 \AA^2) for STM imaging. The sample was then rinsed with acetonitrile, nitrogen dried, and transferred to the STM electrochemical cell containing a 0.1 M HClO_4 solution. The electrode potentials given henceforth are in reference to a Ag/AgCl electrode, although a platinum wire was used as a quasi-reference electrode.

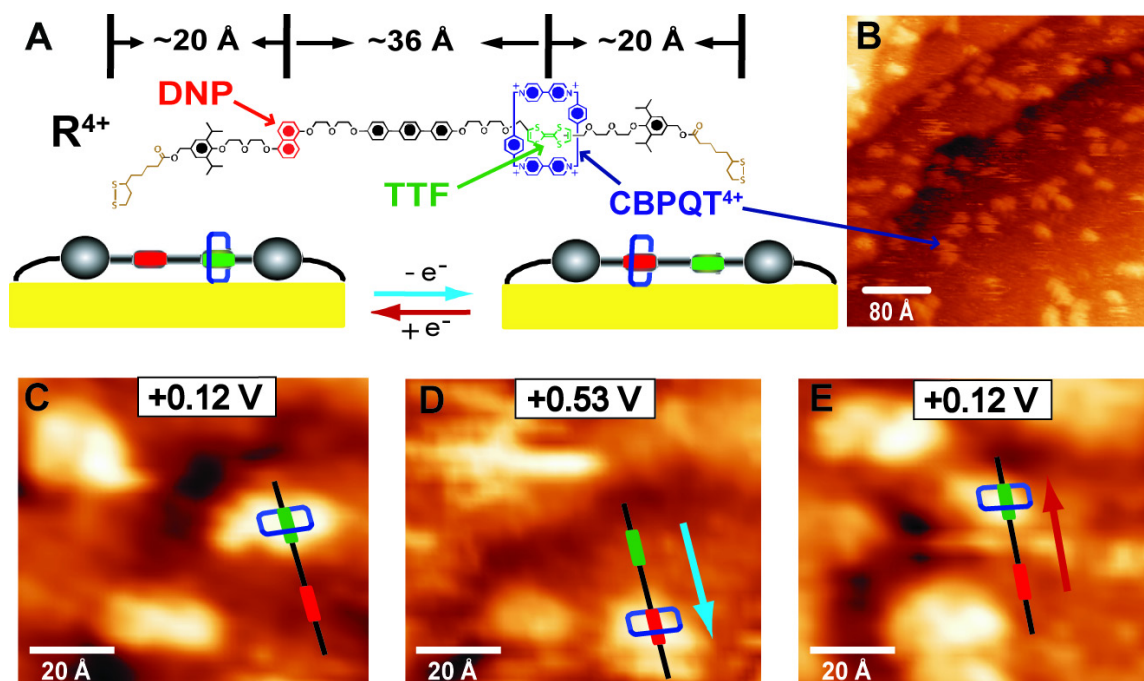


Figure 5.1: Structure and motion of a bistable rotaxane molecule, R , adsorbed on Au{111} investigated using electrochemical scanning tunneling microscopy. (A) The tetracationic cyclobis(paraquat-*para*-phenylene) ring (CBPQT $^{4+}$, blue) is known to move along the thread between two recognition sites (tetrathiafulvalene, TTF, green and 1,5-dioxynaphthalene, DNP, red stations) depending on the redox state of the TTF unit. (B) The protrusions are assigned as CBPQT $^{4+}$ rings. (C) In its reduced state at +0.12 V, the CBPQT $^{4+}$ ring prefers to encircle the TTF station. (D) Upon oxidation (+0.12 V to +0.53 V) of TTF into a radical cation, electrostatic repulsion propels the ring to the DNP station (blue arrow). (E) Upon reduction (+0.53 V to +0.12 V) of TTF to neutrality, the DNP station relaxes back to its thermodynamically favorable position, the TTF station (red arrow). Imaging conditions: $V_s = 0.3$ V; $I_t = 2$ pA. The Faradaic current was typically less than 10 pA.

5.2.2 Electrochemical Scanning Tunneling Microscopy

Refer to Chapter 1 for a description of STM operation. Here, the rotaxane molecule was analyzed using a PicoSPM microscope (Molecular Imaging, AZ) controlled by an RHK STM-100 controller (MI) and electrochemically etched tungsten tips insulated with paraffin wax.

5.2.3 Cyclic Voltammetry

To verify the electrochemical reactivity of the \mathbf{R}^{4+} molecule, a monolayer of \mathbf{R}^{4+} was formed by immersing a gold bead into 0.1 mM \mathbf{R}^{4+} 4PF₆ acetonitrile solution for 48 hours (the increased time and concentrations are used to ensure sufficient coverage for electrochemical studies). Under 0.1 M HClO₄, the cyclic voltammogram (CV) of \mathbf{R}^{4+} adsorbed on Au{111} showed two anodic peaks at +0.15 V and +0.44 V and one cathodic peak at +0.55 V. A previous electrochemical study by Tseng *et al.* [86] observed two anodic peaks and two cathodic peaks associated with two monoelectronic redox processes of adsorbed bistable rotaxane under a non-aqueous electrolyte. The positions of the three peaks and their relative amplitudes in the CV are similar to the corresponding peaks in Tseng *et al.*'s work. However, the second anodic peak, which previously appeared at +0.6-0.7 V, was not clearly resolved in our study. This absence is most likely a consequence of the limited potential window afforded by an aqueous electrolyte. The onset of hydroxide formation on gold surfaces starts near +0.6-0.7 V [206], overwhelming a possible second oxidation peak. Similarly, we are not able to probe the redox reactions of the ring that occur below -0.4 V due to the onset of hydrogen evolution. Integrated charge density associated with the second cathodic peak is

$1.84 \mu\text{C}/\text{cm}^2$. Therefore, we calculate that each molecule occupies about $87 \times 87 \text{ \AA}^2$. This area is compared to the $40 \times 40 \text{ \AA}^2$ footprint of a rotaxane with only one disulfide tether [86]. This observation suggests that with the tethers at both ends, the footprint of \mathbf{R}^{4+} is increased because of its adsorption parallel to the surface.

5.3 Results and Discussion

The thread section of the dumbbell is assumed to assemble parallel to the surface [101]. The distance between the two stations (TTF and DNP) in the fully stretched dumbbell would be 36 \AA . *In situ* STM images of the bistable rotaxane molecules adsorbed on Au{111} showed (Figure 5.1B) apparent protrusions $\sim 3 \text{ \AA}$ high and $10\text{-}12 \text{ \AA}$ laterally. No protrusions were observed when a bare gold surface and a control molecule – *i.e.*, the dumbbell compound without the CBPQT⁴⁺ ring – were treated and imaged under identical conditions as for the bistable rotaxane (Figure 5.2). The dumbbell component was apparently not sufficiently conductive to be resolved by STM. However, the CBPQT⁴⁺ rings, having higher electrical conductivity and greater height relative to the dumbbell, appear as protrusions in STM images [43]. The protrusions are therefore assigned to be the CBPQT⁴⁺ rings (Figure 5.1B), consistent with prior STM studies [205].

To study the station changes in \mathbf{R}^{4+} , we imaged the same surface region repeatedly and tracked the positions of protrusions using image processing routines, developed previously [7,20,44,45,47,76,77,207]. The images were corrected for lateral drift and the coordinates were identified by calculating the centroids of the protrusions.

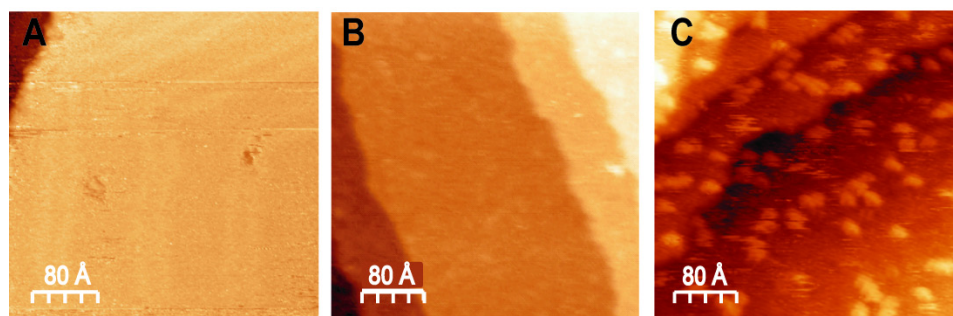


Figure 5.2: Scanning tunneling microscope images of Au{111} under 0.1 M HClO₄ at electrode potential of +0.35 V vs. Ag/AgCl electrode ($V_s = 0.3$ V; $I_t = 2$ pA). **(A)** Control experiment, no molecules (vertical scale: 10 Å); **(B)** dumbbell component of R^{4+} on Au{111} (CH₂Cl₂: 5 sec, 5 μM adsorption) (vertical scale: 15 Å); **(C)** R^{4+} on Au{111}. The protrusions are due to the CBPQT⁴⁺ rings (vertical scale: 20 Å). Imaging conditions: $V_s = 0.3$ V; $I_t = 2$ pA. The Faradaic current was typically less than 10 pA.

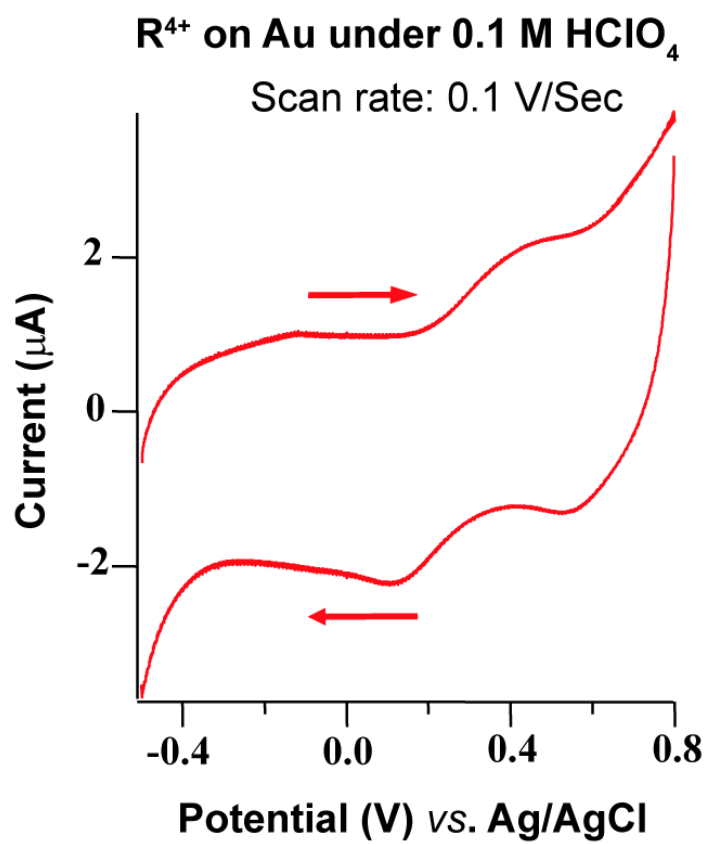


Figure 5.3: Cyclic voltammogram of **R⁴⁺** adsorbed on Au under 0.1 M HClO₄.

Trajectories were determined by minimizing sums of the squares of the displacements. We imaged the molecules at two different electrode potentials, +0.12 V and +0.53 V, for which the TTF station is in the reduced (neutral) state, and in its oxidized (cationic) state, respectively (Figure 5.3). Significant displacements were observed when the potential was stepped from +0.12 V to +0.53 V (vs. Ag/AgCl) and when the potential was returned to +0.12 V. Figure 5.1C,D shows the displacement trajectory (blue arrow) of one such ring. The correlations between the potential change and ring motion suggest that the TTF station becomes positively charged and repels the CBPQT⁴⁺ ring. Subsequently, the potential was stepped down from +0.53 V to +0.12 V and the protrusions underwent further displacements (Figure 5.1D,E; red arrow) suggesting that the CBPQT⁴⁺ ring returns to its thermodynamically more favored position encircling the neutral TTF station [101]. In this example (Figure 5.1C-5.1E), shuttling of the ring between the two positions was $\sim 30 \text{ \AA}$, which corresponds to the approximate distance between the two stations in \mathbf{R}^{4+} . We observed many such motions, but the displacements varied, as described below.

Displacements of all the protrusions arising from the molecules in larger areas ($320 \times 320 \text{ \AA}^2$) of the sample were tracked as station changing was induced by potential steps from +0.12 V to +0.53 V and back (Figure 5.4). The images were superimposed and the protrusion centroids were filtered and correlated with the motions of each CBPQT⁴⁺ ring. The blue and red arrows represent displacements induced by these potential steps (as in Figure 5.1C-E). Figure 5.4 shows a wide range of displacements and angles between the trajectories during first (oxidation) and second (reduction) steps.

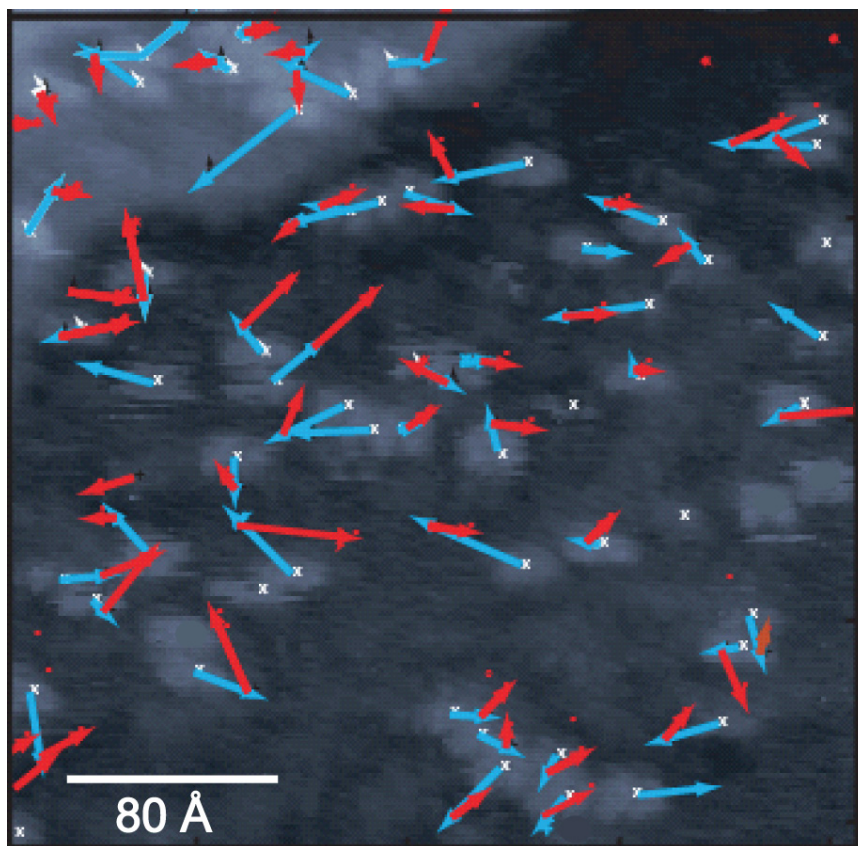


Figure 5.4: A STM image of \mathbf{R}^{4+} adsorbed on Au{111} under 0.1 M HClO₄ solution. The three images with potentials +0.12 V, +0.53 V, and +0.12 V are superimposed and the protrusions on all three images have been marked. The trajectories of a large number of motions of CBPQT⁴⁺ rings after potential steps from +0.12 V to +0.53 V and back to +0.12 V are marked with blue and red lines, respectively, as in Figure 5.1C-E (320 Å × 320 Å).

To understand the motions of CBPQT⁴⁺ rings of **R**⁴⁺ at different potentials, the displacements of a large number of protrusions were plotted in histograms (Figure 5.5). At each potential, the sample was equilibrated for 10 min. The root mean square (rms) displacements observed at +0.12 V and +0.53 V were 5.5 Å and 6.2 Å (Figure 5.5A, 5.5B), respectively. Most of the protrusions remained at the same positions, within the measurement error (3-5 Å), when monitored in successive images under constant potential. A few protrusions (<10) appeared or disappeared between frames, despite appearing in the majority of images; we attribute this observation as most likely the result of conformational changes that reduce the conductance path through the rings to the substrate [20,44]. Here, the rms displacements of more than 90% of molecules are equal to or less than the distance between the two stations in the fully stretched model of **R**⁴⁺, and thus, could be accounted for and attributed to the station changes.

Histograms of displacement with oxidation steps (Figure 5.5C) showed a wide range of values (0-55 Å). The rms displacement was 20 Å, smaller than the distance between two recognition sites (36 Å) in a fully extended bistable rotaxane. Several factors influence the observed displacements. The wide distribution of values suggests the flexible nature of the dumbbell, along which the ring moves. The segment between the two stations (Figure 5.1A) is flexible because of the presence of ethyleneglycol chains, and thus, it is likely to deviate from a linear conformation. On account of bending of the center segment between the TTF and DNP stations, the average displacement of the ring is expected to be smaller than 36 Å. In addition, conformational changes in the dumbbell and tethers would change the apparent ring displacement. A fully extended side segment is 20 Å long (Figure 5.1A) and with wagging of this segment

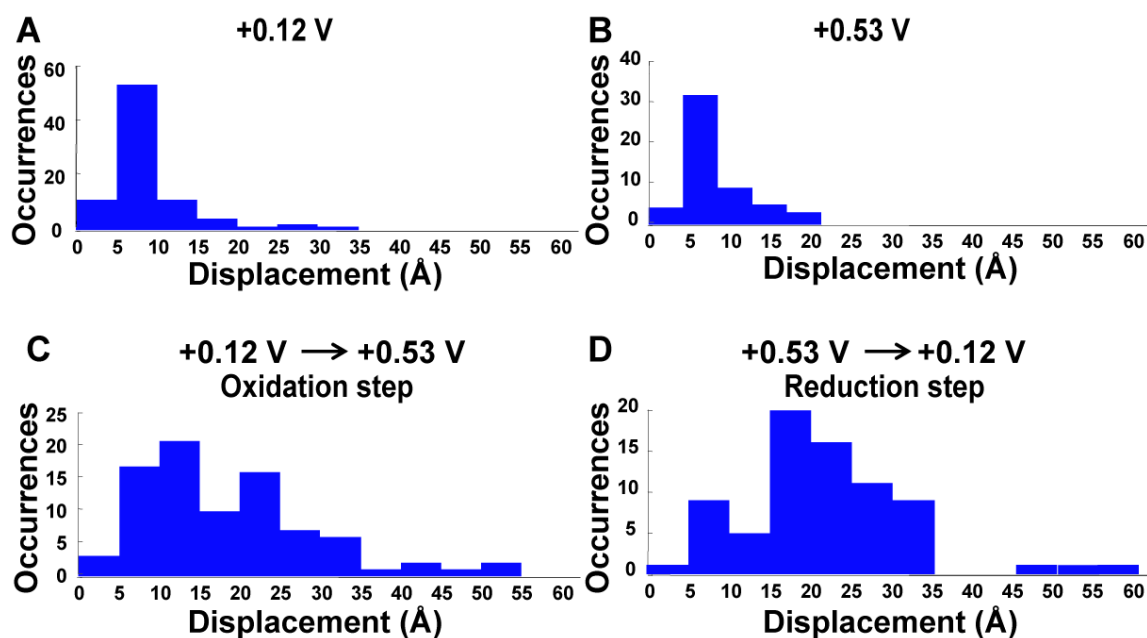


Figure 5.5: Histogram of measured displacements of protrusions over 10 min at different potentials. **(A)** The surface was equilibrated at +0.12 V; **(B)** the surface was equilibrated at +0.53 V; **(C)** the potential was stepped from +0.12 V to +0.53 V and displacements were measured by comparing images acquired before and after the potential step; **(D)** the potential was stepped back from +0.53 V to +0.12 V and again the displacements were measured.

around the thiolate tethers can shift the stations by up to 20 Å. Therefore, we anticipate ring displacements to be 0-56 Å, consistent with the observed range. Conformational changes in the dumbbell component could be induced by the interplay of forces in which the electrochemically driven station changing competes with the π -electron interactions of one of the bipyridinium units in the CBPQT⁴⁺ with the substrate. The result of these forces could be conformational changes in the dumbbell and/or displacement of the thread section of the dumbbell. (If the dumbbell were fully stretched or was rigid by design, this would not be possible.)

Displacements are relatively smaller where the molecules are clustered. Previously, ensemble studies showed that the speed of switching was reduced dramatically when bistable rotaxanes were placed in condensed monolayers or gel matrices [66]. Nonetheless, adsorbed rotaxane molecules can block ion adsorptions, and, in changing state, could lead to coordinated mechanical strain [200] as well as significant changes in optical properties if deliberately assembled on appropriate substrates [208].

By stepping back the potential to +0.12 V (reduction step), a wide range of displacements was once again observed. The rms displacement of 16 Å is within the measurement error of the 20 Å displacement observed during the oxidation step. To understand the correlations between the two sets of motions, we calculated the angles between the trajectories during the first (oxidation) and second (reduction) steps. The angles of the second trajectories were measured and it was found that 75% of the angles are between 90° and 270° (Figure 5.6). By contrast, random walks would not display such anticorrelated directions. By controlling the oxidation state of the TTF units, the CBPQT⁴⁺ rings on individual molecules can be driven back and forth between stations.

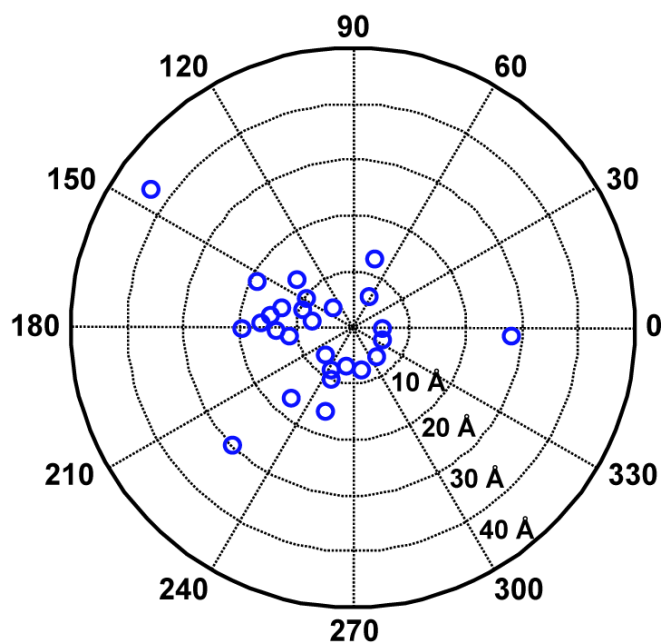


Figure 5.6: Polar graph of displacement vectors after the potential step from +0.53 V to +0.12 V. The angle is referenced against the trajectories after the potential was stepped from +0.12 V to +0.53 V. The angular distribution suggests that the protrusions have the tendency to move in opposite directions when molecules are reduced back to the original state.

Although STM has not directly visualized the stations on the dumbbells, the reversibility provides evidence that electrochemical station changing is driving the motion of the rings. Because of the flexibility of the dumbbells, one does not expect most of the CBPQT⁴⁺ rings to move back and forth between fixed positions.

5.4 Conclusions and Future Directions

Using ECSTM, we observed electrochemically controlled station changes of individual bistable rotaxane molecules *in situ*. Motions of the CBPQT⁴⁺ rings were correlated with redox states of the TTF station and displayed partial reversibility. The trajectories of the rings suggest that once a bistable rotaxane molecule is adsorbed on a surface, the motion of the CBPQT⁴⁺ ring relative to the dumbbell is affected by its local environment and the flexibility of the molecule. Such insights are important for nanoelectromechanical and nanoelectronic devices based on mechanically interlocked compounds. Bistable rotaxane molecules with *rigid* dumbbells should enable consistent and fully reversible motions, as well as direct visualization of the rings *and* the shafts of the molecules. The molecular design and synthesis of such systems are underway.

Chapter 6

MANIPULATION OF DOUBLE-DECKER PHTHALOCYANINE MOLECULES ON HOPG

6.1 Introduction

Precise control of molecular assemblies on substrates is central for development of molecular-scale devices. The formation and characterization of ordered adlayers of porphyrin and/or phthalocyanine (Pc) based DD molecules on metal surfaces are key elements in building functional arrays of DD-based molecular rotors. In this chapter, we demonstrate the ability to control molecular placement in DD arrays using phthalocyanine (Pc) as bottom ligands on highly oriented pyrolytic graphite (HOPG) substrates. We used the STM probe tip to manipulate single DD molecules.

In the last decade, substantial efforts have been made in synthetic and self-assembly techniques that have resulted in increasingly sophisticated supramolecular structures [64,93,209,210]. Sandwich complexes such as DD molecules, where Pc and porphyrins (Por) are connected by rare-earth cations, and are promising candidates for controlled arrays of molecular switches [14] and molecular motors [12,211] because of their unique photophysical and redox properties in the solution phase [24]. Molecular orientation and positions of these DD molecules in crystalline thin films are important for the control of the physical and chemical properties of the films. Double-deckers can also be used to realize coupled single-molecule devices by employing single-molecule manipulation and recognition techniques [212].

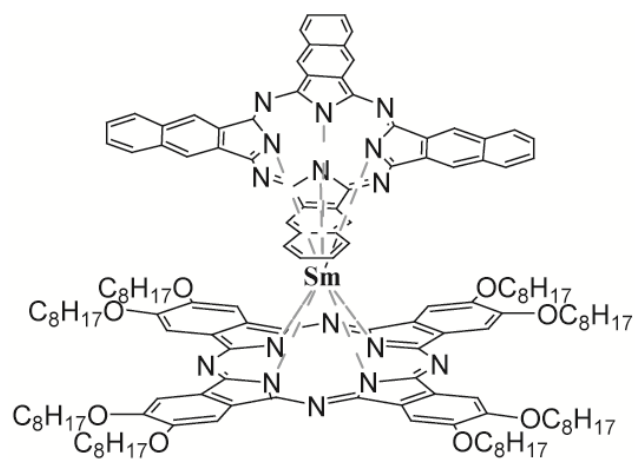
Scanning tunneling microscopy has been utilized to characterize well-ordered arrays of homoleptic DD molecules with octakis(octyloxy)phthalocyaninato ligands, where the periodicity was regulated by the surrounding alkyl chains [213-215]. Long alkyl chains are added to the molecular periphery to immobilize DD molecules on HOPG surfaces [216-223]. Previously, heteroleptic DD molecules with long alkyl chains surrounding the bottom ligands were observed, and isolation of the DD molecules was also demonstrated [224,225]. Ye *et al.* [225] changed the size of the top ligand of the DD molecules to vary the intermolecular distances to study surface structure and their interactions.

In this chapter, we controlled the molecular orientation of naphthalocyanine- (Nc) and Pc-based DD molecular arrays on HOPG. Two-dimensional arrays of DD molecules (Nc)Sm[Pc(OC₈H₁₇)₈] were physisorbed on substrates using metal-free H₂Pc(OC₈H₁₇)₈ as the bottom ligand and were imaged using room-temperature liquid-cell STM. Previously, the STM probe tip has been used to manipulate large molecules at room temperature [226,227]. Here, we demonstrate the STM probe tip lateral manipulation (LM) of single DD molecules in arrays that can be utilized to move and to arrange DD molecules to form defined structures.

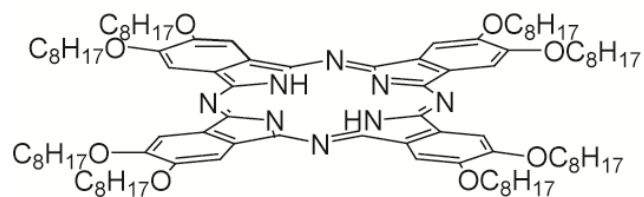
6.2 Experimental Procedure

6.2.1 Sample Preparation

Metal-free H₂Pc(OC₈H₁₇)₈ and heteroleptic double-decker complexes (Nc)Sm[Pc(OC₈H₁₇)₈] were synthesized according to published procedures by our



(Nc)Sm[Pc(OC₈H₁₇)₈]



Pc(OC₈H₁₇)₈

Scheme 6.1: Molecular structures of double-decker molecule (Nc)Sm[Pc(OC₈H₁₇)₈] (upper) and Pc(OC₈H₁₇)₈ (lower). Nc = naphthalocyanine; Pc = phthalocyanine.

collaborators at Shandong University, China [228-231]. The double-decker molecules were dissolved in 1-phenyloctane. For the co-adsorption experiments, the total concentration was kept in the range of 1-10 μM . A solution was prepared with two parts 50% saturated $\text{Pc}(\text{OC}_8\text{H}_{17})_8/\text{PhC}_8\text{H}_{17}$ and one part $(\text{Nc})\text{Sm}[\text{Pc}(\text{OC}_8\text{H}_{17})_8]/\text{Pc}(\text{OC}_8\text{H}_{17})_8$ (1:10). The graphite (HOPG, ZYA, 10 mm \times 10 mm, GE Advanced Ceramics, Strongsville, OH) was immersed under 20-30 μL of solution contained in a Teflon liquid cell. The sample under the solution was annealed at 50 $^\circ\text{C}$ before cooling down to 30 $^\circ\text{C}$.

6.2.2 Scanning Tunneling Microscopy

The STM observations and manipulations were carried out on a liquid cell Pico SPM microscope head (Molecular Imaging) controlled by a low-noise analog controller (SPM 1000, RHK Technology). All STM images were recorded under constant-current mode at -0.5 V sample bias voltage, and tunneling currents of 1-2 pA under 1-phenyloctane solution on HOPG. A mechanically cut Pt-Ir (80%-20%) wire was used as the STM tip. All the horizontal scales of the STM images were calibrated using the hexagonal lattice of HOPG ($a = 0.246$ nm) and all the vertical scales of the STM images were calibrated with monoatomic steps of HOPG ($c/2 = 0.34$ nm).

Lateral manipulation by the STM is used to relocate atoms/molecules across the surface. A typical LM procedure involves three steps: (1) vertical approach of the STM probe tip toward the target molecule, (2) moving the tip parallel to the surface to move the molecule under the influence of the tip, and (3) retracting the tip back to the normal imaging height thereby the molecule is left at the final location on the surface [232,233]. We employed the RHK *manipulation* feature to manipulate the DD molecules. The STM

tip-substrate distance (z) was decreased as compared to the imaging condition tip-substrate distance by increasing the tunneling current (I_t) and/or decreasing the sample bias voltage (V_s). An oscilloscope was used to profile the changes in z during manipulation. A cut-off current was set to trigger the oscilloscope acquisition during each manipulation. During the process, the probe tip was moved to *push* the molecules within the path of the tip (*vide infra*).

6.3 Results and Discussion

6.3.1 Structure of the Thin Films

The structures of $\text{H}_2\text{Pc}(\text{OC}_8\text{H}_{17})_8$ and $(\text{Nc})\text{Sm}[\text{Pc}(\text{OC}_8\text{H}_{17})_8]$ are shown in Scheme 6.1. Scanning tunneling microscope topographic images of thin films of a mixture of $\text{H}_2\text{Pc}(\text{OC}_8\text{H}_{17})_8$ and $(\text{Nc})\text{Sm}[\text{Pc}(\text{OC}_8\text{H}_{17})_8]$ on HOPG are shown in Figure 6.1. A $\text{H}_2\text{Pc}(\text{OC}_8\text{H}_{17})_8$ monolayer forms a well-ordered quasi-hexagonal and square lattice, with lattice constants of 2.5 ± 0.1 nm, consistent with earlier observations [225] (Figure 6.1A). The thin film shows two types of protrusions with apparent height differences of 0.3 – 0.4 nm. A square lattice of 3.0 ± 0.1 nm was observed in the more protruding domains (Figure 6.1A). The less protruding area is assigned as $\text{H}_2\text{Pc}(\text{OC}_8\text{H}_{17})_8$ and the more protruding area is assigned as DD molecules. Figure 6.1B shows an area of the mixed monolayer with DD molecules. Most of the isolated DD molecules were in registry with the surrounding $\text{H}_2\text{Pc}(\text{OC}_8\text{H}_{17})_8$ lattice and the bottom of the $\text{Pc}(\text{OC}_8\text{H}_{17})_8$ ligand of the DD is parallel to the $\text{H}_2\text{Pc}(\text{OC}_8\text{H}_{17})_8$ matrix. The film of mixed monolayer is stable and does not rearrange or degrade at these imaging conditions

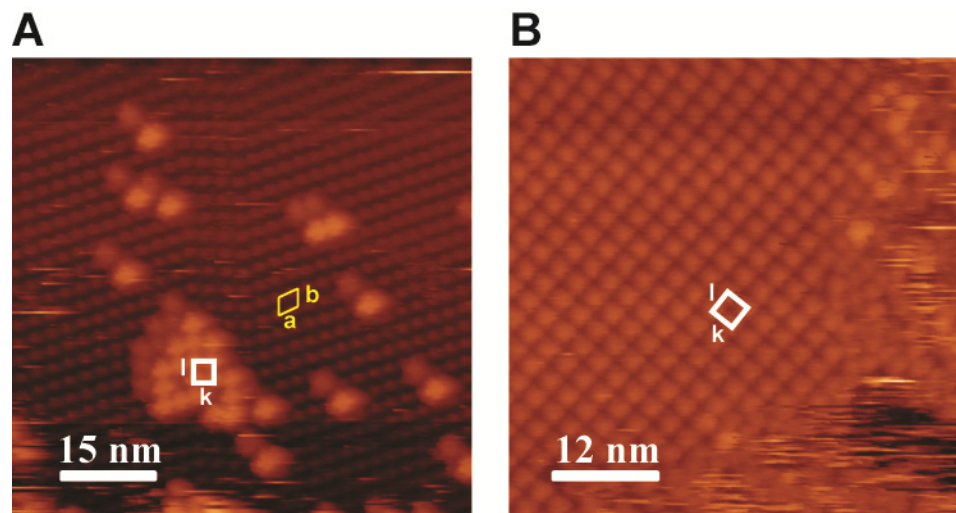


Figure 6.1: (A) Topographic STM images of thin films of a mixture of $\text{H}_2\text{Pc}(\text{OC}_8\text{H}_{17})_8$ and $(\text{Nc})\text{Sm}[\text{Pc}(\text{OC}_8\text{H}_{17})_8]$ on HOPG. (B) An area of the mixed monolayer occupied with DD molecules. Dark areas correspond to $\text{H}_2\text{Pc}(\text{OC}_8\text{H}_{17})_8$, lattice constants: $a = 2.5 \pm 0.1$ nm and $b = 2.4 \pm 0.1$ nm. Lighter areas correspond to DD molecules: lattice constants: $l = 3.0 \pm 0.1$ nm and $k = 3.0 \pm 0.1$ nm. Imaging conditions: $V_s = -0.5$ V and $I_t = 2$ pA.

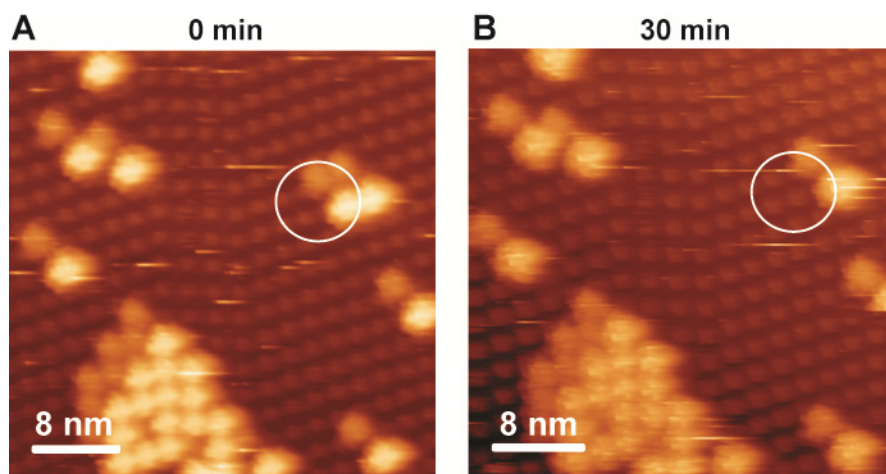


Figure 6.2: With time (30 min), few changes in the mixed monolayer of DD and $\text{H}_2\text{Pc}(\text{OC}_8\text{H}_{17})_8$ molecules were observed in STM images ($I_t = 2 \text{ pA}$; $V_s = -0.5 \text{ V}$). Circles show one desorbed molecule.

Oscilloscope traces for z-position and current

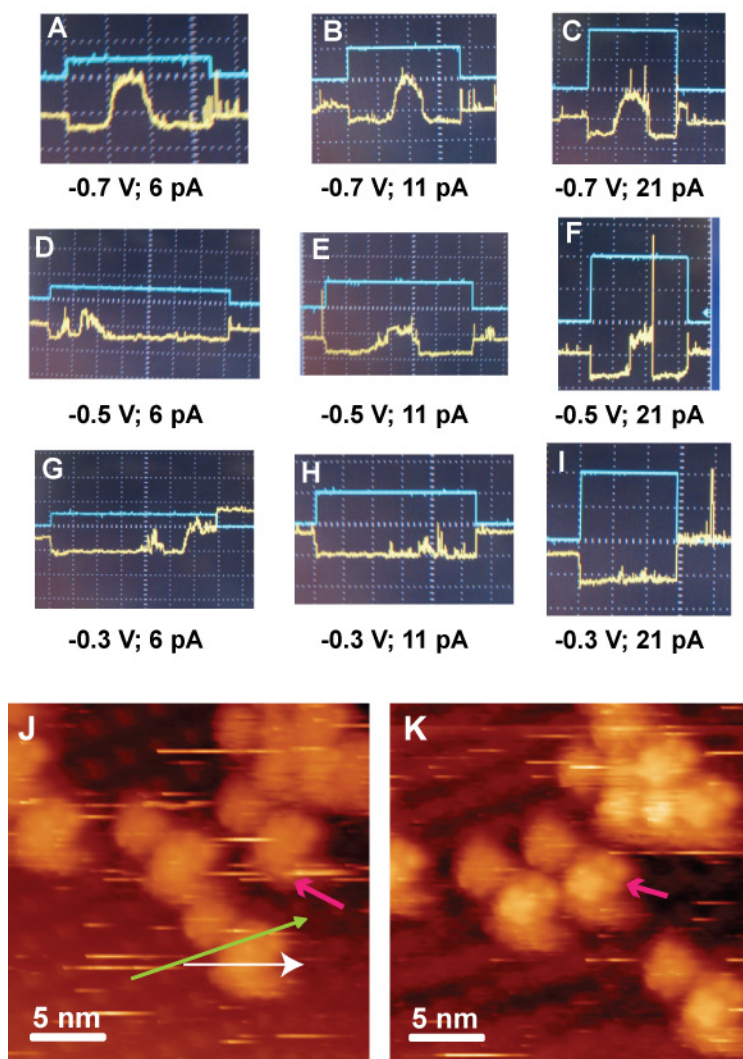


Figure 6.3: A-I. Oscilloscope traces for the STM tip-sample distance (yellow) and tunneling current (blue) during the manipulation step of molecules. The corresponding sample bias voltage and current values are given as (V_s ; I_t). **J.** Mixed monolayer of DD and $H_2Pc(OC_8H_{17})_8$ molecules on HOPG. The green arrow is the direction of tip movement with $(-0.3 \text{ V}; 21 \text{ pA})$. The molecule being manipulated moved along the white arrow. **K.** Image of the area after manipulation. Another molecule was pushed upward (pink arrows). Imaging conditions: $V_s = -0.5 \text{ V}$ and $I_t = 2 \text{ pA}$.

($V_s = -0.5$ V; $I_t = 2$ pA). Figure 6.2 shows two images of the same scan area recorded with a 30 min time difference. After 30 min of imaging under 1-phenyloctane, there is no change in the monolayer, except one desorbed molecule (Figure 6.2, in circle). We believe that the molecule desorbed into the 1-phenyloctane solution.

6.3.2 STM Probe Tip Manipulation of Molecules

We used the STM probe tip to manipulate the physisorbed DD molecules on HOPG. To manipulate the molecules on the surface, we increased the tunneling current and/or decreased the sample bias voltage to bring the probe tip closer to the surface, as compared to the imaging conditions. When the probe tip-substrate distance is smaller than the height of the molecule on the surface, the probe tip is buried into the molecular layer. In this manipulation condition, when the probe tip is moved, it also moved the molecules within its path. To explore the conditions needed to manipulate molecules, we varied the tunneling parameters. Figure 6.3 shows the optimum condition for manipulation for this system ($V_s = -0.3$ V; $I_t = 21$ pA). To monitor the manipulation steps, we employed an oscilloscope to track the tunneling current (Figure 6.3A-6.3I, blue traces). Another trace (yellow) is used to track the motion of STM probe tip in perpendicular direction to the surface, which is happening due to changes in probe tip-substrate distance. Images recorded before and after the manipulation steps were compared.

We started with a lateral manipulation conditions of $V_s = -0.7$ V; $I_t = 5$ pA (Figure 6.3A). The blue trace went up, showing the increase in current from the imaging tunneling current (2 pA) to the manipulation tunneling current (5 pA). The probe tip

moved closer to the surface and we can observe a corresponding decrease in the yellow trace (Figure 6.3A). With this condition, we moved the probe tip in the direction shown in Figure 6.3J along the green line. After this step, we did not observe any change in the imaged area (i.e., manipulation did not move the molecule). We also observed a broad peak-like structure in the yellow trace (Figure 6.3A), which appeared due to the probe tip moving upward and crossing above the molecule; hence, the manipulation conditions were not strong enough to move the molecule coming into the path of the tip. We continued to increase the current and decrease the bias voltage in order to bring the probe tip closer to the surface (shown in Figure 6.3A-6.3I). Only with the conditions of $V_s = -0.3$ V and $I_t = 21$ pA did we not observe any peak-like structure in the yellow trace, and the STM image showed that the molecule moved (Figure 6.3K). Thus, this manipulation condition is sufficient to move the molecule coming into the path of the tip. With this, we established that at the conditions of $V_s \leq -0.3$ V and $I_t \geq 21$ pA, we could manipulate the DD molecules on HOPG. All the molecules appeared as if paired together due to a double tip feature. All images, henceforth, given in this chapter possess this feature.

The mechanism of LM of molecules or atoms using a STM probe-tip interaction has been categorized as three basic modes, “pushing”, “pulling”, and “sliding” [232]. In the pushing mode, repulsive tip-molecule interaction drives the molecule to move in front of the tip. In the pulling mode, the molecule follows the tip due to an attractive tip-molecule interaction. In the sliding mode, the atom is virtually bound or trapped under the tip and it moves across the surface together with the tip.

During the stepwise exploration for effective LM conditions, we tracked the changes in the current and tip-substrate distance using an oscilloscope. In the weak LM condition in Figure **6.3A-6.3C**, we observed an increase in the tip-substrate distance (peak in yellow traces). We believe that the tip-molecule interactions during these steps were not generating sufficient lateral force to overcome the hopping barrier of the DD molecule in the matrix of $\text{H}_2\text{Pc}(\text{OC}_8\text{H}_{17})_8$. The probe tip followed the contour of the molecule while crossing over the molecule without moving or desorbing it. Since, the electrons are tunneling through a more conducting DD molecule, the tip retracts to maintain the current and cross over the molecule, generating a peak in the yellow trace. Only in the LM step shown in Figure **6.3J**, the interactive force is strong enough to overcome the hopping barrier of the molecule and thus move the molecule. During this successful LM step, the tip does not cross over the molecule and we did not observe any peak in the yellow trace. We also observed that instead of following the probe tip manipulation direction (green arrow), the molecule moved along the direction of the white arrow. The independent motion in the molecule may occur due to the *pushing* mode manipulation, where the repulsive tip-molecule interaction drives the molecule in front of the tip. Therefore, the molecule is not bound to follow the tip trajectory and is presumably guided by the underlying $\text{H}_2\text{Pc}(\text{OC}_8\text{H}_{17})_8$ matrix [234,235]. We hypothesize that the DD molecules only moved along the lattice directions or along the domain boundaries within the $\text{H}_2\text{Pc}(\text{OC}_8\text{H}_{17})_8$ lattices. During the intermediate steps (Figure **6.3D-6.3H**), the molecule did not move, however, we do not observe a clear peak in the yellow trace, either. More experiments are needed to understand the tip-molecule interactions during these intermediate steps.

6.3.2.1 Detaching Molecules from an Island using Probe Tip Manipulation

After exploring the optimal conditions for manipulating the DD molecules, we detached a DD molecule from an island of DD molecules with $V_s = -0.3$ V and $I_t = 21$ pA. Figure 6.4B shows the path of probe tip used to manipulate the island. One molecule (black circle in Figure 6.4B) broke out of the island due to 2D desorption of the molecules between the molecule and the island (black arrows). The oscilloscope trace for the z shows a small, broad peak-like signal (Figure 6.4A, yellow trace) due to the probe tip moving above the corner molecule in the island (pink arrow). The probe tip could not move the corner molecule under the above LM conditions. This indicates that the corner molecule is strongly attached to the island and a larger repulsive force is required to successfully *push* it. Again, all of the molecules shown in the images appear as “pairs” due to the double-tip feature.

6.3.2.2 Splitting and Combining a Pair of Molecules Using Probe Tip Manipulation

Probe tip manipulation can also be used to split or to combine a pair of molecules. Figure 6.5A and 6.5B shows the splitting of a pair of molecules. The probe tip was placed in between molecules **1** and **2** with LM conditions of $V_s = -0.1$ V and $I_t = 21$ pA and the probe tip was moved along the path of the green arrow, as shown in Figure 6.5A. The molecules become separated after this step (Figure 6.5B), however, the direction of motion was not along the tip trajectory (green arrow). The probe tip *pushed* only molecule **2**, but we observed that molecules **1** and **2** moved in opposite directions, along

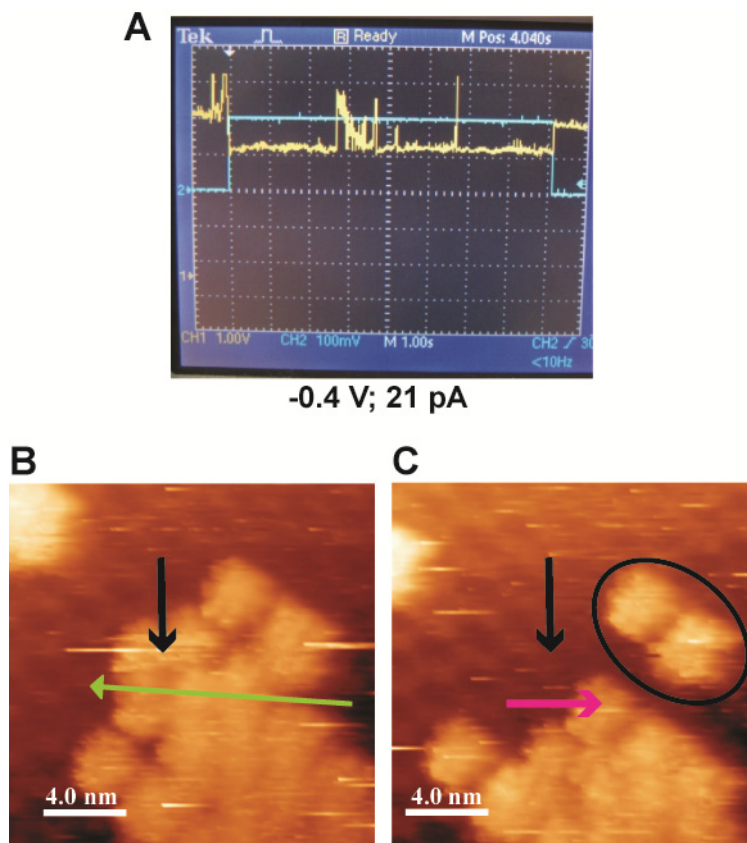


Figure 6.4: **A.** Oscilloscope traces for the manipulation of an island of DD molecules. Manipulation condition was $V_s = -0.3$ V; $I_t = 21$ pA. **B.** Island of DD molecules is manipulated using STM. The probe tip moved along the green arrow, breaking the island. **C.** Circled molecule broke away from island. A few molecules desorbed after manipulation (black arrows). Molecule with pink arrow stayed intact with the island. Imaging conditions: $V_s = -0.5$ V and $I_t = 2$ pA.

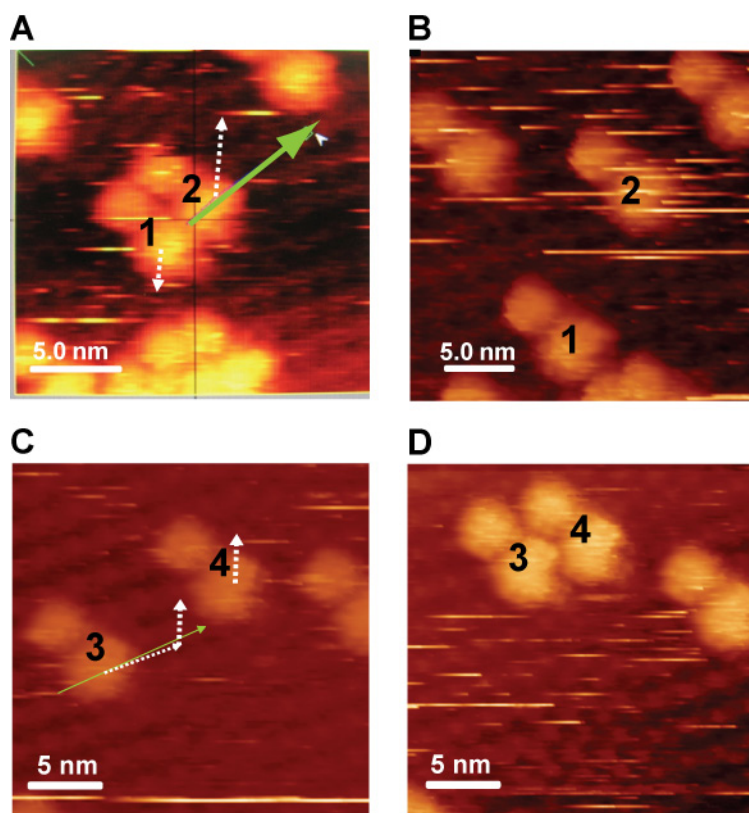


Figure 6.5: A pair of DD molecules is split and combined using manipulation ($V_s = -0.1$ V and $I_t = 21$ pA). **A-B.** The probe tip is placed between the molecules and the manipulation step was applied to split the pair. The probe tip was moved along the green arrow. However, the molecules **1** and **2** moved along the white arrows. **C-D.** Molecule **3** was manipulated to form a pair with **4**. The probe tip was moved along the green line. However, **3** moved along the white lines and pushed **4**, as shown in **6.5C**. Imaging conditions: V_s -0.5 V and $I_t = 2$ pA.

the white arrows. Again, the molecule is not bound to follow the tip trajectory and is moved along the lattice directions or along the domain boundaries within the $\text{H}_2\text{Pc}(\text{OC}_8\text{H}_{17})_8$ lattices [234,235].

We manipulated two molecules to combine them as a pair (Figure **6.5C** and **6.5D**). The tip trajectory is shown by the green arrow and the molecular movements by the white arrows. Together with the motion of molecule **3**, we also observed the molecule **4** move upwards (as depicted). It is not clear if the motion of molecule **4** is triggered due to the impact with molecule **3** or due to repulsive interaction with the probe tip. Directions traced by **3** and **4** were again along the lattice directions of the $\text{H}_2\text{Pc}(\text{OC}_8\text{H}_{17})_8$ lattice.

6.4 Conclusions and Future Directions

In this chapter, we demonstrated that DD molecules can be moved on HOPG under 1-phenyloctane using the STM probe tip. We manipulated two molecules together and split a pair of molecules. Using the LM technique, molecules can be assembled in different geometries. The DD molecules have rotating tops that can be interlocked by placing them next to each other, restricting rotation or transducing rotation like a set of gears [26,196,236,237]. The nature of forces involved in the LM process and the mechanism of the molecule movements need to be explored in more detail.

Chapter 7

CONCLUSIONS AND FUTURE PROSPECTS

This dissertation focused on the design of molecules and their assemblies on substrates for understandings and applications in molecular devices. Chapter 1 provided an introduction to SAM assemblies and STM instrumentation. In Chapters 2 and 3, we controlled the photo-induced isomerization of single azobenzene-functionalized molecules isolated in tailored decanethiolate SAM matrices on Au{111}. We prepared 1D chain structures of these molecules and studied their switching with photons and electrons. Switching of assemblies provided understanding about electron transfer along electronically coupled molecular chains. In Chapters 4 and 5, we studied rotaxane molecules, which behave as artificial muscles. We created nanoscale assemblies of these artificial molecules to generate forces at the microscale. Motion of single rotaxane molecules was studied using ECSTM to understand how they move and to improve the design of the molecules for more efficient work generation. In Chapter 6, we controlled the placement of double-decker molecules using STM probe tip lateral manipulation.

7.1 Switching of Single Molecules and Their One-Dimensional Assemblies

The work in this dissertation represents a contribution towards the understanding of switching of azobenzene-functionalized molecules (**1**) at a single-molecule level as well as in 1D assemblies. The work on molecule **1** has been performed in collaboration with the Tour group at Rice University, who synthesized the molecules, as well as with

the Crespi group at Penn State University, who performed theoretical calculations on our system. In Chapter 2, photo-induced isomerization of isolated single molecules of **1** was achieved. We engineered the design of the molecule to suppress excited-state quenching from the metal substrate and to form rigid assemblies of single tethered **1** molecules in the domains of the monolayer to limit steric constraints, as well as tip-induced and stochastic switching effects. We demonstrate a controlled reversible photoisomerization of single molecules between *trans* and *cis* conformations by exposure to UV and visible light. We imaged the *trans* and *cis* conformations using STM and assigned them to the ON and OFF states of the molecule, respectively.

We prepared 1D chain structures of **1** molecules in the domain boundaries of a decanethiolate SAM matrix on Au{111}. We switched the chain structures from *trans* to *cis* using UV light and observed that the molecules in the chain isomerize in concert. This concerted switching was attributed to the electronic coupling between the molecules within the chains. To demonstrate the extent of the electronic coupling, we employed a STM probe tip for electron-induced isomerization of azobenzenes. We induced the isomerization at one end of the chains and observed the isomerization of the entire >100 Å long chains. The tunneling electrons supplied at one end of the chain, delocalize along the 1D structure, and induce isomerization of all the molecules in the chain. We hypothesized that π -orbital overlap of the molecules in the 1D structures enables the electrons to delocalize along the chain, like a conductor. To understand this phenomenon in greater detail, theoretical calculations are being performed.

The work described in Chapters 2 and 3 has resulted in the following publications:

Reversible Photo-Switching of Single Azobenzene Molecules in Controlled Nanoscale Environments, A. S. Kumar, T. Ye, T. Takami, B. C. Yu, A. K. Flatt, J. M. Tour, and P. S. Weiss, *Nano Letters* **8**, 1644-1648 (2008).

Electronic Dominoes: Transport through Assembled One-Dimensional Supramolecular Wires, A. S. Kumar, B. K. Pathem, D. A. Corley, T. Ye, V. J. Aiello, V. H. Crespi, J. M. Tour, and P. S. Weiss, in preparation.

Quenching of the excitation responsible for isomerization of the azobenzene moiety is observed to reduce by lifting the moiety off the substrate and by minimizing the conductivity of the tether [20,71]. To this end, B. K. Pathem is working on systematically varying the conductivity of the tethers and studying the efficiency of photo-isomerization of the azobenzene moiety. Initial results confirm our hypothesis that photo-isomerization is suppressed when the conductivity of the tether is increased sufficiently. In future, a tether with intermediate conductivity will be employed to investigate the role of tether conductivity on photo-isomerization. This molecule will have a phenyl ring attached to the azobenzene moiety. The phenyl ring has an approximately 30° twist angle with respect to the normal axis, thereby decreasing the degree of π -conjugation and thus decreasing the extent of conductivity through the molecule as compared to a fully conjugated system. This molecule is being synthesized by the Tour group at Rice University. Theoretical calculations for estimating the difference in conductivity of the tethers are being performed by the Jensen group at Penn State University. Correlation of the experimentally observed switching efficiency with the calculated conductivity of the tethers will give a quantitative determination of the role of the tethers in photo-isomerization.

In order to map the roles of collective effects in molecular motion or structural phase transitions in 2D, we need to overcome the problem of steric hindrance in the lattice. For future experiments, we have designed cage, especially adamantanetrithiol-based, molecules functionalized with azobenzenes to create space around each azobenzene unit thereby providing sufficient spatial freedom for switching of the entire monolayer [238,239]. Also, the adamantyl cage would be expected to decouple the azobenzene moiety electronically from the substrate, thereby improving switching efficiency. This molecule is being synthesized by the Tour group at Rice University. Photo-induced isomerization studies should be conducted on these molecules and their switching efficiencies should be compared with that of molecule **1** and molecules with more conducting tethers.

The 1D chain structures can be grown easily, however, further work is required to develop control over their placement on substrates, as well as their lengths. Currently, V. J. Aiello is working to expand the library of molecules that can be assembled as molecular chains in a variety of host matrices. To understand the propagation of electrons in the 1D chains of azobenzenes, different molecules with similar structural properties, yet different electronic properties, such as stilbene, will be mixed in the chain structure [75,240-242]. Electron-induced isomerization experiments in such mixed chains may reveal the pathways of electron travel along the chains.

7.2 Rotaxane: An Artificial Muscle Molecule

The structure of specially designed rotaxane molecules, model systems for an artificial muscle, can be changed reversibly between two (or more) stable states via redox reactions [22,86,194,203]. In Chapter 4, we used the electrochemically-induced nanoscale motion within the molecule to generate *microscale* motions by arranging them to work in unison. We assembled these molecules on microscale levers to produce forces that bend the levers reversibly and to generate microscale motion. Compared with their chemically-driven counterparts, the electrochemically-driven molecular-muscle-based actuators can be operated much faster, more conveniently, and with larger responses. The use of cooperative forces generated by these artificial molecular muscles constitutes a seminal step toward molecular-machine-based nanoelectromechanical systems.

In order to control motion and orientation, in Chapter 5, we controlled the conformational changes in rotaxanes at the single-molecule level using ECSTM, and observed that conformational changes correlate with the known redox states of rotaxanes. The mechanical motions of these interlocked molecules are influenced by their interactions with the surface and with neighboring molecules, as well as by conformations of the thread component.

The work described in Chapters 4 and 5 has resulted in the following publications:

A Mechanical Actuator Driven Electrochemically by Artificial Molecular Muscles, B. K. Juluri, A. S. Kumar, Y. Liu, T. Ye, Y. W. Yang, A. H. Flood, L. Fang, J. F. Stoddart, P. S. Weiss, and T. J. Huang, *ACS Nano* **3**, 291-300 (2009).

Changing Stations in Single Bistable Rotaxane Molecules under Electrochemical Control, T. Ye, A. S. Kumar, S. Saha, T. Takami, T. J. Huang, J. F. Stoddart, and P. S. Weiss, submitted for publication.

In future, bistable rotaxane molecules with *rigid* dumbbells should be studied to enable consistent and fully reversible motions, as well as for the direct visualization of the rings *and* the shafts of the molecules. The molecular design and synthesis of such systems are underway by the Stoddart group at Northwestern University. The rigid backbone will also help us align the molecules in specific directions thereby generating greater force in actuation applications.

7.3 Double-Decker Rotors

Double-decker molecules, having two parallel porphyrin or phthalocyanine rings connected by rare earth metal cations, were assembled on HOPG to study both rotary motion dynamics of isolated DDs, and the collective interactions of ensembles whose rotors interact as intermeshed gears. In Chapter 6, we demonstrated the STM probe tip lateral manipulation of single DD molecules in arrays that can be utilized to move and to arrange DD molecules to form defined structures. Using this manipulation technique, molecules can be assembled in different geometries. In future work, better control over the DD molecules, having a rotating top, should be developed to interlock molecules by placing them next to each other, thereby restricting rotation or transducing rotation like a set of gears.

7.4 Concluding Remarks

The research described in this dissertation is primarily related to the design of molecules and their assemblies on substrates for their application in molecular electronics and molecular motors. Novel instrumentation was employed to induce and to understand

motion, structural changes, and electronic changes in single molecules and their assemblies. Our results have elucidated new directions for the development of future electronic circuitry, and have revealed new factors that strongly affect the behavior of surface-bound molecules. The results presented here demonstrate the continued importance of self-assembly as a host matrix to support a bottom-up method of constructing nanoscale machineries.

REFERENCES

- [1] J. V. Barth, G. Costantini, and K. Kern, *Engineering Atomic and Molecular Nanostructures at Surfaces*, *Nature* **437**, 671-679 (2005).
- [2] B. L. Feringa, *The Art of Building Small: From Molecular Switches to Molecular Motors*, *Journal of Organic Chemistry* **72**, 6635-6652 (2007).
- [3] V. Balzani, A. Credi, F. M. Raymo, and J. F. Stoddart, *Artificial Molecular Machines*, *Angewandte Chemie-International Edition* **39**, 3349-3391 (2000).
- [4] R. A. Bissell, E. Cordova, A. E. Kaifer, and J. F. Stoddart, *A Chemically and Electrochemically Switchable Molecular Shuttle*, *Nature* **369**, 133-137 (1994).
- [5] M. Gomez-Lopez, J. A. Preece, and J. F. Stoddart, *The Art and Science of Self-Assembling Molecular Machines*, *Nanotechnology* **7**, 183-192 (1996).
- [6] C. Joachim, J. K. Gimzewski, and A. Aviram, *Electronics Using Hybrid-Molecular and Mono-Molecular Devices*, *Nature* **408**, 541-548 (2000).
- [7] P. S. Weiss, *Functional Molecules and Assemblies in Controlled Environments: Formation and Measurements*, *Accounts of Chemical Research* **41**, 1772-1781 (2008).
- [8] C. M. Niemeyer, *Progress In "Engineering Up" Nanotechnology Devices Utilizing DNA as a Construction Material*, *Applied Physics A - Materials Science & Processing* **68**, 119-124 (1999).
- [9] E. R. Kay, D. A. Leigh, and F. Zerbetto, *Synthetic Molecular Motors and Mechanical Machines*, *Angewandte Chemie-International Edition* **46**, 72-191 (2007).
- [10] A. M. Moore and P. S. Weiss, *Functional and Spectroscopic Measurements with Scanning Tunneling Microscopy*, *Annual Review of Analytical Chemistry* **1**, 857-882 (2008).
- [11] K. Kinbara and T. Aida, *Toward Intelligent Molecular Machines: Directed Motions of Biological and Artificial Molecules and Assemblies*, *Chemical Reviews* **105**, 1377-1400 (2005).
- [12] G. S. Kottas, L. I. Clarke, D. Horinek, and J. Michl, *Artificial Molecular Rotors*, *Chemical Reviews* **105**, 1281-1376 (2005).

- [13] V. Balzani, M. Venturi, and A. Credi, *Molecular Devices and Machines: A Journey into the Nanoworld* (Wiley-VCH, 2003).
- [14] B. L. Feringa, *Molecular Switches* (Wiley-VCH, Weinheim, Germany, 2001).
- [15] V. Bermudez, N. Capron, T. Gase, F. G. Gatti, F. Kajzar, D. A. Leigh, F. Zerbetto, and S. W. Zhang, *Influencing Intramolecular Motion with an Alternating Electric Field*, *Nature* **406**, 608-611 (2000).
- [16] A. M. Elizarov, S. H. Chiu, and J. F. Stoddart, *An Acid-Base Switchable [2]Rotaxane*, *Journal of Organic Chemistry* **67**, 9175-9181 (2002).
- [17] T. Ikeda, S. Saha, I. Aprahamian, K. C. F. Leung, A. Williams, W. Q. Deng, A. H. Flood, W. A. Goddard, and J. F. Stoddart, *Toward Electrochemically Controllable Tristable Three-Station [2]Catenanes*, *Chemistry - An Asian Journal* **2**, 76-93 (2007).
- [18] S. Saha and J. F. Stoddart, *Photo-Driven Molecular Devices*, *Chemical Society Reviews* **36**, 77-92 (2007).
- [19] N. Katsonis, M. Lubomska, M. M. Pollard, B. L. Feringa, and P. Rudolf, *Synthetic Light-Activated Molecular Switches and Motors on Surfaces*, *Progress in Surface Science* **82**, 407-434 (2007).
- [20] A. S. Kumar, T. Ye, T. Takami, B. C. Yu, A. K. Flatt, J. M. Tour, and P. S. Weiss, *Reversible Photo-Switching of Single Azobenzene Molecules in Controlled Nanoscale Environments*, *Nano Letters* **8**, 1644-1648 (2008).
- [21] B. L. Feringa, R. A. van Delden, N. Koumura, and E. M. Geertsema, *Chiroptical Molecular Switches*, *Chemical Reviews* **100**, 1789-1816 (2000).
- [22] J. D. Badjic, V. Balzani, A. Credi, S. Silvi, and J. F. Stoddart, *A Molecular Elevator*, *Science* **303**, 1845-1849 (2004).
- [23] N. Koumura, R. W. J. Zijlstra, R. A. van Delden, N. Harada, and B. L. Feringa, *Light-Driven Unidirectional Molecular Rotor*, *Nature* **401**, 152-155 (1999).
- [24] K. Tashiro, K. Konishi, and T. Aida, *Metal Bisporphyrinate Double-Decker Complexes as Redox-Responsive Rotating Modules. Studies on Ligand Rotation Activities of the Reduced and Oxidized Forms Using Chirality as a Probe*, *Journal of the American Chemical Society* **122**, 7921-7926 (2000).
- [25] R. A. van Delden, M. K. J. ter Wiel, M. M. Pollard, J. Vicario, N. Koumura, and B. L. Feringa, *Unidirectional Molecular Motor on a Gold Surface*, *Nature* **437**, 1337-1340 (2005).

- [26] J. K. Gimzewski, C. Joachim, R. R. Schlittler, V. Langlais, H. Tang, and I. Johannsen, *Rotation of a Single Molecule within a Supramolecular Bearing*, *Science* **281**, 531-533 (1998).
- [27] Y. Shirai, A. J. Osgood, Y. M. Zhao, K. F. Kelly, and J. M. Tour, *Directional Control in Thermally Driven Single-Molecule Nanocars*, *Nano Letters* **5**, 2330-2334 (2005).
- [28] W. Biglow, D. Pickett, and W. Zisman, *Oleophobic Monolayers. I. Films Adsorbed from Solution in Non-Polar Liquids*, *Journal of Colloid and Interface Science* **1**, 513-538 (1946).
- [29] J. C. Love, L. A. Estroff, J. K. Kriebel, R. G. Nuzzo, and G. M. Whitesides, *Self-Assembled Monolayers of Thiolates on Metals as a Form of Nanotechnology*, *Chemical Reviews* **105**, 1103-1169 (2005).
- [30] R. G. Nuzzo and D. L. Allara, *Adsorption of Bifunctional Organic Disulfides on Gold Surfaces*, *Journal of the American Chemical Society* **105**, 4481-4483 (1983).
- [31] R. G. Nuzzo, L. H. Dubois, and D. L. Allara, *Fundamental-Studies of Microscopic Wetting on Organic-Surfaces. I. Formation and Structural Characterization of a Self-Consistent Series of Polyfunctional Organic Monolayers*, *Journal of the American Chemical Society* **112**, 558-569 (1990).
- [32] R. G. Nuzzo, B. R. Zegarski, and L. H. Dubois, *Fundamental-Studies of the Chemisorption of Organosulfur Compounds on Au(111) - Implications for Molecular Self-Assembly on Gold Surfaces*, *Journal of the American Chemical Society* **109**, 733-740 (1987).
- [33] G. E. Poirier, *Mechanism of Formation of Au Vacancy Islands in Alkanethiol Monolayers on Au(111)*, *Langmuir* **13**, 2019-2026 (1997).
- [34] G. E. Poirier, *Characterization of Organosulfur Molecular Monolayers on Au(111) Using Scanning Tunneling Microscopy*, *Chemical Reviews* **97**, 1117-1127 (1997).
- [35] G. E. Poirier and E. D. Pylant, *The Self-Assembly Mechanism of Alkanethiols on Au(111)*, *Science* **272**, 1145-1148 (1996).
- [36] G. E. Poirier and M. J. Tarlov, *The C(4x2) Superlattice of n-Alkanethiol Monolayers Self-Assembled on Au(111)*, *Langmuir* **10**, 2853-2856 (1994).
- [37] G. E. Poirier, M. J. Tarlov, and H. E. Rushmeier, *2-Dimensional Liquid-Phase and the $px.sqroot.3$ Phase of Alkanethiol Self-Assembled Monolayers on Au(111)*, *Langmuir* **10**, 3383-3386 (1994).

- [38] D. L. Allara and R. G. Nuzzo, *Spontaneously Organized Molecular Assemblies. 1. Formation, Dynamics, and Physical-Properties of Normal-Alkanoic Acids Adsorbed from Solution on an Oxidized Aluminum Surface*, *Langmuir* **1**, 45-52 (1985).
- [39] D. L. Allara and R. G. Nuzzo, *Spontaneously Organized Molecular Assemblies. 2. Quantitative Infrared Spectroscopic Determination of Equilibrium Structures of Solution-Adsorbed Normal-Alkanoic Acids on an Oxidized Aluminum Surface*, *Langmuir* **1**, 52-66 (1985).
- [40] P. Han, A. R. Kurland, A. N. Giordano, S. U. Nanayakkara, M. M. Blake, C. M. Pochas, and P. S. Weiss, *Heads and Tails: Simultaneous Exposed and Buried Interface Imaging of Monolayers*, *ACS Nano* **3**, 3115-3121 (2009).
- [41] S. V. Atre, B. Liedberg, and D. L. Allara, *Chain-Length Dependence of the Structure and Wetting Properties in Binary Composition Monolayers of OH-Terminated and CH₃-Terminated Alkanethiolates on Gold*, *Langmuir* **11**, 3882-3893 (1995).
- [42] M. D. Porter, T. B. Bright, D. L. Allara, and C. E. D. Chidsey, *Spontaneously Organized Molecular Assemblies. 4. Structural Characterization of Normal-Alkyl Thiol Monolayers on Gold by Optical Ellipsometry, Infrared-Spectroscopy, and Electrochemistry*, *Journal of the American Chemical Society* **109**, 3559-3568 (1987).
- [43] L. A. Bumm, J. J. Arnold, M. T. Cygan, T. D. Dunbar, T. P. Burgin, L. Jones, D. L. Allara, J. M. Tour, and P. S. Weiss, *Are Single Molecular Wires Conducting?*, *Science* **271**, 1705-1707 (1996).
- [44] Z. J. Donhauser, B. A. Mantooth, K. F. Kelly, L. A. Bumm, J. D. Monnell, J. J. Stapleton, D. W. Price, A. M. Rawlett, D. L. Allara, J. M. Tour, and P. S. Weiss, *Conductance Switching in Single Molecules through Conformational Changes*, *Science* **292**, 2303-2307 (2001).
- [45] Z. J. Donhauser, B. A. Mantooth, T. P. Pearl, K. F. Kelly, S. U. Nanayakkara, and P. S. Weiss, *Matrix-Mediated Control of Stochastic Single Molecule Conductance Switching*, *Japanese Journal of Applied Physics*, 4871-4877 (2002).
- [46] A. M. Moore, A. A. Dameron, B. A. Mantooth, R. K. Smith, D. J. Fuchs, J. W. Ciszek, F. Maya, Y. X. Yao, J. M. Tour, and P. S. Weiss, *Molecular Engineering and Measurements to Test Hypothesized Mechanisms in Single-Molecule Conductance Switching*, *Journal of the American Chemical Society* **128**, 1959-1967 (2006).

- [47] A. M. Moore, B. A. Mantooth, Z. J. Donhauser, F. Maya, D. W. Price, Y. X. Yao, J. M. Tour, and P. S. Weiss, *Cross-Step Place-Exchange of Oligo(phenylene-ethynylene) Molecules*, *Nano Letters* **5**, 2292-2297 (2005).
- [48] A. M. Moore, B. A. Mantooth, Z. J. Donhauser, Y. Yao, J. M. Tour, and P. S. Weiss, *Real-Time Measurements of Conductance Switching and Motion of Oligo(phenylene-ethynylene)s*, *Journal of the American Chemical Society* **129**, 10352 (2007).
- [49] H. Klein, N. Battaglini, B. Bellini, and P. Dumas, *STM of Mixed Alkylthiol Self-Assembled Monolayers on Au(111)*, *Materials Science & Engineering C - Biomimetic and Supramolecular Systems* **19**, 279-283 (2002).
- [50] P. A. Lewis, Z. J. Donhauser, B. A. Mantooth, R. K. Smith, L. A. Bumm, K. F. Kelly, and P. S. Weiss, *Control and Placement of Molecules via Self-Assembly*, *Nanotechnology* **12**, 231-237 (2001).
- [51] S. J. Stranick, S. V. Atre, A. N. Parikh, M. C. Wood, D. L. Allara, N. Winograd, and P. S. Weiss, *Nanometer-Scale Phase Separation in Mixed Composition Self-Assembled Monolayers*, *Nanotechnology* **7**, 438-442 (1996).
- [52] G. Binnig and H. Rohrer, *Scanning Tunneling Microscopy*, *Helvetica Physica Acta* **55**, 726-735 (1982).
- [53] G. Binnig and H. Rohrer, *Scanning Tunneling Microscopy*, *IBM Journal of Research and Development* **30**, 355-369 (1986).
- [54] G. Binnig and H. Rohrer, *Scanning Tunneling Microscopy: From Birth to Adolescence*, *Reviews of Modern Physics* **59**, 615-625 (1987).
- [55] D. A. Bonnell, *Scanning Probe Microscopy and Spectroscopy: Theory, Techniques, and Applications* (Wiley-VCH, Inc., 2001).
- [56] C. J. Chen, *Introduction to Scanning Tunneling Microscopy* (Oxford University press, 1993).
- [57] J. E. Griffith and G. P. Kochanski, *Scanning Tunneling Microscopy*, *Annual Review of Materials Science* **20**, 219-244 (1990).
- [58] J. Tersoff and D. R. Hamann, *Theory and Application for the Scanning Tunneling Microscope*, *Physical Review Letters* **50**, 1998-2001 (1983).
- [59] N. Garcia, *Theory of Scanning Tunneling Microscopy and Spectroscopy - Resolution, Image and Field States, and Thin Oxide Layers*, *IBM Journal of Research and Development* **30**, 533-542 (1986).

- [60] A. A. Gewirth and B. K. Niece, *Electrochemical Applications of in Situ Scanning Probe Microscopy*, *Chemical Reviews* **97**, 1129-1162 (1997).
- [61] A. Aviram and M. A. Ratner, *Molecular Rectifiers*, *Chemical Physics Letters* **29**, 277-283 (1974).
- [62] S. J. Tans, A. R. M. Verschueren, and C. Dekker, *Room-Temperature Transistor Based on a Single Carbon Nanotube*, *Nature* **393**, 49-52 (1998).
- [63] M. T. Cygan, T. D. Dunbar, J. J. Arnold, L. A. Bumm, N. F. Shedlock, T. P. Burgin, L. Jones, D. L. Allara, J. M. Tour, and P. S. Weiss, *Insertion, Conductivity, and Structures of Conjugated Organic Oligomers in Self-Assembled Alkanethiol Monolayers on Au{111}*, *Journal of the American Chemical Society* **120**, 2721-2732 (1998).
- [64] B. A. Mantooth and P. S. Weiss, *Fabrication, Assembly, and Characterization of Molecular Electronic Components*, *Proceedings of the IEEE* **91**, 1785-1802 (2003).
- [65] M. Alemani, M. V. Peters, S. Hecht, K. H. Rieder, F. Moresco, and L. Grill, *Electric Field-Induced Isomerization of Azobenzene by STM*, *Journal of the American Chemical Society* **128**, 14446-14447 (2006).
- [66] B. Y. Choi, S. J. Kahng, S. Kim, H. Kim, H. W. Kim, Y. J. Song, J. Ihm, and Y. Kuk, *Conformational Molecular Switch of the Azobenzene Molecule: A Scanning Tunneling Microscopy Study*, *Physical Review Letters* **96**, 156106-1-4 (2006).
- [67] F. Moresco, G. Meyer, K. H. Rieder, H. Tang, A. Gourdon, and C. Joachim, *Conformational Changes of Single Molecules Induced by Scanning Tunneling Microscopy Manipulation: A Route to Molecular Switching*, *Physical Review Letters* **86**, 672-675 (2001).
- [68] P. A. Lewis, C. E. Inman, Y. X. Yao, J. M. Tour, J. E. Hutchison, and P. S. Weiss, *Mediating Stochastic Switching of Single Molecules Using Chemical Functionality*, *Journal of the American Chemical Society* **126**, 12214-12215 (2004).
- [69] P. A. Lewis, C. E. Inman, F. Maya, J. M. Tour, J. E. Hutchison, and P. S. Weiss, *Molecular Engineering of the Polarity and Interactions of Molecular Electronic Switches*, *Journal of the American Chemical Society* **127**, 17421-17426 (2005).
- [70] S. Yasuda, T. Nakamura, M. Matsumoto, and H. Shigekawa, *Phase Switching of a Single Isomeric Molecule and Associated Characteristic Rectification*, *Journal of the American Chemical Society* **125**, 16430-16433 (2003).

- [71] M. J. Comstock, N. Levy, A. Kirakosian, J. Cho, F. Lauterwasser, J. H. Harvey, D. A. Strubbe, J. M. J. Frechet, D. Trauner, S. G. Louie, and M. F. Crommie, *Reversible Photomechanical Switching of Individual Engineered Molecules at a Metallic Surface*, Physical Review Letters **99**, 038301-1-4 (2007).
- [72] G. Pace, V. Ferri, C. Grave, M. Elbing, C. von Hanisch, M. Zharnikov, M. Mayor, M. A. Rampi, and P. Samori, *Cooperative Light-Induced Molecular Movements of Highly Ordered Azobenzene Self-Assembled Monolayers*, Proceedings of the National Academy of Sciences of the United States of America **104**, 9937-9942 (2007).
- [73] R. Eelkema, M. M. Pollard, J. Vicario, N. Katsonis, B. S. Ramon, C. W. M. Bastiaansen, D. J. Broer, and B. L. Feringa, *Nanomotor Rotates Microscale Objects*, Nature **440**, 163-163 (2006).
- [74] N. Katsonis, T. Kudernac, M. Walko, S. J. van der Molen, B. J. van Wees, and B. L. Feringa, *Reversible Conductance Switching of Single Diarylethenes on a Gold Surface*, Advanced Materials **18**, 1397-1400 (2006).
- [75] C. S. Tsai, J. K. Wang, R. T. Skodje, and A. C. Lin, *A Single Molecule View of Bistilbene Photoisomerization on a Surface Using Scanning Tunneling Microscopy*, Journal of the American Chemical Society **127**, 10788-10789 (2005).
- [76] J. He, F. Chen, P. A. Liddell, J. Andreasson, S. D. Straight, D. Gust, T. A. Moore, A. L. Moore, J. Li, O. F. Sankey, and S. M. Lindsay, *Switching of a Photochromic Molecule on Gold Electrodes: Single-Molecule Measurements*, Nanotechnology **16**, 695-702 (2005).
- [77] B. A. Mantooth, E. C. H. Sykes, P. Han, A. M. Moore, Z. J. Donhauser, V. H. Crespi, and P. S. Weiss, *Analyzing the Motion of Benzene on Au{111}: Single Molecule Statistics from Scanning Probe Images*, Journal of Physical Chemistry C **111**, 6167-6182 (2007).
- [78] M. J. Comstock, N. Levy, J. Cho, L. Berbil-Bautista, M. F. Crommie, D. A. Poulsen, and J. M. J. Frechet, *Measuring Reversible Photomechanical Switching Rates for a Molecule at a Surface*, Applied Physics Letters **92**, 123107-1-3 (2008).
- [79] X. L. Zhou, X. Y. Zhu, and J. M. White, *Photochemistry at Adsorbate Metal Interfaces*, Surface Science Reports **13**, 73-220 (1991).
- [80] L. Ruan, F. Besenbacher, I. Stensgaard, and E. Laegsgaard, *Atom-Resolved Discrimination of Chemically Different Elements on Metal-Surfaces*, Physical Review Letters **70**, 4079-4082 (1993).

- [81] A. Riposan and G. Y. Liu, *Significance of Local Density of States in the Scanning Tunneling Microscopy Imaging of Alkanethiol Self-Assembled Monolayers*, *Journal of Physical Chemistry B* **110**, 23926-23937 (2006).
- [82] L. A. Bumm, J. J. Arnold, L. F. Charles, T. D. Dunbar, D. L. Allara, and P. S. Weiss, *Directed Self-Assembly to Create Molecular Terraces with Molecularly Sharp Boundaries in Organic Monolayers*, *Journal of the American Chemical Society* **121**, 8017-8021 (1999).
- [83] A. M. Napper, H. Y. Liu, and D. H. Waldeck, *The Nature of Electronic Coupling between Ferrocene and Gold through Alkanethiolate Monolayers on Electrodes: The Importance of Chain Composition, Interchain Coupling, and Quantum Interference*, *Journal of Physical Chemistry B* **105**, 7699-7707 (2001).
- [84] Z. J. Donhauser, D. W. Price, J. M. Tour, and P. S. Weiss, *Control of Alkanethiolate Monolayer Structure Using Vapor-Phase Annealing*, *Journal of the American Chemical Society* **125**, 11462-11463 (2003).
- [85] U. Wiesner, M. Antonietti, C. Boeffel, and H. W. Spiess, *Dynamics of Photoinduced Isomerization of Azobenzene Moieties in Liquid-Crystalline Polymers*, *Macromolecular Chemistry and Physics* **191**, 2133-2149 (1990).
- [86] H.-R. Tseng, D. M. Wu, N. X. L. Fang, X. Zhang, and J. F. Stoddart, *The Metastability of an Electrochemically Controlled Nanoscale Machine on Gold Surfaces*, *ChemPhysChem* **5**, 111-116 (2004).
- [87] T. Nagele, R. Hoche, W. Zinth, and J. Wachtveitl, *Femtosecond Photoisomerization of cis-Azobenzene*, *Chemical Physics Letters* **272**, 489-495 (1997).
- [88] H. Rau, *Photochromism: Molecules and Systems* (Elsevier, 2003).
- [89] Z. F. Liu, K. Morigaki, T. Enomoto, K. Hashimoto, and A. Fujishima, *Kinetic-Studies on the Thermal cis-trans Isomerization of an Azo Compound in the Assembled Monolayer Film*, *Journal of Physical Chemistry* **96**, 1875-1880 (1992).
- [90] G. P. Lopinski, D. D. M. Wayner, and R. A. Wolkow, *Self-Directed Growth of Molecular Nanostructures on Silicon*, *Nature* **406**, 48-51 (2000).
- [91] P. G. Piva, G. A. DiLabio, J. L. Pitters, J. Zikovsky, M. Rezeq, S. Dogel, W. A. Hofer, and R. A. Wolkow, *Field Regulation of Single-Molecule Conductivity by a Charged Surface Atom*, *Nature* **435**, 658-661 (2005).
- [92] J. A. Theobald, N. S. Oxtoby, M. A. Phillips, N. R. Champness, and P. H. Beton, *Controlling Molecular Deposition and Layer Structure with Supramolecular Surface Assemblies*, *Nature* **424**, 1029-1031 (2003).

- [93] T. Yokoyama, S. Yokoyama, T. Kamikado, Y. Okuno, and S. Mashiko, *Selective Assembly on a Surface of Supramolecular Aggregates with Controlled Size and Shape*, *Nature* **413**, 619-621 (2001).
- [94] R. Madueno, M. T. Raisanen, C. Silien, and M. Buck, *Functionalizing Hydrogen-Bonded Surface Networks with Self-Assembled Monolayers*, *Nature* **454**, 618-621 (2008).
- [95] G. M. Whitesides and B. Grzybowski, *Self-Assembly at All Scales*, *Science* **295**, 2418-2421 (2002).
- [96] W. T. Geng, M. Oda, J. Nara, H. Kondo, and T. Ohno, *Electron Transport in a pi-Stacking Molecular Chain*, *Journal of Physical Chemistry B* **112**, 2795-2800 (2008).
- [97] A. Rochefort, P. Boyer, and B. Nacer, *Resonant Tunneling Transport in Highly Organized Oligoacene Assemblies*, *Organic Electronics* **8**, 1-7 (2007).
- [98] A. Rochefort, R. Martel, and P. Avouris, *Electrical Switching in pi-Resonant 1D Intermolecular Channels*, *Nano Letters* **2**, 877-880 (2002).
- [99] R. Temirov, S. Soubatch, A. Luican, and F. S. Tautz, *Free-Electron-Like Dispersion in an Organic Monolayer Film on a Metal Substrate*, *Nature* **444**, 350-353 (2006).
- [100] G. Kirczenow, P. G. Piva, and R. A. Wolkow, *Linear Chains of Styrene and Methylstyrene Molecules and Their Heterojunctions on Silicon: Theory and Experiment*, *Physical Review B* **72**, 17 (2005).
- [101] X. Y. Liu, J. E. Reynolds, C. Wells, J. Welch, and T. S. Cale, *First-Principles Modeling of Electronic Transport in pi-Stacked Molecular Junctions*, *Journal of Applied Physics* **98**, 4 (2005).
- [102] M. Akai-Kasaya, K. Shimizu, Y. Watanabe, A. Saito, M. Aono, and Y. Kuwahara, *Electronic Structure of a Polydiacetylene Nanowire Fabricated on Highly Ordered Pyrolytic Graphite*, *Physical Review Letters* **91**, 4 (2003).
- [103] L. Chen, H. Li, and A. T. S. Wee, *One-Dimensional Molecular Chains with Dispersive Electronic States*, *Nano Letters* **9**, 4292-4296 (2009).
- [104] J. Henzl, M. Mehlhorn, H. Gawronski, K. H. Rieder, and K. Morgenstern, *Reversible cis-trans Isomerization of a Single Azobenzene Molecule*, *Angewandte Chemie-International Edition* **45**, 603-606 (2006).

- [105] Y. F. Wang, X. Ge, G. Schull, R. Berndt, H. Tang, C. Bornholdt, F. Koehler, and R. Herges, *Switching Single Azopyridine Supramolecules in Ordered Arrays on Au(111)*, *Journal of the American Chemical Society* **132**, 1196-1197 (2010).
- [106] W. B. Caldwell, D. J. Campbell, K. M. Chen, B. R. Herr, C. A. Mirkin, A. Malik, M. K. Durbin, P. Dutta, and K. G. Huang, *A Highly Ordered Self-Assembled Monolayer Film of an Azobenzenealkanethiol on Au(111): Electrochemical Properties and Structural Characterization by Synchrotron in-Plane X-Ray Diffraction, Atomic Force Microscopy, and Surface-Enhanced Raman Spectroscopy*, *Journal of the American Chemical Society* **117**, 6071-6082 (1995).
- [107] G. H. Yang, Y. L. Qian, C. Engtrakul, L. R. Sita, and G. Y. Liu, *Arenethiols Form Ordered and Incommensurate Self-Assembled Monolayers on Au(111) Surfaces*, *Journal of Physical Chemistry B* **104**, 9059-9062 (2000).
- [108] G. Binnig, H. Rohrer, C. Gerber, and E. Weibel, *Surface Studies by Scanning Tunneling Microscopy*, *Physical Review Letters* **49**, 57-61 (1982).
- [109] A. J. Heinrich, C. P. Lutz, J. A. Gupta, and D. M. Eigler, *Molecule Cascades*, *Science* **298**, 1381-1387 (2002).
- [110] G. Fuchsel, T. Klamroth, J. Dokic, and P. Saalfrank, *On the Electronic Structure of Neutral and Ionic Azobenzenes and Their Possible Role as Surface Mounted Molecular Switches*, *Journal of Physical Chemistry B* **110**, 16337-16345 (2006).
- [111] S. E. Lyshevski, *Nano- and Micro-Electromechanical Systems: Fundamentals of Nano- and Microengineering* (CRC Press, 2005).
- [112] G. A. Ozin, I. Manners, S. Fournier-Bidoz, and A. Arsenault, *Dream Nanomachines*, *Advanced Materials* **17**, 3011-3018 (2005).
- [113] C. Liu, *Foundations of Mems* (Pearson Education, 2006).
- [114] Y. Gianchandani, O. Tabata, and H. Zappe, *Comprehensive Microsystems* (Elsevier, 2007).
- [115] W. R. Browne and B. L. Feringa, *Making Molecular Machines Work*, *Nature Nanotechnology* **1**, 25-35 (2006).
- [116] E. Baranoff, F. Barigelletti, S. Bonnet, J. P. Collin, L. Flamigni, P. Mobian, and J. P. Sauvage, *From Photoinduced Charge Separation to Light-Driven Molecular Machines*, *Structure & Bonding* **123**, 41-78 (2007).
- [117] J. E. Green, J. W. Choi, A. Boukai, Y. Bunimovich, E. Johnston-Halperin, E. DeIonno, Y. Luo, B. A. Sheriff, K. Xu, Y. S. Shin, H.-R. Tseng, J. F. Stoddart,

- and J. R. Heath, *A 160-Kilobit Molecular Electronic Memory Patterned at 10(11) Bits Per Square Centimetre*, *Nature* **445**, 414-417 (2007).
- [118] H. G. Craighead, *Nanoelectromechanical Systems*, *Science* **290**, 1532-1535 (2000).
- [119] R. H. Baughman, C. X. Cui, A. A. Zakhidov, Z. Iqbal, J. N. Barisci, G. M. Spinks, G. G. Wallace, A. Mazzoldi, D. De Rossi, A. G. Rinzler, O. Jaschinski, S. Roth, and M. Kertesz, *Carbon Nanotube Actuators*, *Science* **284**, 1340-1344 (1999).
- [120] S. Juodkazis, N. Mukai, R. Wakaki, A. Yamaguchi, S. Matsuo, and H. Misawa, *Reversible Phase Transitions in Polymer Gels Induced by Radiation Forces*, *Nature* **408**, 178-181 (2000).
- [121] J. Fritz, M. K. Baller, H. P. Lang, H. Rothuizen, P. Vettiger, E. Meyer, H. J. Guntherodt, C. Gerber, and J. K. Gimzewski, *Translating Biomolecular Recognition into Nanomechanics*, *Science* **288**, 316-318 (2000).
- [122] L. Bay, K. West, P. Sommer-Larsen, S. Skaarup, and M. Benslimane, *A Conducting Polymer Artificial Muscle with 12% Linear Strain*, *Advanced Materials* **15**, 310-313 (2003).
- [123] T. Braun, N. Backmann, M. Vogtli, A. Bietsch, A. Engel, H.-P. Lang, C. Gerber, and M. Hegner, *Conformational Change of Bacteriorhodopsin Quantitatively Monitored by Microcantilever Sensors*, *Biophysical Journal* **90**, 2970-2977 (2006).
- [124] T. J. Huang and B. K. Juluri, *Biological and Biomimetic Molecular Machines*, *Nanomedicine* **3**, 107-124 (2008).
- [125] H. F. Ji, Y. Feng, X. H. Xu, V. Purushotham, T. Thundat, and G. M. Brown, *Photon-Driven Nanomechanical Cyclic Motion*, *Chemical Communications* **22**, 2532-2533 (2004).
- [126] M. Lahav, C. Durkan, R. Gabai, E. Katz, I. Willner, and M. E. Welland, *Redox Activation of a Polyaniline-Coated Cantilever: An Electro-Driven Microdevice*, *Angewandte Chemie-International Edition* **40**, 4219-4221 (2001).
- [127] B. Raguse, K. H. Muller, and L. Wiczorek, *Nanoparticle Actuators*, *Advanced Materials* **15**, 922-926 (2003).
- [128] Q. Ren, Y. P. Zhao, L. Han, and H. B. Zhao, *A Nanomechanical Device Based on Light-Driven Proton Pumps*, *Nanotechnology* **17**, 1778-1785 (2006).

- [129] W. M. Shu, D. S. Liu, M. Watari, C. K. Riener, T. Strunz, M. E. Welland, S. Balasubramanian, and R. A. McKendry, *DNA Molecular Motor Driven Micromechanical Cantilever Arrays*, *Journal of the American Chemical Society* **127**, 17054-17060 (2005).
- [130] V. Tabard-Cossa, M. Godin, P. Grütter, I. Burgess, and R. B. Lennox, *Redox-Induced Surface Stress of Polypyrrole-Based Actuators*, *Journal of Physical Chemistry B* **109**, 17531-17537 (2005).
- [131] G. Wu, H. Ji, K. Hansen, T. Thundat, R. Datar, R. Cote, M. F. Hagan, A. K. Chakraborty, and A. Majumdar, *Origin of Nanomechanical Cantilever Motion Generated from Biomolecular Interactions*, *Proceedings of the National Academy of Sciences of the United States of America* **98**, 1560-1564 (2001).
- [132] A. H. Flood, R. J. A. Ramirez, W. Q. Deng, R. P. Muller, W. A. Goddard, and J. F. Stoddart, *Meccano on the Nanoscale - a Blueprint for Making Some of the World's Tiniest Machines*, *Australian Journal of Chemistry* **57**, 301-322 (2004).
- [133] T. J. Huang, A. H. Flood, B. Brough, Y. Liu, P. A. Bonvallet, S. S. Kang, C. W. Chu, T. F. Guo, W. X. Lu, Y. Yang, J. F. Stoddart, and C. M. Ho, *Understanding and Harnessing Biomimetic Molecular Machines for NEMS Actuation Materials*, *IEEE Transactions on Automation Science and Engineering* **3**, 254-259 (2006).
- [134] T. J. Huang, H.-R. Tseng, L. Sha, W. X. Lu, B. Brough, A. H. Flood, B. D. Yu, P. C. Celestre, J. P. Chang, J. F. Stoddart, and C. M. Ho, *Mechanical Shuttling of Linear Motor-Molecules in Condensed Phases on Solid Substrates*, *Nano Letters* **4**, 2065-2071 (2004).
- [135] T. J. Huang, *Recent Developments in Artificial Molecular Machine-Based Active Nanomaterials and Nanosystems*, *MRS Bulletin* **33**, 226-231 (2008).
- [136] T. A. V. Khuong, J. E. Nunez, C. E. Godinez, and M. A. Garcia-Garibay, *Crystalline Molecular Machines: A Quest Toward Solid-State Dynamics and Function*, *Accounts of Chemical Research* **39**, 413-422 (2006).
- [137] B. Champin, P. Mobian, and J. P. Sauvage, *Transition Metal Complexes as Molecular Machine Prototypes*, *Chemical Society Reviews* **36**, 358-366 (2007).
- [138] E. R. Kay and D. A. Leigh, *Beyond Switches: Rotaxane- and Catenane-Based Synthetic Molecular Motors*, *Pure and Applied Chemistry* **80**, 17-29 (2008).
- [139] N. N. P. Moonen, A. H. Flood, J. M. Fernandez, and J. F. Stoddart, *Towards a Rational Design of Molecular Switches and Sensors from Their Basic Building Blocks*, *Molecular Machines* **262**, 99-132 (2005).

- [140] J. D. Badjic, C. M. Ronconi, J. F. Stoddart, V. Balzani, S. Silvi, and A. Credi, *Operating Molecular Elevators*, *Journal of the American Chemical Society* **128**, 1489-1499 (2006).
- [141] J. R. Heath and M. A. Ratner, *Molecular Electronics*, *Physics Today* **56**, 43-49 (2003).
- [142] A. H. Flood, J. F. Stoddart, D. W. Steuerman, and J. R. Heath, *Whence Molecular Electronics?*, *Science* **306**, 2055-2056 (2004).
- [143] C. P. Collier, G. Mattersteig, E. W. Wong, Y. Luo, K. Beverly, J. Sampaio, F. M. Raymo, J. F. Stoddart, and J. R. Heath, *A [2]Catenane-Based Solid State Electronically Reconfigurable Switch*, *Science* **289**, 1172-1175 (2000).
- [144] A. R. Pease, J. O. Jeppesen, J. F. Stoddart, Y. Luo, C. P. Collier, and J. R. Heath, *Switching Devices Based on Interlocked Molecules*, *Accounts of Chemical Research* **34**, 433-444 (2001).
- [145] Y. Luo, C. P. Collier, J. O. Jeppesen, K. A. Nielsen, E. DeIonno, G. Ho, J. Perkins, H.-R. Tseng, T. Yamamoto, J. F. Stoddart, and J. R. Heath, *Two-Dimensional Molecular Electronics Circuits*, *ChemPhysChem* **3**, 519-525 (2002).
- [146] H.-R. Tseng, S. A. Vignon, P. C. Celestre, J. Perkins, J. O. Jeppesen, A. Di Fabio, R. Ballardini, M. Gandolfi, M. Venturi, V. Balzani, and J. F. Stoddart, *Redox-Controllable Amphiphilic [2]Rotaxanes*, *Chemistry - A European Journal* **10**, 155-172 (2004).
- [147] S. S. Jang, Y. H. Jang, Y. H. Kim, W. A. Goddard, J. W. Choi, J. R. Heath, B. W. Laursen, A. H. Flood, J. F. Stoddart, K. Norgaard, and T. Bjornholm, *Molecular Dynamics Simulation of Amphiphilic Bistable [2]Rotaxane Langmuir Monolayers at the Air/Water Interface*, *Journal of the American Chemical Society* **127**, 14804-14816 (2005).
- [148] W. Q. Deng, A. H. Flood, J. F. Stoddart, and W. A. Goddard, *An Electrochemical Color-Switchable RGB Dye: Tristable [2]Catenane*, *Journal of the American Chemical Society* **127**, 15994-15995 (2005).
- [149] W. R. Dichtel, J. R. Heath, and J. F. Stoddart, *Designing Bistable [2]Rotaxanes for Molecular Electronic Devices*, *Philosophical Transactions of the Royal Society A - Mathematical Physical and Engineering Sciences* **365**, 1607-1625 (2007).
- [150] T. D. Nguyen, Y. Liu, S. Saha, K. C. F. Leung, J. F. Stoddart, and J. I. Zink, *Design and Optimization of Molecular Nanovalves Based on Redox-Switchable Bistable Rotaxanes*, *Journal of the American Chemical Society* **129**, 626-634 (2007).

- [151] T. D. Nguyen, H.-R. Tseng, P. C. Celestre, A. H. Flood, Y. Liu, J. F. Stoddart, and J. I. Zink, *A Reversible Molecular Valve*, Proceedings of the National Academy of Sciences of the United States of America **102**, 10029-10034 (2005).
- [152] S. Saha, K. C. F. Leung, T. D. Nguyen, J. F. Stoddart, and J. I. Zink, *Nanovalves*, Advanced Functional Materials **17**, 685-693 (2007).
- [153] S. Angelos, E. Johansson, J. F. Stoddart, and J. I. Zink, *Meslostructured Silica Supports for Functional Materials and Molecular Machines*, Advanced Functional Materials **17**, 2261-2271 (2007).
- [154] S. Angelos, Y.-W. Yang, K. Patel, J. F. Stoddart, and J. I. Zink, *Supramolecular Nanovalves Based on Cucurbit[6]uril Pseudorotaxanes*, Angewandte Chemie-International Edition **47**, 2222-2226 (2008).
- [155] K. Patel, S. Angelos, W. R. Dichtel, A. Coskun, Y.-W. Yang, J. I. Zink, and J. F. Stoddart, *Enzyme-Responsive Snap-Top Covered Silica Nanocontainers*, Journal of the American Chemical Society **130**, 2382-2383 (2008).
- [156] D. W. Steuerman, H.-R. Tseng, A. J. Peters, A. H. Flood, J. O. Jeppesen, K. A. Nielsen, J. F. Stoddart, and J. R. Heath, *Molecular-Mechanical Switch-Based Solid-State Electrochromic Devices*, Angewandte Chemie-International Edition **116**, 6648-6653 (2004).
- [157] I. Aprahamian, T. Yasuda, T. Ikeda, S. Saha, W. R. Dichtel, K. Isoda, T. Kato, and J. F. Stoddart, *A Liquid-Crystalline Bistable [2]Rotaxane*, Angewandte Chemie-International Edition **46**, 4675-4679 (2007).
- [158] T. Ikeda, I. Aprahamian, and J. F. Stoddart, *Blue-Colored Donor-Acceptor [2]Rotaxane*, Organic Letters **9**, 1481-1484 (2007).
- [159] J. Berna, D. A. Leigh, M. Lubomska, S. M. Mendoza, E. M. Perez, P. Rudolf, G. Teobaldi, and F. Zerbetto, *Macroscopic Transport by Synthetic Molecular Machines*, Nature Materials **4**, 704-710 (2005).
- [160] J. F. Stoddart, *Whither and Thither Molecular Machines*, Chemistry in Australia **59**, 576-581 (1992).
- [161] H.-R. Tseng, S. A. Vignon, and J. F. Stoddart, *Toward Chemically Controlled Nanoscale Molecular Machinery*, Angewandte Chemie-International Edition **42**, 1491-1495 (2003).
- [162] I. Aprahamian, O. S. Miljanic, W. R. Dichtel, K. Isoda, T. Yasuda, T. Kato, and J. F. Stoddart, *Clicked Interlocked Molecules*, Bulletin of Chemical Society of Japan **80**, 1856-1869 (2007).

- [163] J. O. Jeppesen, S. Nygaard, S. A. Vignon, and J. F. Stoddart, *Honing up a Genre of Amphiphilic Bistable [2]Rotaxanes for Device Settings*, *European Journal of Organic Chemistry* **1**, 196-220 (2005).
- [164] T. J. Huang, B. Brough, C. M. Ho, Y. Liu, A. H. Flood, P. A. Bonvallet, H. R. Tseng, J. F. Stoddart, M. Baller, and S. Magonov, *A Nanomechanical Device Based on Linear Molecular Motors*, *Applied Physics Letters* **85**, 5391-5393 (2004).
- [165] Y. Liu, A. H. Flood, P. A. Bonvallet, S. A. Vignon, B. H. Northrop, H. R. Tseng, J. O. Jeppesen, T. J. Huang, B. Brough, M. Baller, S. Magonov, S. D. Solares, W. A. Goddard, C. M. Ho, and J. F. Stoddart, *Linear Artificial Molecular Muscles*, *Journal of the American Chemical Society* **127**, 9745-9759 (2005).
- [166] G. T. A. Kovacs, *Micromachined Transducers Sourcebook* (McGraw-Hill, 1998).
- [167] H. Hess, *Materials Science - Toward Devices Powered by Biomolecular Motors*, *Science* **312**, 860-861 (2006).
- [168] J. W. Choi, A. H. Flood, D. W. Steuerman, S. Nygaard, A. B. Braunschweig, N. N. P. Moonen, B. W. Laursen, Y. Luo, E. DeIonno, A. J. Peters, J. O. Jeppesen, K. Xu, J. F. Stoddart, and J. R. Heath, *Ground-State Equilibrium Thermodynamics and Switching Kinetics of Bistable [2]Rotaxanes Switched in Solution, Polymer Gels, and Molecular Electronic Devices*, *Chemistry - A European Journal* **12**, 261-279 (2006).
- [169] D. S. Goodsell, *Our Molecular Nature: The Body's Motors, Machines, and Messages* (Copernicus, 1996).
- [170] M. A. Geeves, *Stretching the Lever-Arm Theory*, *Nature* **415**, 129-131 (2002).
- [171] J. A. Spudich and R. S. Rock, *A Crossbridge Too Far*, *Nature Cell Biology* **4**, E8-E10 (2002).
- [172] A. H. Flood, A. J. Peters, S. A. Vignon, D. W. Steuerman, H.-R. Tseng, S. Kang, J. R. Heath, and J. F. Stoddart, *The Role of Physical Environment on Molecular Electromechanical Switching*, *Chemistry - A European Journal* **10**, 6558-6564 (2004).
- [173] H. Ibach, C. E. Bach, M. Giesen, and A. Grossmann, *Potential-Induced Stress in the Solid-Liquid Interface: Au(111) and Au(100) in an HClO₄ Electrolyte*, *Surface Science* **375**, 107-119 (1997).
- [174] V. Tabard-Cossa, M. Godin, L. Y. Beaulieu, and P. Grütter, *A Differential Microcantilever-Based System for Measuring Surface Stress Changes Induced by*

- Electrochemical Reactions, Sensors and Actuators B: Chemical* **107**, 233-241 (2005).
- [175] F. Quist, V. Tabard-Cossa, and A. Badia, *Nanomechanical Cantilever Motion Generated by a Surface-Confined Redox Reaction*, *Journal of Physical Chemistry B* **107**, 10691-10695 (2003).
- [176] F. Zhou, P. M. Biesheuvel, E. Y. Chol, W. Shu, R. Poetes, U. Steiner, and W. T. S. Huck, *Polyelectrolyte Brush Amplified Electroactuation of Microcantilevers*, *Nano Letters* **8**, 725-730 (2008).
- [177] K. S. Alleman, K. Weber, and S. E. Creager, *Electrochemical Rectification at a Monolayer-Modified Electrode*, *Journal of Physical Chemistry B* **100**, 17050-17058 (1996).
- [178] C. E. D. Chidsey and D. N. Loiacono, *Chemical Functionality in Self-Assembled Monolayers: Structural and Electrochemical Properties*, *Langmuir* **6**, 682-691 (1990).
- [179] H. O. Finklea, S. Avery, M. Lynch, and T. Furtch, *Blocking Oriented Monolayers of Alkyl Mercaptans on Gold Electrodes*, *Langmuir* **3**, 409-413 (1987).
- [180] T. J. Mullen, A. A. Dameron, and P. S. Weiss, *Directed Assembly and Separation of Self-Assembled Monolayers via Electrochemical Processing*, *Journal of Physical Chemistry B* **110**, 14410-14417 (2006).
- [181] J. B. Nelson and D. T. Schwartz, *Electrochemical Factors Controlling the Patterning of Metals on SAM-Coated Substrates*, *Langmuir* **23**, 9661-9666 (2007).
- [182] R. K. Smith, P. A. Lewis, and P. S. Weiss, *Patterning Self-Assembled Monolayers*, *Progress in Surface Science* **75**, 1-68 (2004).
- [183] N. E. Dowling, *Mechanical Behavior of Materials* (Prentice Hall, 1999).
- [184] V. H. Ebron, Z. Yang, D. J. Seyer, M. E. Kozlov, J. Oh, H. Xie, J. Razal, L. J. Hall, J. P. Ferraris, A. G. MacDiarmid, and R. H. Baughman, *Fuel-Powered Artificial Muscles*, *Science* **311**, 1580-1583 (2006).
- [185] T. E. Herod and J. B. Schlenoff, *Doping-Induced Strain in Polyaniline: Stretchoelectrochemistry*, *Chemistry of Materials* **5**, 951-955 (1993).
- [186] M. Hughes and G. M. Spinks, *Multiwalled Carbon Nanotube Actuators*, *Advanced Materials* **17**, 443-446 (2005).

- [187] T. Mirfakhrai, J. Oh, M. Kozlov, E. C. W. Fok, M. Zhang, S. Fang, R. H. Baughman, and J. D. W. Madden, *Electrochemical Actuation of Carbon Nanotube Yarns*, *Smart Materials and Structures* **16**, S243-S249 (2007).
- [188] E. Smela, W. Lu, and B. R. Mattes, *Polyaniline Actuators: Part I. PANI(AMPS) in HCl*, *Synthetic Metals* **151**, 25-42 (2005).
- [189] S. J. Stranick, A. N. Parikh, D. L. Allara, and P. S. Weiss, *A New Mechanism for Surface Diffusion: Motion of a Substrate-Adsorbate Complex*, *Journal of Physical Chemistry B* **98**, 11136-11142 (1994).
- [190] M. Yu, N. Bovet, C. J. Satterley, S. Bengio, K. R. J. Lovelock, P. K. Milligan, R. G. Jones, D. P. Woodruff, and V. Dhanaket, *True Nature of an Archetypal Self-Assembly System: Mobile Au-Thiolate Species on Au(111)*, *Physical Review Letters* **97**, 166102-1-4 (2006).
- [191] W. A. Brantley, *Calculated Elastic-Constants for Stress Problems Associated with Semiconductor Devices*, *Journal of Applied Physics* **44**, 534-535 (1973).
- [192] B. Brough, B. H. Northrop, J. J. Schmidt, H.-R. Tseng, K. N. Houk, J. F. Stoddart, and C. M. Ho, *Evaluation of Synthetic Linear Motor-Molecule Actuation Energetics*, *Proceedings of the National Academy of Sciences of the United States of America* **103**, 8583-8588 (2006).
- [193] N. B. Holland, T. Hugel, G. Neuert, A. Cattani-Scholz, C. Renner, D. Oesterhelt, L. Moroder, M. Seitz, and H. E. Gaub, *Single Molecule Force Spectroscopy of Azobenzene Polymers: Switching Elasticity of Single Photochromic Macromolecules*, *Macromolecules* **36**, 2015-2023 (2003).
- [194] D. B. Amabilino and J. F. Stoddart, *Interlocked and Intertwined Structures and Superstructures*, *Chemical Reviews* **95**, 2725-2828 (1995).
- [195] V. Balzani, M. Gomez-Lopez, and J. F. Stoddart, *Molecular Machines*, *Accounts of Chemical Research* **31**, 405-414 (1998).
- [196] J. Michl and E. C. H. Sykes, *Molecular Rotors and Motors: Recent Advances and Future Challenges*, *ACS Nano* **3**, 1042-1048 (2009).
- [197] J. F. Stoddart, *The Master of Chemical Topology Jean-Pierre Sauvage*, *Chemical Society Reviews* **38**, 1521-1529 (2009).
- [198] I. Aprahamian, W. R. Dichtel, T. Ikeda, J. R. Heath, and J. F. Stoddart, *A Clicked Bistable [2]Rotaxane*, *Organic Letters* **9**, 1287-1290 (2007).

- [199] M. Z. Hossain, H. S. Kato, and M. Kawai, *Valence States of One-Dimensional Molecular Assembly Formed by Ketone Molecules on the Si(100)-(2 x 1)-H Surface*, *Journal of Physical Chemistry C* **113**, 10751-10754 (2009).
- [200] B. K. Juluri, A. S. Kumar, Y. Liu, T. Ye, Y. W. Yang, A. H. Flood, L. Fang, J. F. Stoddart, P. S. Weiss, and T. J. Huang, *A Mechanical Actuator Driven Electrochemically by Artificial Molecular Muscles*, *ACS Nano* **3**, 291-300 (2009).
- [201] A. M. Brouwer, C. Frochot, F. G. Gatti, D. A. Leigh, L. Mottier, F. Paolucci, S. Roffia, and G. W. H. Wurpel, *Photoinduction of Fast, Reversible Translational Motion in a Hydrogen-Bonded Molecular Shuttle*, *Science* **291**, 2124-2128 (2001).
- [202] J. P. Collin, C. Dietrich-Buchecker, P. Gavina, M. C. Jimenez-Molero, and J. P. Sauvage, *Shuttles and Muscles: Linear Molecular Machines Based on Transition Metals*, *Accounts of Chemical Research* **34**, 477-487 (2001).
- [203] P. L. Anelli, N. Spencer, and J. F. Stoddart, *A Molecular Shuttle*, *Journal of the American Chemical Society* **113**, 5131-5133 (1991).
- [204] M. Feng, L. Gao, S. X. Du, Z. T. Deng, Z. H. Cheng, W. Ji, D. Q. Zhang, X. F. Guo, X. Lin, L. F. Chi, D. B. Zhu, H. Fuchs, and H. J. Gao, *Observation of Structural and Conductance Transition of Rotaxane Molecules at a Submolecular Scale*, *Advanced Functional Materials* **17**, 770-776 (2007).
- [205] H. Shigekawa, K. Miyake, J. Sumaoka, A. Harada, and M. Komiyama, *The Molecular Abacus: STM Manipulation of Cyclodextrin Necklace*, *Journal of the American Chemical Society* **122**, 5411-5412 (2000).
- [206] A. Hamelin, *Cyclic Voltammetry at Gold Single-Crystal Surfaces. I. Behaviour at Low-Index Faces*, *Journal of Electroanalytical Chemistry* **407**, 1-11 (1996).
- [207] B. A. Mantooth, Z. J. Donhauser, K. F. Kelly, and P. S. Weiss, *Cross-Correlation Image Tracking for Drift Correction and Adsorbate Analysis*, *Review of Scientific Instruments* **73**, 313-317 (2002).
- [208] Y. B. Zheng, Y. W. Yang, L. Jensen, L. Fang, B. K. Juluri, A. H. Flood, P. S. Weiss, J. F. Stoddart, and T. J. Huang, *Active Molecular Plasmonics: Controlling Plasmon Resonances with Molecular Switches*, *Nano Letters* **9**, 819-825 (2009).
- [209] S. Stepanow, M. Lingenfelder, A. Dmitriev, H. Spillmann, E. Delvigne, N. Lin, X. B. Deng, C. Z. Cai, J. V. Barth, and K. Kern, *Steering Molecular Organization and Host-Guest Interactions Using Two-Dimensional Nanoporous Coordination Systems*, *Nature Materials* **3**, 229-233 (2004).

- [210] S. De Feyter and F. C. De Schryver, *Self-Assembly at the Liquid/Solid Interface: STM Reveals*, Journal of Physical Chemistry B **109**, 4290-4302 (2005).
- [211] R. A. van Delden, M. K. J. ter Wiel, N. Koumura, and B. L. Feringa, *Molecular Motors* (Wiley-VCH, Weinheim, Germany, 2003).
- [212] P. Liljeroth, J. Repp, and G. Meyer, *Current-Induced Hydrogen Tautomerization and Conductance Switching of Naphthalocyanine Molecules*, Science **317**, 1203-1206 (2007).
- [213] H. Y. Ma, L. Y. O. Yang, N. Pan, S. L. Yau, J. Z. Hang, and K. Itaya, *Ordered Molecular Assemblies of Substituted Bis(phthalocyaninato) Rare Earth Complexes on Au(111): In Situ Scanning Tunneling Microscopy and Electrochemical Studies*, Langmuir **22**, 2105-2111 (2006).
- [214] T. Takami, D. P. Arnold, A. V. Fuchs, G. D. Will, R. Goh, E. R. Waclawik, J. M. Bell, P. S. Weiss, K. Sugiura, W. Liu, and J. Z. Jiang, *Two-Dimensional Crystal Growth and Stacking of Bis(phthalocyaninato) Rare Earth Sandwich Complexes at the 1-Phenyloctane/Graphite Interface*, Journal of Physical Chemistry B **110**, 1661-1664 (2006).
- [215] Z. Y. Yang, L. H. Gan, S. B. Lei, L. J. Wan, C. Wang, and J. Z. Jiang, *Self-Assembly of PcOC8 and Its Sandwich Lanthanide Complex Pr(PcOC8)₂ with Oligo(phenylene-ethynylene) Molecules*, Journal of Physical Chemistry B **109**, 19859-19865 (2005).
- [216] J. S. Foster, J. E. Frommer, and P. C. Arnett, *Molecular Manipulation Using a Tunnelling Microscope*, Nature **331**, 324-326 (1988).
- [217] P. Samori, H. Engelkamp, P. de Witte, A. E. Rowan, R. J. M. Nolte, and J. P. Rabe, *Self-Assembly and Manipulation of Crown Ether Phthalocyanines at the Gel-Graphite Interface*, Angewandte Chemie-International Edition **40**, 2348-2350 (2001).
- [218] J. P. Rabe and S. Buchholz, *Commensurability and Mobility in 2-Dimensional Molecular-Patterns on Graphite*, Science **253**, 424-427 (1991).
- [219] P. Samori, A. Fechtenkotter, F. Jackel, T. Bohme, K. Mullen, and J. P. Rabe, *Supramolecular Staircase via Self-Assembly of Disklike Molecules at the Solid-Liquid Interface*, Journal of the American Chemical Society **123**, 11462-11467 (2001).
- [220] L. C. Giancarlo and G. W. Flynn, *Raising Flags: Applications of Chemical Marker Groups to Study Self-Assembly, Chirality, and Orientation of Interfacial Films by Scanning Tunneling Microscopy*, Accounts of Chemical Research **33**, 491-501 (2000).

- [221] Y. H. Liu, S. B. Lei, S. X. Yin, S. L. Xu, Q. Y. Zheng, Q. D. Zeng, C. Wang, L. J. Wan, and C. L. Bai, *Molecular Trapping Phenomenon of the 2-D Assemblies of Octa-Alkoxy-Substituted Phthalocyanine Studied by Scanning Tunneling Microscopy*, *Journal of Physical Chemistry B* **106**, 12569-12574 (2002).
- [222] X. H. Qiu, C. Wang, Q. D. Zeng, B. Xu, S. X. Yin, H. N. Wang, S. D. Xu, and C. L. Bai, *Alkane-Assisted Adsorption and Assembly of Phthalocyanines and Porphyrins*, *Journal of the American Chemical Society* **122**, 5550-5556 (2000).
- [223] T. Takami, T. Ye, D. P. Arnold, K. Sugiura, R. M. Wang, J. Z. Jiang, and P. S. Weiss, *Controlled Adsorption Orientation for Double-Decker Complexes*, *Journal of Physical Chemistry C* **111**, 2077-2080 (2007).
- [224] J. Otsuki, S. Kawaguchi, T. Yamakawa, M. Asakawa, and K. Miyake, *Arrays of Double-Decker Porphyrins on Highly Oriented Pyrolytic Graphite*, *Langmuir* **22**, 5708-5715 (2006).
- [225] T. Ye, T. Takami, R. M. Wang, J. Z. Jiang, and P. S. Weiss, *Tuning Interactions between Ligands in Self-Assembled Double-Decker Phthalocyanine Arrays*, *Journal of the American Chemical Society* **128**, 10984-10985 (2006).
- [226] T. A. Jung, R. R. Schlittler, J. K. Gimzewski, H. Tang, and C. Joachim, *Controlled Room-Temperature Positioning of Individual Molecules: Molecular Flexure and Motion*, *Science* **271**, 181-184 (1996).
- [227] P. A. Sloan and R. E. Palmer, *Two-Electron Dissociation of Single Molecules by Atomic Manipulation at Room Temperature*, *Nature* **434**, 367-371 (2005).
- [228] H. C. Zhang, R. M. Wang, P. H. Zhu, Z. F. Lai, J. Han, C. F. Choi, D. K. P. Ng, X. G. Cui, C. Q. Ma, and J. Z. Jiang, *The First Slipped Pseudo-Quadruple-Decker Complex of Phthalocyanines*, *Inorganic Chemistry* **43**, 4740-4742 (2004).
- [229] R. J. Li, X. X. Zhang, P. H. Zhu, D. K. P. Ng, N. Kobayashi, and J. Z. Jiang, *Electron-Donating or -Withdrawing Nature of Substituents Revealed by the Electrochemistry of Metal-Free Phthalocyanines*, *Inorganic Chemistry* **45**, 2327-2334 (2006).
- [230] R. M. Wang, Y. Li, R. J. Li, D. Y. Y. Cheng, P. H. Zhu, D. K. P. Ng, M. Bao, X. Cui, N. Kobayashi, and J. Z. Jiang, *Heteroleptic Rare Earth Double-Decker Complexes with Naphthalocyaninato and Phthalocyaninato Ligands. General Synthesis, Spectroscopic, and Electrochemical Characteristics*, *Inorganic Chemistry* **44**, 2114-2120 (2005).
- [231] Y. Z. Bian, R. M. Wang, J. Z. Jiang, C. H. Lee, J. Z. Wang, and D. K. P. Ng, *Synthesis, Spectroscopic Characterisation and Structure of the First Chiral*

Heteroleptic Bis(phthalocyaninato) Rare Earth Complexes, Chemical Communications, 1194-1195 (2003).

- [232] L. Bartels, G. Meyer, and K. H. Rieder, *Basic Steps of Lateral Manipulation of Single Atoms and Diatomic Clusters with a Scanning Tunneling Microscope Tip*, Physical Review Letters **79**, 697-700 (1997).
- [233] S. W. Hla, *Scanning Tunneling Microscopy Single Atom/Molecule Manipulation and Its Application to Nanoscience and Technology*, Journal of Vacuum Science & Technology B **23**, 1351-1360 (2005).
- [234] S. W. Hla, K. F. Braun, and K. H. Rieder, *Single-Atom Manipulation Mechanisms During a Quantum Corral Construction*, Physical Review B **67** (2003).
- [235] A. Kuhnle, G. Meyer, S. W. Hla, and K. H. Rieder, *Understanding Atom Movement During Lateral Manipulation with the STM Tip Using a Simple Simulation Method*, Surface Science **499**, 15-23 (2002).
- [236] H. L. Tierney, A. E. Baber, E. C. H. Sykes, A. Akimov, and A. B. Kolomeisky, *Dynamics of Thioether Molecular Rotors: Effects of Surface Interactions and Chain Flexibility*, Journal of Physical Chemistry C **113**, 10913-10920 (2009).
- [237] H. L. Tierney, C. E. Calderon, A. E. Baber, E. C. H. Sykes, and F. Wang, *Understanding the Rotational Mechanism of a Single Molecule: STM and DFT Investigations of Dimethyl Sulfide Molecular Rotors on Au(111)*, Journal of Physical Chemistry C **114**, 3152-3155
- [238] T. Kitagawa, Y. Idomoto, H. Matsubara, D. Hobara, T. Kakiuchi, T. Okazaki, and K. Komatsu, *Rigid Molecular Tripod with an Adamantane Framework and Thiol Legs. Synthesis and Observation of an Ordered Monolayer on Au(111)*, Journal of Organic Chemistry **71**, 1362-1369 (2006).
- [239] S. Zarwell and K. Ruck-Braun, *Synthesis of an Azobenzene-Linker-Conjugate with Tetrahedral Shape*, Tetrahedron Letters **49**, 4020-4025 (2008).
- [240] P. M. Schmidt, K. Horn, J. H. Dil, and T. U. Kampen, *Conformational Isomers of Stilbene on Si(100)*, Surface Science **601**, 1775-1780 (2007).
- [241] D. H. Waldeck, *Photoisomerization Dynamics of Stilbenes*, Chemical Reviews **91**, 415-436 (1991).
- [242] W. G. Han, T. Lovell, T. Q. Liu, and L. Noodleman, *Density Functional Studies of the Ground- and Excited-State Potential-Energy Curves of Stilbene cis-trans Isomerization*, ChemPhysChem **3**, 167-178 (2002).

VITA

AJEET KUMAR

Education

Ph.D. in Chemistry; The Pennsylvania State University
University Park, Pennsylvania, 2005-2010.

Integrated M.S. in Chemistry; Indian Institute of Technology Bombay
Mumbai, India, 2000-2005.

Professional Experience

Graduate Research Assistant; The Pennsylvania State University
Thesis Advisor: Prof. Paul S. Weiss (2005-2010)
Thesis Title: Control and Measurement of Single Molecules and their Nanoscale Assemblies to Develop Molecular Machinery

Teaching Assistant; The Pennsylvania State University
General Chemistry Laboratory, Physical Chemistry Laboratory

Undergraduate Research; Indian Institute of Technology Bombay
Advisor: Prof. Chebrolu P. Rao (2003-2005)
Thesis Title: Calix[4]arene Derivatives: Binding Studies

Honors and Awards

2008 Miller Fellowship Award, The Pennsylvania State University
2007 Graduate Fellowship, The Pennsylvania State University
2007 Best Poster Award, American Chemical Society
2006 Incoming Graduate Student Award, The Pennsylvania State University
2006 Dan H. Waugh Memorial Teaching Award, The Pennsylvania State University
2005 Roberts Fellowship, The Pennsylvania State University

Professional Affiliations

American Vacuum Society
American Chemical Society